

Winter 2007

The design and performance of pressure pipe liners under static and cyclic loading

Shanhai Guan
Louisiana Tech University

Follow this and additional works at: <https://digitalcommons.latech.edu/dissertations>



Part of the [Civil Engineering Commons](#)

Recommended Citation

Guan, Shanhai, "" (2007). *Dissertation*. 549.
<https://digitalcommons.latech.edu/dissertations/549>

This Dissertation is brought to you for free and open access by the Graduate School at Louisiana Tech Digital Commons. It has been accepted for inclusion in Doctoral Dissertations by an authorized administrator of Louisiana Tech Digital Commons. For more information, please contact digitalcommons@latech.edu.

THE DESIGN AND PERFORMANCE OF PRESSURE PIPE LINERS
UNDER STATIC AND CYCLIC LOADING

by

Shanhai Guan, M.S.

A Dissertation Presented in Partial Fulfillment of the
Requirement for the Degree of
Doctor of Philosophy

COLLEGE OF ENGINEERING AND SCIENCE
LOUISIANA TECH UNIVERSITY

March 2007

UMI Number: 3264696

INFORMATION TO USERS

The quality of this reproduction is dependent upon the quality of the copy submitted. Broken or indistinct print, colored or poor quality illustrations and photographs, print bleed-through, substandard margins, and improper alignment can adversely affect reproduction.

In the unlikely event that the author did not send a complete manuscript and there are missing pages, these will be noted. Also, if unauthorized copyright material had to be removed, a note will indicate the deletion.

UMI[®]

UMI Microform 3264696

Copyright 2007 by ProQuest Information and Learning Company.

All rights reserved. This microform edition is protected against unauthorized copying under Title 17, United States Code.

ProQuest Information and Learning Company
300 North Zeeb Road
P.O. Box 1346
Ann Arbor, MI 48106-1346

LOUISIANA TECH UNIVERSITY

THE GRADUATE SCHOOL

February 23, 2007

Date

We hereby recommend that the dissertation prepared under our supervision
by Shanghai Guan
entitled The Design and Performance of Pressure Pipe Liners under Static and Cyclic Loading

be accepted in partial fulfillment of the requirements for the Degree of
PhD in Engineering



Supervisor of Dissertation Research

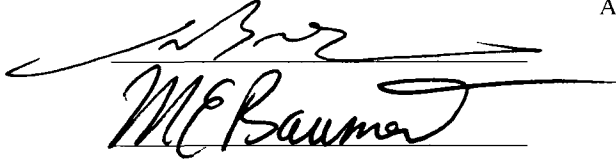
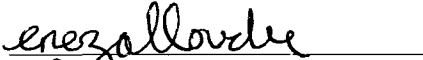


Head of Department

Engineering

Department

Recommendation concurred in:



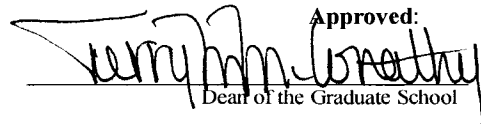
Advisory Committee

Approved:




Director of Graduate Studies

Approved:



Dean of the Graduate School



Dean of the College

ABSTRACT

Cured-in-place pipe (CIPP), is a widely used trenchless technology. Based on the current liner design method, American Society for Testing and Materials (ASTM) F2207-02, several aspects are studied for the effect on estimating the long-term performance of the liners.

While estimating the liner burst pressure, the effect from host pipe material properties, liner material properties, defect geometry, liner creep properties and loading condition should be considered. The burst pressure calculated based on the existing method is overestimated and this allows an increased risk of structural failure before the expected design life is reached.

Compared with cast-iron, a PVC host pipe provides less constraint for the liner and causes a lower liner burst pressure.

The existing method is safe to calculate the liner burst pressure when the defect size is at the high end of the range of defect sizes in comparison with the host pipe size. When the defect size decreases, the estimate becomes less safe. To maintain the same safety factor, a correction should be applied to reduce the estimated liner burst pressure.

To estimate the liner burst pressure for defect shapes other than square and circular, the defect area should be measured and transformed to a square shape with same area. Based on the length of the square, the ASTM method can be used to calculate the

liner burst pressure. It is also recommended to use different correction factors based on the extension direction of the defect.

The creep property of the liner is not an ignorable factor. The displacement could increase about 100% due to the creep effect.

A cyclic loading condition shows a noticeable effect on the development of displacement and strain. The strain development shows that a liner's Young's Modulus gradually decreases under a cyclic loading condition. This means that a liner could fail under a cyclic loading condition at a lower pressure level.

Based on this research, correction factors, according to each of the different aspects of liner behavior outlined above, are recommended for estimating an appropriate liner burst pressure.

Recommendations for further research are also provided.

APPROVAL FOR SCHOLARLY DISSEMINATION

The author grants to the Prescott Memorial Library of Louisiana Tech University the right to reproduce, by appropriate methods, upon request, any or all portions of this Dissertation. It is understood that "proper request" consists of the agreement, on the part of the requesting party, that said reproduction is for his personal use and that subsequent reproduction will not occur without written approval of the author of this Dissertation. Further, any portions of the Dissertation used in books, papers, and other works must be appropriately referenced to this Dissertation.

Finally, the author of this Dissertation reserves the right to publish freely, in the literature, at any time, any or all portions of this Dissertation.

Author Shankar Kumar

Date Feb. 23rd. 2007

TABLE OF CONTENTS

ABSTRACT	iii
LIST OF TABLES	viii
LIST OF FIGURES	x
ACKNOWLEDGEMENTS	xv
CHAPTER ONE INTRODUCTION	1
1.1 Background and Research Need	2
1.2 Objective and Scope	2
CHAPTER TWO LITERATURE REVIEW	4
2.1 Theoretical Model for Liner Burst Pressure and Long Term Performance	7
2.1.1 Equilibrium	7
2.1.2 Strain Displacement	8
2.1.3 Constitutive Equations	9
2.1.4 Compatibility Equations	9
2.1.5 Failure Criteria	10
2.2 Liner Experiments for Tensile Properties	11
2.3 FE Modeling for Burst Pressure Study	13
2.4 Creep Experiments for Long Term Properties	14
2.5 FE Modeling for Creep Study	16
2.6 Cyclic Load Experiments	18
CHAPTER THREE MATHEMATIC MODEL FOR LINER BURST PRESSURE	20
3.1 Material Characterization Tensile Experiment	20
3.1.1 Experiment Setup	20
3.1.2 Data Processing	23
3.2 Analytical Calculations for Burst Pressure and Parametric Study	30
3.3 Conclusions	35
CHAPTER FOUR FEA FOR BURST PRESSURE AND COMPARISON	37
4.1 Model Setup	37
4.1.1 Material Models	37
4.1.2 Basic Geometrical Parameters and Material Properties	38
4.1.3 Element Selection	43
4.1.4 Contact Conditions and Boundary Conditions	43

4.1.5 Failure Criteria.....	44
4.2 Parameters Study	44
4.2.1 Host Pipe Material Properties	49
4.2.2 Shape of Gap in Host Pipe.....	53
4.3 Results Comparisons between Different Methods.....	57
4.4 Finite Element Model Verification and Conclusions	63
CHAPTER FIVE INFLUENCE OF CREEP EFFECT ON LINER LONG TERM PERFORMANCE.....	65
5.1 Creep Experiment	66
5.2 Liner Creep Variation for FE Modeling	70
5.2.1 Creep Material Models	70
5.2.2 Data Fitting Methods and Results.....	72
5.3 Finite Element Analysis for Liner Long Term Performance	75
5.4 Parametric Study.....	81
5.5 Conclusions.....	85
CHAPTER SIX CYCLIC LOADING EXPERIMENTS	86
6.1 Cyclic Loading Experiment Setup	86
6.2 Cyclic Loading Experimental Results	91
6.3 Conclusions.....	102
CHAPTER SEVEN POSSIBLE MODIFICATION ON THE DESIGN OF PIPELINE REHABILITATION LINERS	104
7.1 Factor for Host Pipe and Defect Variation	104
7.2 Factor for Creep Effect and Cyclic Loading Condition.....	105
7.3 Conclusions and Recommendations	106
CHAPTER EIGHT FURTHER INVESTIGATION OF LINER DESIGN.....	107
APPENDIX A LINER TENSILE EXPERIMENTAL DATA	109
APPENDIX B MATHCAD® SPREADSHEETS FOR BURST PRESSURE	114
B.1 Calculations of Burst Pressure Using Maximum Stress Criteria	115
B.2 Calculations of Burst Pressure in ASTM F2207-02 Using Interactive Criteria	118
B.3 Interactive Criteria Conclusion: Liner "Life" and Max Operating Pressure ...	122
APPENDIX C LINER CREEP EXPERIMENTAL DATA.....	123
APPENDIX D CYCLIC LOADING EXPERIMENT DATA.....	127
REFERENCES	131

LIST OF TABLES

Table 3.1	Axial strain results for axial orientation.....	25
Table 3.2	Transverse strain results for axial orientation.....	25
Table 3.3	Poisson’s ratio for axial orientation	26
Table 3.4	Axial strain results for hoop orientation	27
Table 3.5	Transverse strain results for hoop orientation.....	27
Table 3.6	Poisson’s ratio for hoop orientation.....	28
Table 3.7	Interaction compliance coefficients	30
Table 3.8	Effect of defect size on burst pressure	32
Table 4.1	Basic geometrical parameters of PVC pipe and liner	39
Table 4.2	Material properties for liner	41
Table 4.3	Material properties used for ADINA material models	42
Table 4.4	Liner burst pressure result for 1.5 inch defect with different mesh sizes	46
Table 4.5	Burst pressure results for mesh sizes of 0.3” and 0.5”	48
Table 4.6	Burst pressures with circular defects for two host pipes.....	50
Table 4.7	Burst pressures with different shape defects for two host pipes.....	54
Table 4.8	Burst pressures for circular defects: comparison between finite element analysis and ASTM predictions.	58
Table 4.9	Burst pressures with different defect shapes: Comparison between finite element analysis and ASTM predictions	59
Table 4.10	Comparison of experimental and simulated burst pressures for a 6 inch x 8 inch elliptical defect.....	64

Table 5.1	Dimensions of creep test specimens	67
Table 5.2	Applied load and stress level for each specimen	68
Table 5.3	Parameters for Creep Law 1	73
Table 5.4	Parameters for Creep Law 3	74
Table 5.5	Displacement results from finite element analysis and experiments	76
Table 5.6	Displacement results with and without creep effect (Cast-iron pipe).....	82
Table 5.7	Displacement results with and without creep effect for a PVC pipe	82
Table 6.1	Baselines for LVDTs and stain gauges	93

LIST OF FIGURES

Figure 2.1	Three component system	5
Figure 2.2	Liner bulging out of the hole in a host pipe	8
Figure 2.3	Liner sample with the orientation of the coupons.....	11
Figure 2.4	Liner flattened between two metal sheets.....	11
Figure 2.5	Typical coupon dimensions (inches).	12
Figure 3.1	Approximate coupon size (inches).....	21
Figure 3.2	Coupon flattened by metal plate with clamps.....	21
Figure 3.3	Small environmental chamber	21
Figure 3.4	MTS multi-purpose testing machine.....	22
Figure 3.5	Extensometers	23
Figure 3.6	Typical load/width-axial strain curve	24
Figure 3.7	Average load/width-axial strain curve for axial orientation	28
Figure 3.8	Average load/width-axial strain curve for hoop orientation	29
Figure 3.9	The burst pressure and the defect size	31
Figure 3.10	Radius of bulge curvature in the axial direction	33
Figure 3.11	Radius of bulge curvature in the hoop direction.....	33
Figure 3.12	Ratio of actual pressure to assumed value (percent).....	34
Figure 3.13	Ratio between w and $D \cdot \sin^{-1}(w/D)$	34
Figure 4.1	Plastic bilinear material model.....	38

Figure 4.2	True and engineering stress-strain curves.....	39
Figure 4.3	True and engineering bilinear model for axial orientation	40
Figure 4.4	True and engineering bilinear model for hoop orientation	40
Figure 4.5	Stress-strain curve for class 200 “Blue Brute” PVC pipe.....	42
Figure 4.6	Liner burst pressure varies with mesh size	47
Figure 4.7	Burst pressure difference with mesh size.....	47
Figure 4.8	Burst pressure results for two mesh sizes	48
Figure 4.9	Liner burst pressure for cast iron and PVC host pipe with different defect sizes	51
Figure 4.10	Simulated liner burst pressure difference between PVC and cast iron host pipes	51
Figure 4.11	Magnified deformation for a 2” diameter defect in a cast iron host pipe.....	52
Figure 4.12	Magnified deformation for a 2” diameter defect in a PVC host pipe.....	52
Figure 4.13	Rectangle defect (1.732*5.196) in the axial direction	55
Figure 4.14	Rectangle defect in the hoop direction.....	55
Figure 4.15	Deformation of a straight plate under pressure.....	57
Figure 4.16	Deformation of a curved plate under pressure.....	57
Figure 4.17	FEA results and ASTM 2207-02 predicted values <i>versus</i> defect diameter .	60
Figure 4.18	Strain distribution for a cast-iron host pipe with a 1.5 inch circular defect.	61
Figure 4.19	Strain distribution for a cast-iron host pipe with a 6 inch circular defect....	61
Figure 4.20	Strain distribution for a cast-iron host pipe with a 3×3 inch square defect.....	62
Figure 4.21	Strain distribution for a cast-iron host pipe with a 1.732×5.1963 inch rectangular defect.....	62
Figure 4.22	Cast-iron host pipe with 8” long and 6” wide defect.....	63

Figure 5.1	Tension loading device	66
Figure 5.2	Creep strain curve for specimen B5.....	69
Figure 5.3	Liner block model.....	75
Figure 5.4	Displacement developments for specimen B5 over 5,000 hours.....	76
Figure 5.5	Strain comparison between experimental results and analysis results.....	77
Figure 5.6	Magnified deformation of the liner at 5,000 hours (4" diameter hole in cast-iron pipe)	78
Figure 5.7	Magnified deformation for a 4" diameter defect in a cast iron host pipe (creep is neglected)	79
Figure 5.8	Magnified deformation of the liner after 5,000 hours (pressure at 300 psi).....	79
Figure 5.9	Element labels in model.....	80
Figure 5.10	Displacement <i>versus</i> time (pressure at 300 psi).....	80
Figure 5.11	Effective creep strain <i>versus</i> time (element 1951; pressure at 300 psi).....	81
Figure 5.12	Displacement with and without creep effect for cast iron pipe	83
Figure 5.13	Percentage difference with and without creep effect.....	83
Figure 5.14	Displacement comparison with and without creep effect (PVC pipe).....	84
Figure 5.15	Percentage difference with and without creep effect (PVC)	84
Figure 6.1	Customer-made pressure testing system.....	87
Figure 6.2	Control unit of customer-made pressure testing system	87
Figure 6.3	Machined PVC host pipe and steel ring.....	88
Figure 6.4	LVDTs and strain gauges.....	89
Figure 6.5	Electro-pneumatic regulator T3111	89
Figure 6.6	Adjustable power supplies and signal monitor	90

Figure 6.7	Loading cycle illustrations.....	91
Figure 6.8	Measurement drift at LVDT2 without load	92
Figure 6.9	Measurement drift at strain gauge 1 without load	92
Figure 6.10	LVDT1 displacement developments.....	94
Figure 6.11	LVDT1 displacement increase percentages.....	94
Figure 6.12	Strain developments at 4 inch circular defect.....	95
Figure 6.13	Strain increase percentages	95
Figure 6.14	Displacement net gain <i>versus</i> hole size.	97
Figure 6.15	Displacement increase percentage <i>versus</i> hole size.....	97
Figure 6.16	Strain net gain <i>versus</i> hole size.....	98
Figure 6.17	Strain increase percentage <i>versus</i> hole size.	98
Figure 6.18	Displacement development for 4 inch circular defect for 552 hours.....	100
Figure 6.19	Displacement development <i>versus</i> time (effect of creep considered; notice primary and secondary creep mechanisms).	100
Figure 6.20	Comparison between displacement from LVDT1 and finite element analysis.....	101
Figure 6.21	Comparison between strain from strain gauge 1 and finite element analysis.....	102
Figure A.1	Load/width <i>versus</i> axial strain of axial specimen 1	110
Figure A.2	Load/width <i>versus</i> axial strain of axial specimen 2	110
Figure A.3	Load/width <i>versus</i> axial strain of axial specimen 3	110
Figure A.4	Load/width <i>versus</i> axial strain of axial specimen 4	111
Figure A.5	Load/width <i>versus</i> axial strain of axial specimen 5	111
Figure A.6	Load/width <i>versus</i> transverse strain of axial specimen 6.....	111
Figure A.7	Load/width <i>versus</i> transverse strain of axial specimen 7.....	112

Figure A.8	Load/width <i>versus</i> transverse strain of axial specimen 8.....	112
Figure A.9	Load/width <i>versus</i> transverse strain of axial specimen 9.....	112
Figure A.10	Load/width <i>versus</i> transverse strain of axial specimen 10.....	113
Figure C.1	Liner creep experimental data.....	124
Figure C.2	Liner creep experimental data and fitting for specimens. (a) A1, (b) A2, (c) A4, and (d) A5	125
Figure C.3	Liner creep experimental data and fitting for specimens. (a) B1, (b) B2, (c) B3, (d) B4, and (e) B5	126
Figure D.1	LVDT1 (a) displacement and (b) increase percentage	128
Figure D.2	LVDT2 (a) displacement and (b) increase percentage	128
Figure D.3	LVDT3 (a) displacement and (b) increase percentage	128
Figure D.4	LVDT4 (a) displacement and (b) increase percentage	129
Figure D.5	Strain Gauge 1 (a) strain development and (b) increase percentage.....	129
Figure D.6	Strain Gauge 2 (a) strain development and (b) increase percentage.....	129
Figure D.7	Strain Gauge 3 (a) strain development and (b) increase percentage.....	130
Figure D.8	Strain Gauge 4 (a) strain development and (b) increase percentage.....	130

ACKNOWLEDGEMENTS

I am very grateful to my dissertation advisor, Dr. Raymond L. Sterling, for his kindness, insightful guidance and support in my research work throughout last four and half years.

I want to thank my co-advisor, Dr. Erez Allouche, for his every effort and hard work that he put into my research in the last two years.

I also want to thank Dr. Michael E. Baumert, for his help on the cyclic loading system and all the weekends he spent on this project. I want to thank Dr. Zingran "Jay" Wang, for his guidance on finite element analysis and ADINA. I also want to thank Dr. David E. Hall, for his suggestions in my dissertation study.

I want to give thanks to the staff from the mechanical shop, Jimmy, McKinney, Dusty, FeiFei Xu, and Qing Cai, for their help in building up the test system, preparing the test materials, and collecting the test data.

I'd like to give my special thanks to Mr. Lloyd D. Smith and Mr. Brady J. Broom from CMC Joist Company, for their understanding and support in the last seven months.

I really appreciate my parents and parents-in-law, for their unreserved support and love. I give my deepest appreciation to my wife for all the help and encouragement since we met. Also thanks to my little two-year-old daughter, her magic smile always gives me strength to keep going.

CHAPTER ONE

INTRODUCTION

Pipe systems constructed of different materials have been in use for many centuries. The early development of pipe systems was related to the growth of cities. The early pipes were made of clay, lead, bronze and wood. With the development of newer materials, cast iron and ductile iron were introduced into pipe systems. Many buried pipeline systems, built in the post WWII era, have deteriorated significantly and are in need of repair. Numerous research activities have been conducted to develop better and more cost efficient repair methods.

Trenchless methods, while their earliest record goes back to Roman times, became a new technology wave for pipeline installation and repair about 20 years ago. Cured-in-place pipe (CIPP), a trenchless repair method, is a cost effective technique used to rehabilitate defective pipes without disturbing the pavement, sidewalk, landscaping, and adjacent utilities. The process is carried out by impregnating a flexible tube with a cross sectional perimeter equal to the inner circumference of the host pipe. The tube is then pressure inverted against the wall of the host pipe from a suitable access point, and heated in-situ (using water, steam or air) to cure the resin, thus forming a structurally competent lining.

For the CIPP lining method, there are aspects which should be considered while estimating the long-term performance of the liners. These include the conditions of the

defects in the host pipe, long term material properties, geometrical imperfections in the liner, and the magnitude and nature of the loading condition.

1.1 Background and Research Need

More than 300,000 miles of underground utilities, including water, sewer, and gas, electrical power, cable television, and telephone, are constructed around the world each year, with an estimated market value of greater than \$35 billion. An estimate of the total U.S. pipeline-renewal market is about \$330 billion. As one of the most widely used methods of trenchless pipeline renewal, CIPP has gained a significant share of this market.

1.2 Objective and Scope

The objective of this research is to better understand the long-term performance of glass fiber reinforced CIPP liners installed in partially deteriorated water pressure pipes. The effect of a host pipe defect's shape and size on the liner's pressure capacity and the liner creep properties on its long term performance were investigated experimentally as well as numerically.

A three-dimensional (3-D) Finite Element (FE) model was developed to study the effect of the shape and size of defects in the host pipe on a liner's performance. An experimental creep test was performed to quantify the liner's creep variations, which are used in the 3-D FE model to study the effect of creep properties on a liner's long term behavior.

The research consisted of the following parts:

- a) A literature review of the design models and finite element models used for rehabilitation liner applications.
- b) An experimental material characterization program undertaken to determine the key liner properties in the longitudinal and latitudinal directions.
- c) Use of a 3-D FE model to study the relationship between failure pressure and the shape and size of a defect in the wall of a fully deteriorated host pipe.
- d) Comparison of the failure pressure results with ASTM F2207-02.
- e) Creep tests to collect creep data and build up a creep model for the FE analysis.
- f) Use of a 3-D FE model to study the effect of creep properties on a liner's long-term performance.
- g) Cyclic loading tests and data collection for different defect sizes for studying the effect of cyclic loading condition on a liner's long term performance.

CHAPTER TWO

LITERATURE REVIEW

Cast iron pipe was first used in the United States around the beginning of the nineteenth century. It was imported from England and Scotland to be used in the water-supply and gas-lighting systems of the larger cities, principally those in the northeastern portion of the country. The utilization of gray cast-iron pipe in North America continued until the 1940s, when they were gradually replaced with ductile iron pipes.

CIPP is a commonly employed technique for the rehabilitation of gravity sewer pipes. The application of CIPP to pressure pipes such as water and gas mains is a newer development in North America. CIPP is classified as a “close fitting liner” and is designed to perform as a hybrid pipe system along with the partially deteriorated host pipe. A cured-in-place liner may be either a two-component system or a three-component system. In a two-component system the CIP pipe lining system consists of a flexible tube and an adhesive. In a three-component system the CIP pipe lining system consists of an elastomer skin, a jacket and an adhesive (Figure 2.1).

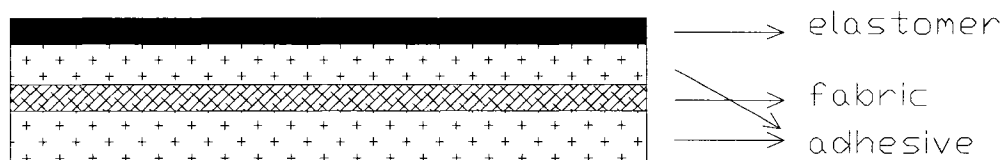


Figure 2.1. Three component system.

The elastomer skin is a membrane, which is typically made of polyurethane or polyester, allowing for both inversion of the liner during the installation process and to be pressure tight during in-service operation. When the flexible tubing is inverted into the pipeline to be rehabilitated, the elastomer skin becomes the inner surface of the newly rehabilitated pipe. For a three-component system, the flexible tubing consists of a jacket with an elastomer skin that functions as a barrier. For a two-component system, the flexible tubing functions as the barrier.

The jacket is a textile product that is manufactured into a cylindrical form. It is made of synthetic materials, typically polyester and glass fiber composite cloth, and provides the tensile strength and elasticity necessary to resist the specified sustained pressure when installed in a partially deteriorated pipe. The jacket and the elastomer skin should be compatible with liquids such as water, gasoline, gas condensate, methanol, triethylene glycol, brine, mineral oil, isopropanol, sulfuric acid, surfactants and mercaptans [1].

The adhesive system is a two part system consisting of a resin and a hardener. Three primary resin systems used by the CIPP industry are unsaturated polyester, vinyl ester and epoxy. Vinyl ester and epoxy resin systems are commonly used in industrial and high pressure/high temperature applications, where their special corrosion and/or

solvent resistance and higher temperature performance are needed. Unsaturated polyester is commonly used in low pressure applications (e.g., gravity sewers).

In potable water distribution systems, epoxy resins are commonly used. Common requirements of any resin system are:

- a) low viscosity,
- b) high physical strength,
- c) good adhesion,
- d) low shrinkage on cure,
- e) low sensitivity to water and other fluids mentioned above, and
- f) fast cure with controlled exotherm.

Liner burst pressure is decided by the interaction of the composite components. Liner burst pressure tests were conducted for a 6.313 inch internal diameter cast-iron with a 2 inch circular defect that were lined with four different liner types including: a) 1.5 mm coated felt with epoxy resin; b) 2 mm uncoated felt with carbon fiber and epoxy resin; c) 3 mm uncoated felt with polyurethane resin; and, d) 3 mm uncoated felt with epoxy resin [2]. The observed liner burst pressures ranged from 390 psi to 1400 psi corresponding to the different liner materials. It was noticed that tears in the liner occurred at the edges of the circular opening in the host pipe or beneath cracks and tears in the felt and/or carbon fiber layer. In all cases, bursting of the liners was ultimately caused by tearing of the liner as it flexed over the sharp cracks or breaks in the outer felt and/or carbon fiber layer [2].

2.1 Theoretical Model for Liner Burst Pressure and Long Term Performance

A mathematical model is provided in ASTM F 2207-02 for liners used in the rehabilitation of pressurized gas pipeline systems. This model is applicable to an elastomer-fabric liner whose shear stiffness is small compared with its tensile stiffness in the axial and hoop directions. The purpose of the model is to use uniaxial tensile test data of the liner in combination with hole size data to determine the liner's design pressure and service life. This model solves equilibrium equations, strain displacement equations, constitutive equations and compatibility equations in conjunction with a failure criterion to predict the burst pressure of the liner for a given opening size in the host pipe. The following sections provide a simplified description of this mathematical model.

2.1.1 Equilibrium

The static equilibrium of the exposed liner is expressed by the following equation:

$$\frac{N_h}{r_h} + \frac{N_a}{r_a} = P \quad (2.1)$$

Where:

N_h is the hoop load per unit width from the uni-axial tensile test on the hoop direction coupon,

N_a is the axial load per unit width from the uni-axial tensile test on axial direction coupon,

r_h is the radius of curvature of the liner in the hoop direction,

r_a is the radius of curvature of the liner in the axial direction (see Figure 2.2).

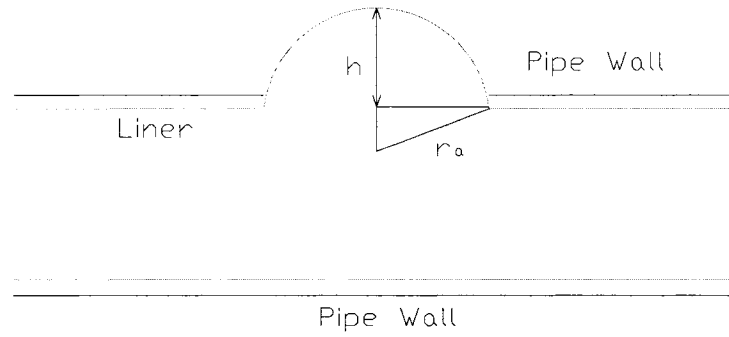


Figure 2.2. Liner bulging out of the hole in a host pipe.

2.1.2 Strain Displacement

It is assumed that a defect can be adequately characterized by two dimensions, w in the hoop direction and L in the axial direction. For circular defects, $L=w$. It is assumed that the liner deforms into a circular arc at the hole in each of these directions (Figure 2.2).

Under such conditions, the strains are given by the following expressions:

$$\varepsilon_h = \frac{2 \cdot r_h \cdot \sin^{-1}\left(\frac{w}{2 \cdot r_h}\right)}{D \cdot \sin^{-1}\left(\frac{w}{D}\right)} - 1 \quad (2.2)$$

$$\varepsilon_a = \frac{2 \cdot r_a \cdot \sin^{-1}\left(\frac{w}{2 \cdot r_a}\right)}{L} - 1 \quad (2.3)$$

Where:

ε_h is the strain in the hoop direction,

ε_a is the strain in the axial direction, and

D is the internal diameter of the host pipe.

2.1.3 Constitutive Equations

The liner is assumed to be an orthotropic membrane without any shear stiffness.

Thus the relationship between stress and strain is given by the following equations:

$$\varepsilon_h = \frac{1}{E_h} \cdot N_h + S_{12} \cdot N_a \quad (2.4)$$

$$\varepsilon_a = S_{12} \cdot N_h + \frac{1}{E_a} \cdot N_a \quad (2.5)$$

Where:

E_a is the modulus in axial direction,

E_h is the modulus in hoop direction,

S_{12} is the interactive compliance factor = Poisson's ratio/modulus in the corresponding orientations.

2.1.4 Compatibility Equations

As the liner bulges out of the gap in the host pipe, it is constrained to pass through the end points of the gap. This requirement, in conjunction with the assumption that the shape of the liner in the axial and hoop directions is a circular arc, gives the following relationships for the radius of curvature in each direction:

$$r_a = \frac{L^2}{8h} + \frac{h}{2} \quad (2.6)$$

$$r_h = \frac{w^2}{8h} + \frac{h}{2} \quad (2.7)$$

Where:

h is the height of the liner bulge beyond the pipe's internal wall.

2.1.5 Failure Criteria

Both the maximum stress criterion and the interactive stress criterion have been used successfully for predicting a liner's failure load. In the maximum stress criterion, failure is said to occur when either the hoop load/width reaches the ultimate hoop load/width ratio or the axial load/width ratio reaches the ultimate axial load/width ratio. This is stated mathematically as follows:

$$\frac{N_h}{(N_{uts})_h} = 1 \quad (2.8)$$

$$\frac{N_a}{(N_{uts})_a} = 1 \quad (2.9)$$

In interactive failure criterion, failure occurs when the following condition is reached:

$$\left(\frac{N_h}{(N_{uts})_h}\right)^2 - \frac{N_h \cdot N_a}{(N_{uts})_h^2} + \left(\frac{N_a}{(N_{uts})_a}\right)^2 = 1 \quad (2.10)$$

The failure pressure is calculated by solving the Equations 2.8 through 2.10. The solution is a two-step iterative process. In the first step the yield load/width and strains are determined by using a yield criterion:

$$\epsilon_a^2 + \epsilon_h^2 = \epsilon_y^2 \quad (2.11)$$

Where ϵ_y is the yield strain from the tensile test.

In the second step, the burst pressure is calculated by incrementing the load/width ratio and strain using the secondary modulus. The equations are solved using iterative techniques such as the Newton-Raphson method.

2.2 Liner Experiments for Tensile Properties

According to ASTM F2207-02, tensile properties in both hoop and axial orientations should be determined. Coupons for tensile testing are cut in both axial and hoop directions (See Figure 2.3).

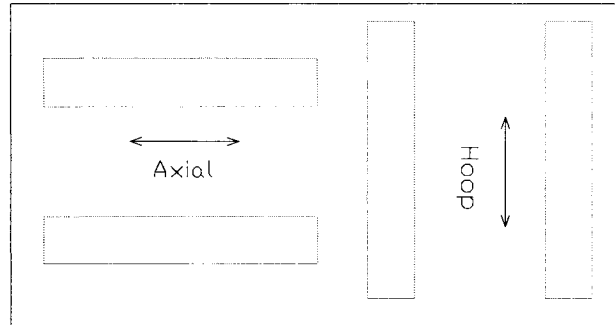


Figure 2.3. Liner sample with the orientation of the coupons.

The portions of the liner that contained folds were avoided because of non-uniformity in thickness. The liner is flattened between two sheets of metal with the adhesive applied as in practice (See Figure 2.4).

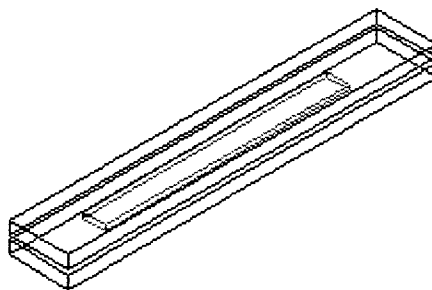


Figure 2.4. Liner flattened between two metal sheets.

The specimen is required be sufficiently wide (0.75 to 1.00 in.) so that a representative number of fibers are included (See Figure 2.5).

For strains higher than 5 %, the true stress and true strain should be used as the input material parameters for finite element analyses [3]. The true stress is defined as the ratio of applied load (P) to instantaneous cross-section (A). Assuming that volume change in the specimen during tensile testing is negligible, true stress can be calculated using the following relationships:

$$A \cdot L = A_0 \cdot L_0 \quad (2.12)$$

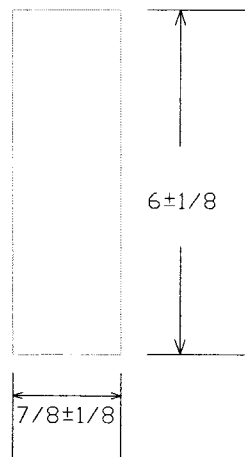


Figure 2.5. Typical coupon dimensions (inches).

Where A , L represent the instantaneous cross-sectional area and length of portion of specimen under stretching, respectively, while A_0 and L_0 correspond to the original dimensions of the specimen.

The true stress (σ_T) can be obtained from:

$$\sigma_T = \frac{P}{A} \cdot \frac{L}{L_0} = \sigma_e(1 + \varepsilon_e) \quad (2.13)$$

Where σ_e and ε_e are the engineering stress and strain, respectively. Similarly, true strain is given by:

$$\varepsilon_T = \ln\left(\frac{L_0 + \delta L}{L_0}\right) = \ln(1 + \varepsilon_e) \quad (2.14)$$

Where δL is the incremental strain.

2.3 FE Modeling for Burst Pressure Study

The accuracy of predictions made by a finite element model is influenced by several factors, including:

- a) Physical representation and extent of idealization,
- b) Material models,
- c) Boundary and loading conditions,
- d) Failure criterion, and
- e) Choice of elements.

Considering a host pipe with a defect, a 2-D model is not capable of simulating the stress and strain distribution. Thus, a 3-D model should be used in this case.

Non-linear behaviors need to be considered in a finite element analysis when one or more of the following conditions exist:

- a) Physical non-linearity or material non-linearity.
- b) Geometric non-linearity.
- c) Boundary non-linearity.

Further discussion of nonlinear behavior is offered in Chapter Five.

Considering that the stiffness of cast iron is much greater than that of the liner, two different material models should be used for the host pipe (cast-iron) and the liner.

Many theories have been proposed to predict the failure of materials under the action of loading. Since the liner material used in this research undergoes plastic loading for the most part of the uniaxial test, the theory used to predict failure of the liner is based on accumulated plastic strain. Rupture is assumed to occur when the accumulated plastic strain in the complex stress state reaches the maximum plastic strain in the tensile test. When the accumulated plastic strain reaches this value in any integration point of an element, that element is considered 'dead' and is removed from the analysis [4]. The load corresponding to the dead element is distributed to neighboring elements. Failure (i.e., critical pressure) is assumed to be the pressure corresponding to the last load step that resulted in the convergence of the FE model.

Contact surfaces are considered to simulate the surface of the liner and that of the host pipe. The contact between the liner and the host pipe is assumed to be frictionless ($\mu = 0$). Further discussion of contact elements is offered in Chapter Five.

2.4 Creep Experiments for Long Term Properties

When a thermoplastic material is held under sustained stress, its strain continues to increase with time, and the magnitude of stress needed to produce failure diminishes. This characteristic can be described by a long-term modulus, E_v , that is the curve which relates creep strain to time under sustained stress is plotted. Then the relationship between E_v and time, t , can be developed [5].

Several investigations [6] have presented different approaches to creep characterization. Generally, approaches to the creep can be divided into theoretical methods and experimental methods. The Maxwell model, Kelvin model and the combined creep model [7] are commonly used models to represent creep properties. A

common experimental approach is the one proposed by Findley [8], which was successfully used to predict up to 26 years of creep behavior.

A tensile creep process is controlled by several factors and a number of methods [9] have been proposed to describe the tensile creep behavior of plastics in terms of stress, strain, and loading time. Findley (1944, [10]) found that tensile creep of several reinforced thermosetting materials could be described by following expression:

$$\varepsilon = \varepsilon_0 + \varepsilon_t t^n \quad (2.15)$$

Where: ε = total elastic plus time-dependent strain

ε_0 = stress-dependent, time-independent initial elastic strain

ε_t = stress-dependent, time-dependent coefficient of time-dependent strain

n = material constant, substantially independent of stress magnitude

t = time after loading (hours)

Equation 2.15 was developed from tensile creep tests, but, in some cases, it can successfully describe the behavior of compression, and combinations of tensile and shear stresses as well [11].

Horsley [12] suggested the equation (which is a simplification of Findley's equation):

$$\varepsilon = m_0 t^n \sinh \frac{\sigma}{\sigma_0} \quad (2.16)$$

Where:

ε = total elastic plus time-dependent strain

σ = sustained stress

σ_0, n, m_0 = empirical material constants

t = time after loading (hours only)

Bergen and Wolstenholme [13] suggested the following equation to model creep behavior:

$$\varepsilon - \varepsilon_0 = A(1 - e^{-Ba_t}) \quad (2.17)$$

Where:

$$\varepsilon_0 = ks$$

s = applied stress

ε = time-dependent strain

t = time after loading

k, B, A = material constants

a_t = shift factor, which is a function of temperature

This equation is not appropriate to predict creep for a longer period.

2.5 FE Modeling for Creep Study

The finite element (FE) method is a powerful analysis tool because of its flexibility in dealing with complicated geometry and boundary conditions. FE modeling is widely used in parametric studies, stress/strain visualization and boundary condition analyses. In CIPP studies, the FE method has been applied in modeling the liner buckling process under external pressure by a number of researchers [14-18]. Most of these researchers verified their modeling with their own experimental data and/or published test data. Good agreement between the predicted and observed results was reported in all cases.

The liner is subjected to several loads acting alone or in combinations. These loads can be classified as internal loads, external loads and installation loads.

External Loads include:

- a) Over burden soil loads,
- b) Traffic loads,
- c) Hydrostatic loads
- d) Loads due to ground movements and ground settlements,
- e) Loads due to bending of pipes due to poor bedding, frost action, swelling of soil surrounding the pipeline, poor compaction, etc.,
- f) Thermal loads, and
- g) Point loads caused by irregularities in existing pipeline caused by internal corrosion.

Internal Loads:

- a) Design and operating pressures,
- b) Pressure transients-positive and negative (e.g. water hammer, pressure cycling, vacuum),
- c) Thermal loads due to temperature changes in transported fluid, and
- d) Friction of transported fluid.

Installation loads:

- a) Lining pipe preparation forces (e.g. section reduction),
- b) Insertion forces (i.e., tensile, bending, compressive, torsion),
- c) Grouting forces (i.e., external pressure, floatation), and
- d) Residual stresses due the installation forces listed above.

Most studies focus on buckling in low pressure pipes under external hydrostatic or earth pressures. Research on modeling liner performance under variable internal pressure was conducted by GTI [2]. Allouche et al [19] examined the effect of internal loads on liner in a partially deteriorated pressure pipe. Arun [20] conducted an experimental and numerical study of the effect of longitudinal folds on the pressure rating of structural liners. However, studies on the long term performance of structural liners under variable internal pressure in the presence of a partially deteriorated host pipe are still insufficient.

2.6 Cyclic Load Experiments

Surge pressures are always considered as one of the main design factors for pressure pipes. Surge pressures (commonly termed “water hammer”) are generated in any pressurized piping system when the flowing liquid changes velocity. As the flow velocity changes, part or all of the kinetic energy of the moving fluid is converted into potential energy; resulting in pressure waves that travel upstream and downstream from the point of origin. Common causes for pressure surges include:

- a) Opening and closing (partial or full) of valves,
- b) Starting and stopping of pumps,
- c) Changes in flow demand,
- d) Changes in reservoir elevation,
- e) Reservoir wave action, and
- f) Entrapped air inside the pipelines.

Surges can be generally divided into transient and cyclic surges. Cyclic surges occur regularly over time. This type of surge is generally generated by equipment such as reciprocating pumps and pressure reducing valves. Small oscillatory surges can grow

rapidly and can become damaging if the frequency is close to the natural resonant frequency of the piping system. Transient surges may be best described as the intermediate conditions that exist in a system as it moves from one steady state to another. The closing of a single valve is a classical example of a transient surge.

When studying the effect of cyclic loading on a liner long term performance, it is important to understand the failure mechanism of composite materials. Normally, one component in a composite is often a high tensile fiber that gives the material its tensile strength, while another component is a resin that binds the fibers together, transferring load from broken fibers to unbroken ones and among fibers that are not oriented along lines of the principal stress. The last component will be the matrix material in which the fibers are embedded.

Under cyclic loading condition, several damage modes could happen in composite materials.

- a) Matrix tensile cracking or matrix compressive/shear failure. Matrix mode failure is characterized by cracks running parallel to the fibers.
- b) Ply separation (delamination). A delamination is a crack which runs in the resin rich area between plies with different fiber. Normally, delamination only occurs in the presence of matrix cracks.
- c) Fiber breakage (tensile or compressive).

CHAPTER THREE

MATHEMATIC MODEL FOR LINER BURST PRESSURE

A mathematic model provided by ASTM 2207-02 can be used to predict the liner burst pressure and long-term performance for a glass-fiber-reinforced (GFR) structural liner. This chapter describes the application of ASTM 2207-02 to a structural liner for potable water applications. Both experimental and mathematical calculations are used to derive the needed material properties. Analytically obtained predictions will be compared with liner burst test data and also with predictions obtained using three-dimensional finite modeling in later chapters.

3.1 Material Characterization Tensile Experiment

3.1.1 Experiment Setup

Coupons for tensile tests were cut in both axial and hoop orientations (see Figure 2.3). The approximate coupon dimensions are shown as Figure 3.1. Coupons were held by two metal plates with clamps (see Figure 3.2) and placed in a small environmental chamber at a temperature of 140F (Figure 3.3) for a period of 24 hours. Thereafter, the coupons were removed from the chamber and left to cool at room temperature (70 F) for another 24 hours before being released from the clamps and tested.

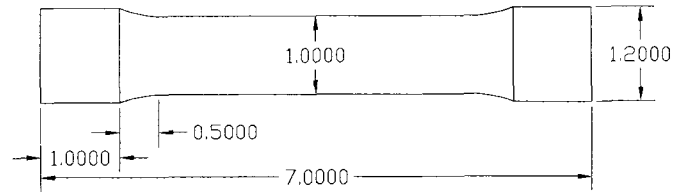


Figure 3.1. Approximate coupon size (inches).

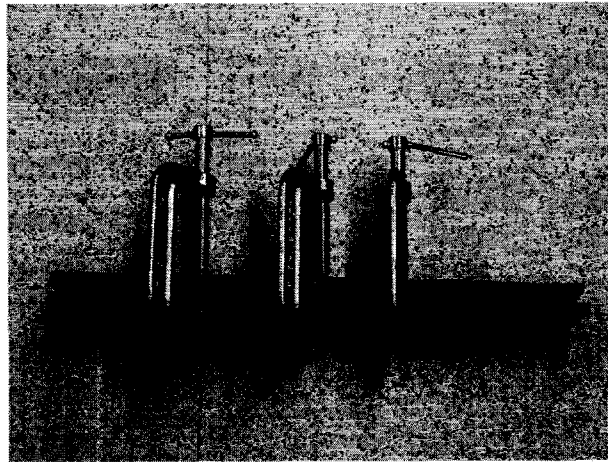


Figure 3.2. Coupon flattened by metal plate with clamps.

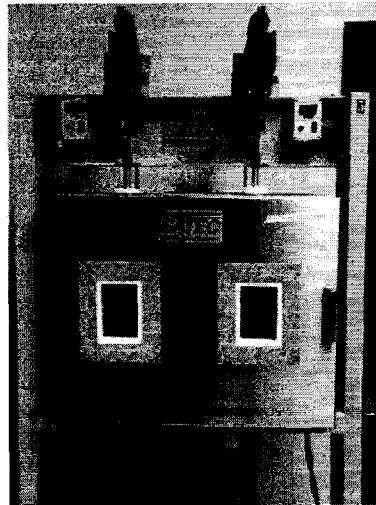


Figure 3.3. Small environmental chamber.

All tensile tests were conducted using a 22kip MTS 810 servo controller test system with a TestStar II controller (see Figure 3.4). An integrated data acquisition system was used to record the applied load and corresponding strain in the specimen. All tests were done at a temperature of 70F. Self-tightening grips were used to avoid slippage during testing. The extensometer and load-indicating mechanisms were capable of recording 100 readings per second. The speed of testing was set to 0.05 inches per minute. Time (seconds), axial load (pounds), axial strain (%) and axial displacement (inches) were recorded continuously from the start till failure of the specimen.

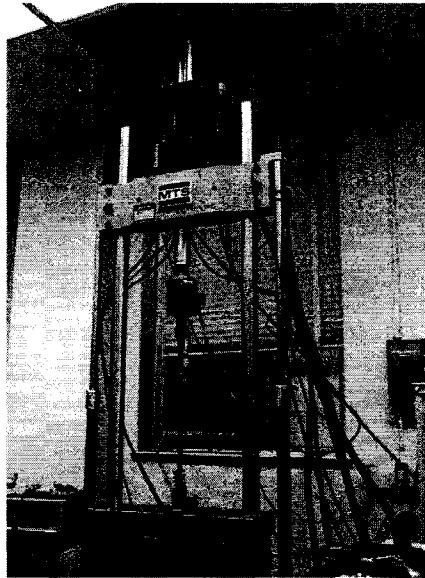


Figure 3.4. MTS multi-purpose testing machine.

Two extensometers are used in this study (see Figure 3.5). An extensometer capable of measuring a maximum of 50% elongation was used for measurement of the axial strain. A second extensometer capable of measuring a maximum of 10% elongation was used for transverse strain measurement. Rubber bands were used to ensure that the extensometers move with the coupon, especially for the transverse strain measurements.

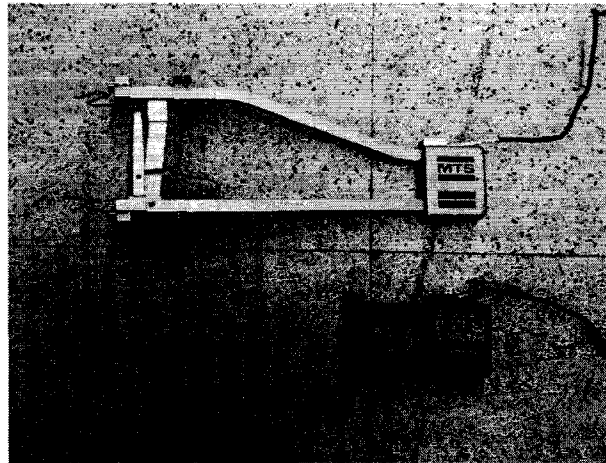


Figure 3.5. Extensometers.

3.1.2 Data Processing

A typical load/width-axial strain curve is shown in Figure 3.6. The curve can be divided into two portions. The first portion is dominated by the strength of the resin, while the second portion of the load-deformation curve is dominated by the strength of the fiber-elastomer liner. Thus, a bilinear model can be used to capture the strain curve. The vertical and horizontal coordinates of the intersection of the two lines represents the yield LPW and the yield strain, respectively. A least squares linear regression gives the following equations for the bilinear approximation as:

$$y = m_{a1}x + c_{a1} \quad (3.1)$$

$$y = m_{a2}x + c_{a2} \quad (3.2)$$

Where m_{a1} and m_{a2} are the slopes of the primary and secondary linear curves, respectively.

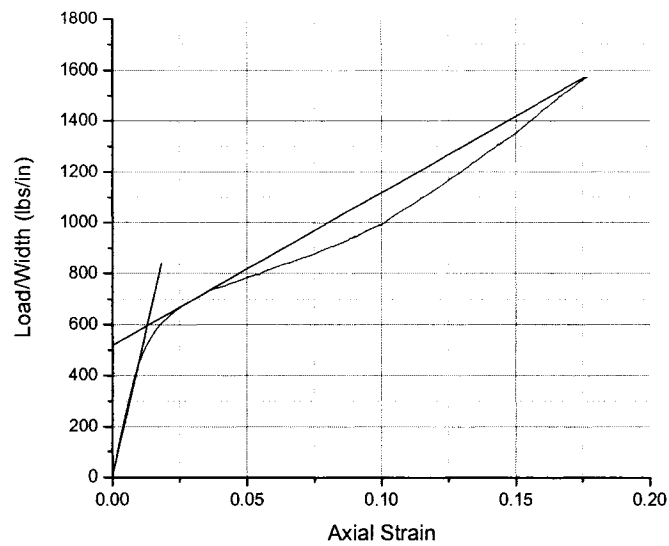


Figure 3.6. Typical load/width-axial strain curve.

According to ASTM F2207-02, the following properties are also required to be determined for the liner in the axial and transverse orientation:

- a) Yield strain (ϵ_y),
- b) Load/Width at yield (N_y),
- c) Primary modulus (E_1),
- d) Secondary modulus (E_2),
- e) Primary Poisson ratio (ν_{12_1}),
- f) Secondary Poisson ratio (ν_{12_2}), and
- g) Ultimate load/width (N_{uts})

Tables 3.1 and 3.2 provide a summary of the results from tensile tests of the axial orientation coupons. Load-deformation plots and details for each test are given in Appendix A.

Table 3.1. Axial strain results for axial orientation.

ID No	W_c (in)	t (in)	N_{uts}	ϵ_y	N_y	m_{a1}	m_{a2}
No.1	0.9282	0.1736	1574.36382	0.0125	600	48000	6025.8
No.2	0.9464	0.1716	1453.71936	0.015	600	40000	5048.3
No.3	0.9446	0.1692	1526.35528	0.015	580	38667	5689.6
No.4	0.966	0.1764	1638.93768	0.0125	600	48000	5872
No.5	0.8504	0.1788	1334.33102	0.012	540	45000	4731.5
AVG	0.92712	0.17392	1505.54143	0.0134	584	43933.4	5473.44

Table 3.2. Transverse strain results for axial orientation.

ID No	W_c (in)	t (in)	N_{uts}	ϵ_y	N_y	m_{a1}	m_{a2}
No.6	0.9524	0.1678	1407.0861	0.0045	620	137780	13169
No.7	0.95	0.1766	1361.02011	0.004	580	145000	12959
No.8	0.9256	0.1742	1620.2567	0.006	720	120000	15676
No.9	0.9456	0.174	1402.24915	0.005	640	128000	11814
No.10	0.9622	0.1798	1664.3069	0.003	600	200000	13284
AVG	0.94716	0.17448	1490.98379	0.0045	632	146156	13380.4

The primary Poisson ratio is given by:

$$v_{ah_1} = -\frac{m_{a1}}{m_{t1}} \quad (3.3)$$

The secondary Poisson ratio is given by:

$$v_{ah_2} = -\frac{m_{a2}}{m_{t2}} \quad (3.4)$$

Table 3.3 shows the Poisson ratios for the primary and secondary load ranges at the axial orientation.

Table 3.3. Poisson's ratio for axial orientation.

γ_1	γ_2
$43933.4/146156 = 0.301$	$5473.44/13380.4 = 0.409$

Tables 3.4 and 3.5 list the results from tensile tests for the hoop orientation.

Load-deformation plots and details for each test are given in Appendix A.

Table 3.4. Axial strain results for hoop orientation.

ID No	W_c (in)	t (in)	N_{uts}	ϵ_y	N_y	m_{a1}	m_{a2}
No.1	1.007	0.174	1898.55353	0.01	600	40000	17646
No.2	0.895	0.1778	2013.39106	0.011	650	45455	16613
No.3	1.0114	0.168	1570.69527	0.01	475	37500	14228
No.4	1.0128	0.1678	1223.79731	0.007	400	57143	12852
No.5	0.998	0.173	1628.89709	0.005	270	48000	16520
AVG	0.98484	0.17212	1667.067	0.0086	479	45619.6	15571.8

Table 3.5. Transverse strain results for hoop orientation.

ID No	W_c (in)	t (in)	N_{uts}	ϵ_y	N_y	m_{t1}	m_{t2}
No.6	1.0072	0.174	1501.69241	0.003	400	133330	33074
No.7	1.0708	0.17276	1400.55062	0.0025	330	132000	33319
No.8	1.0832	0.1758	1180.60137	0.0025	360	144000	37182
No.9	1.0138	0.171	1275.36901	0.0015	220	146670	51683
AVG	1.04375	0.17339	1339.553	0.002375	327.5	139000	38814.5

Table 3.6 shows the Poisson's ratios for the primary and secondary load ranges for the hoop orientation.

Table 3.6. Poisson's ratio for hoop orientation.

ν_1	ν_2
$45619.6/139000 = 0.328$	$15571.8/38814.5 = 0.40119$

The average values for the N_{uts} and ε_y were used to construct a representative load-deformation curve used in the analytical calculations and FE Modeling. The curves for the axial and hoop orientations are given in Figures 3.7 and 3.8, respectively.

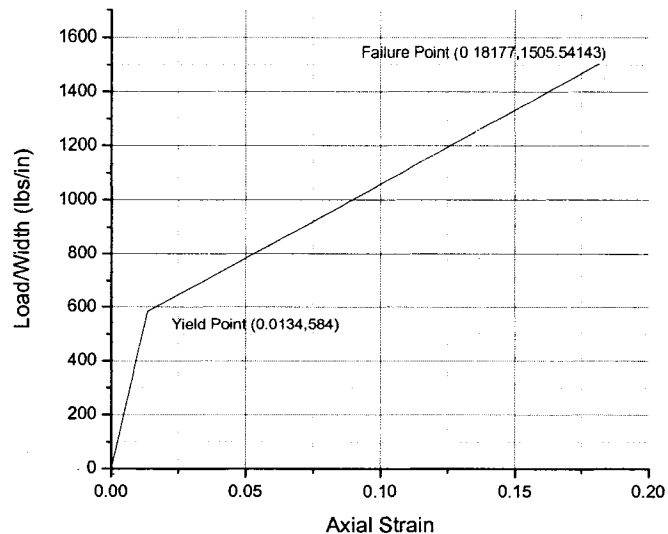


Figure 3.7. Average load/width-axial strain curve for axial orientation.

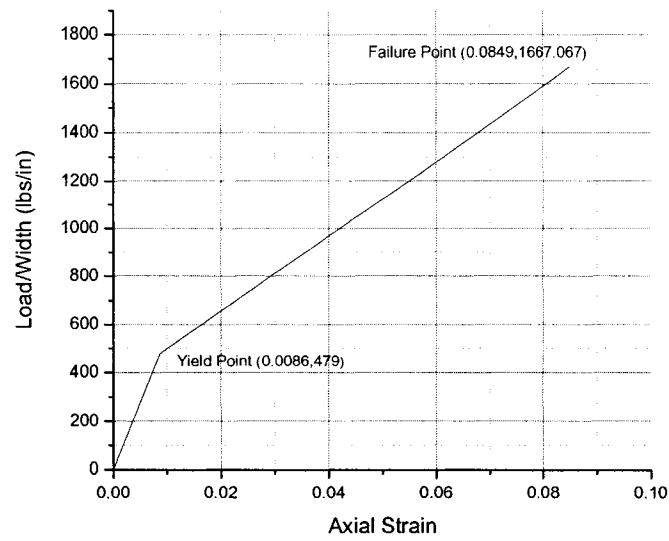


Figure 3.8. Average load/width-axial strain curve for hoop orientation.

The primary and secondary interaction compliance coefficients S_{12} and S_{21} were calculated for both orientations and are listed in Table 3.7. These interaction coefficients are used to present the interaction of two orientations.

$$S_{12-1} = \frac{-\nu_{12-1}}{E_1} \quad (3.5)$$

$$S_{12-2} = \frac{-\nu_{12-2}}{E_2} \quad (3.6)$$

$$S_{21-2} = \frac{-\nu_{21-2}}{E_2} \quad (3.7)$$

Table 3.7. Interaction compliance coefficients.

Orientation	S_{12_1}	S_{12_2}	S_{21_2}
Axial	6.85128E-6	7.47245E-5	
Hoop	7.18989E-6		2.576E-5
Average	7.02058E-6		

3.2 Analytical Calculations for Burst Pressure and Parametric Study

The material properties derived in Section 3.1 were inputted into the ASTM F2207-02 mathematical model. Detailed calculations for the burst pressure of a 1" diameter circular hole in a 7" outside diameter pipe are given in Appendix B using both the maximum stress criterion and the interactive stress criterion. As shown in Appendix B, the burst pressure is 2,445 psi using the maximum stress criterion and 2,581 psi using the interactive criterion.

In ASTM F2207-02, the defect is assumed to be uniquely characterized by two dimensions, w in the hoop direction, and L in the axial direction. For a circular defect $L=w$. The defect size is assumed to be the main factor that affects the burst pressure. Figure 3.9 and Table 3.8 show the effect of defect size on the predicted burst pressure for a 7" outside diameter host pipe. It is assumed that the defect is either square or circular (i.e. $w=L$).

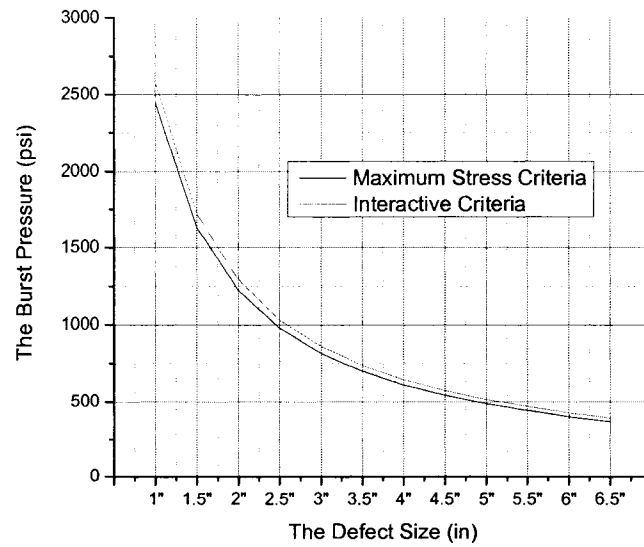


Figure 3.9. The burst pressure and the defect size.

Figure 3.9 shows the relationship between burst pressure and defect size as predicted by ASTM 2207-02 assuming a perfectly circular hole and the material properties presented earlier.

Table 3.8. Effect of defect size on burst pressure.

Defect Size	Burst Pressure (psi)	
	Maximum Stress Criteria	Interactive Criteria
1"	2,445	2,581
1.5"	1,630	1,720
2"	1,223	1,290
2.5"	978.156	1,032
3"	815.13	860.215
3.5"	698.683	737.327
4"	611.347	645.161
4.5"	543.42	573.477
5"	489.078	516.129
5.5"	444.616	469.208
6"	407.565	430.107
6.5"	376.214	397.022

While presenting a convenient tool for predicting the burst pressure of a structural liner with an unknown set of mechanical properties, ASTM 2207-02 presents several shortcomings:

a) Equations 3.8 and 3.9 give the relationships for the radius of curvature of the bulge in each direction. But equation 3.9 uses an approximation, for which its effect on the model's prediction should be quantified.

$$r_a = \frac{L^2}{8h} + \frac{h}{2} \quad (3.8)$$

$$r_h = \frac{w^2}{8h} + \frac{h}{2} \quad (3.9)$$

Figure 3.10 and 3.11 show the radius of bulge curvature in each direction, respectively. The actual equation for r_h should be as follows:

$$r_h = \frac{h + R - \sqrt{R^2 - (w/2)^2}}{2} + \frac{w^2}{8 * (h + R - \sqrt{R^2 - (w/2)^2})} \quad (3.8)$$

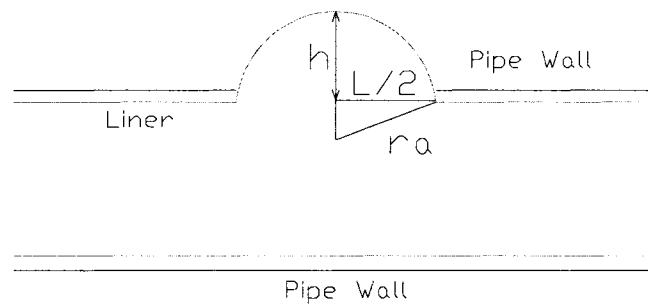


Figure 3.10. Radius of bulge curvature in the axial direction.

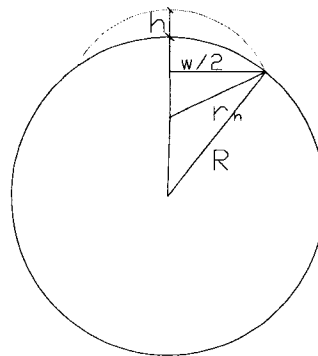


Figure 3.11. Radius of bulge curvature in the hoop direction.

Assume a 7" diameter host pipe with height of liner bulge $h = 0.5"$. Figure 3.12 shows the percentage of difference between assumed and actual value for the radius of the bulge curvature in the hoop direction.

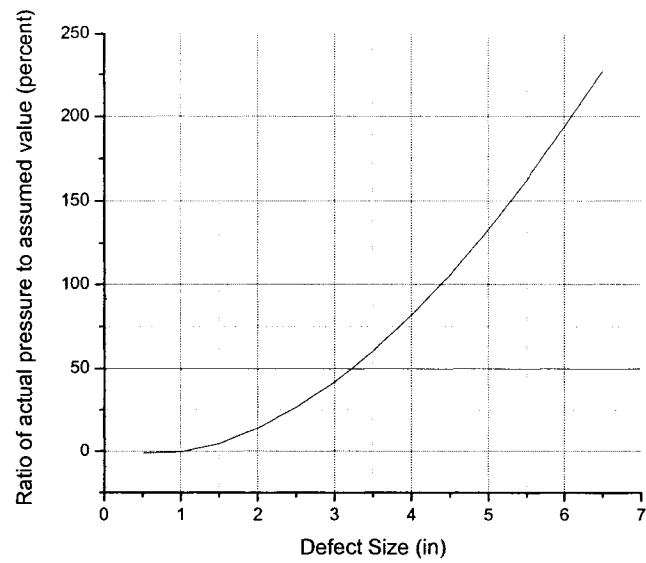


Figure 3.12. Ratio of actual pressure to assumed value (percent).

For a defect size of 6.5 inches, the assumed value is twice that of the actual value.

b) In the model, w is used as an approximation for the term $D \cdot \sin^{-1}(w/D)$.

Figure 3.13 shows that these two terms are close only when w is very small.

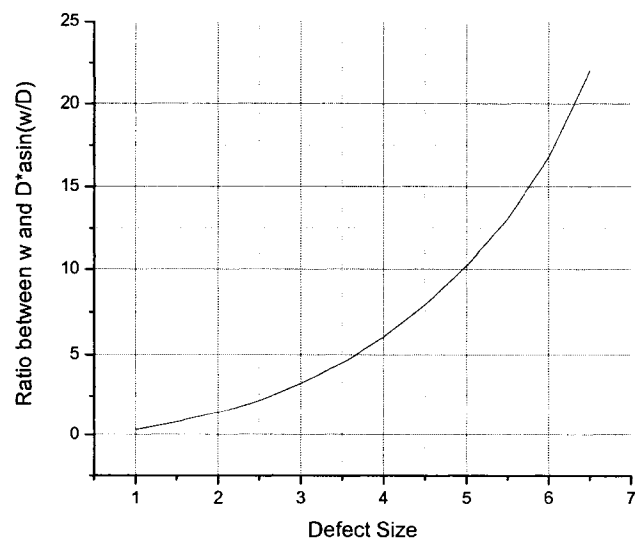


Figure 3.13. Ratio between w and $D \cdot \sin^{-1}(w/D)$.

c) When L is not equal to w , which means that the defect is neither square nor circular, no solution can be found by the current solution procedure. Thus, the effect of defect geometry needs to be accounted for.

d) The model does not account for loading history (i.e. cyclic loading and resulting accumulating plastic strain).

e) The model currently does not account for geometrical imperfections (e.g. folds), a parameter which was shown to play a crucial role in the actual burst pressure of structural liners [20,21]. This research proposed a method to account for longitudinal folds in ASTM 2207-02.

f) The combined effect of the assumptions and simplifications above can result in a burst pressure which is substantially lower than that predicted by ASTM F2207-02 [1]. Depending on the gap geometry and loading conditions, the model prediction could be 3-5 times higher than the actual burst pressure compared to a currently used typical safety factor of 2.0.

3.3 Conclusions

The mathematical method provided by ASTM F2207-02 [1] is capable of predicting the burst pressure for an ideal liner as a function of defect size. Further research, physical experimentation and finite element simulation are needed to validate the accuracy of this mathematic method for water main applications of structural liners. Specifically, the effect of defect size and shape on the burst pressure needs to be examined since the mathematical model uses several assumptions and simplifications in its calculation and is not able to consider the impact of an oval or irregular shaped defect. Moreover, the effect of load history such as the impact of cyclic loading due to water

hammer effect needs to be considered. This is particularly important due to the fact that a liner is a thermo-plastic material for which its stiffness declines under a fixed repeated or monotonic loading.

CHAPTER FOUR

FEA FOR BURST PRESSURE AND COMPARISON

4.1 Model Setup

The objective of the finite element modeling was to study the short term performance (burst pressure) of the structural liner for cases representing different defect geometries and dimensions and to compare these analyses with the results obtained using the analytical method given in ASTM F2207-02 [1] and the physical burst pressure test results.

4.1.1 Material Models

Considering the difference of Young's Modulus between cast iron and rigid PVC, both materials will be used as host pipe in finite element analysis to examine the effect of host pipe properties on the liner's performance.

The stiffness of either cast iron or rigid PVC is much greater than that of the liner. Therefore, the strain and displacement of the host pipe were considered to be negligible when compared with that of the liner. For these reasons, a linear elastic isotropic material model was used for host pipe.

In the ADINA software, a plastic bilinear model is commonly employed for such liner elastic isotropic material. A schematic shape of this material model is given in

Figure 4.1. This material model is based on von Mises yield condition and is temperature and rate independent.

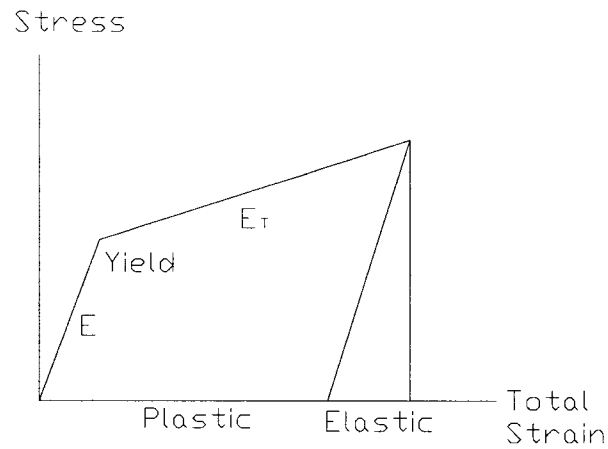


Figure 4.1. Plastic bilinear material model.

4.1.2 Basic Geometrical Parameters and Material Properties

Table 4.1 shows the basic geometrical parameters of the PVC pipe and liner. True stress and true strain values were used in this study to calculate the needed liner material parameters for the finite element analysis. Figure 4.2 displays the true stress-strain and engineering stress-strain curves derived from the uni-axial tensile tests. It can be seen that the true stress and engineering stress overlap prior to yielding. The true stress-strain curve features a stiffer response after yielding, and its maximum strain is somewhat smaller than that obtained from the engineering stress-strain curve.

Table 4.1. Basic geometrical parameters of PVC pipe and liner.

Geometrical Parameters		Value (inch)
PVC Pipe	Outside Diameter	9.05
	Pipe Thickness	0.5
	Inside Diameter	8.05
Liner Thickness		0.1734

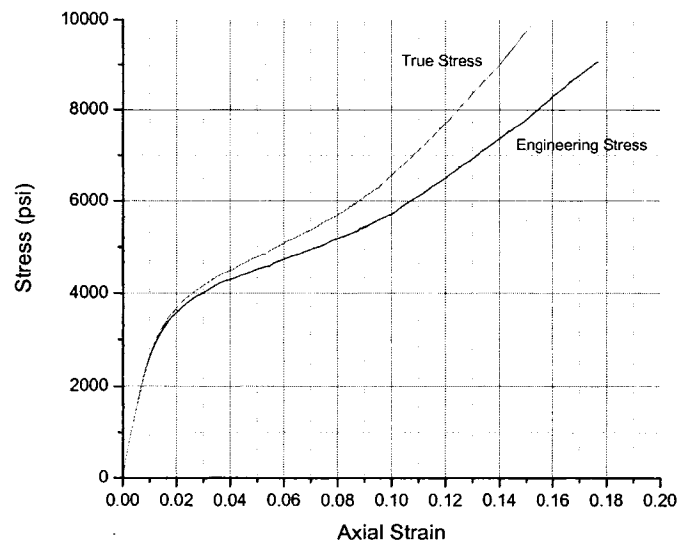


Figure 4.2. True and engineering stress-strain curves.

Idealized bilinear constitutive models were developed for the liner's axial and hoop directions based on the true stress-strain plots obtained from the experimental uni-axial tests. These are plotted in Figures 4.3 and 4.4 for the axial and hoop orientations, respectively. Key values are summarized in Table 4.2.

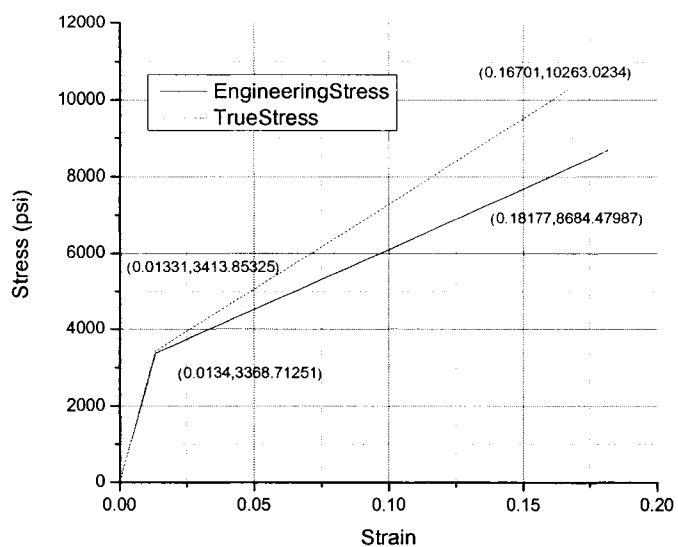


Figure 4.3. True and engineering bilinear model for axial orientation.

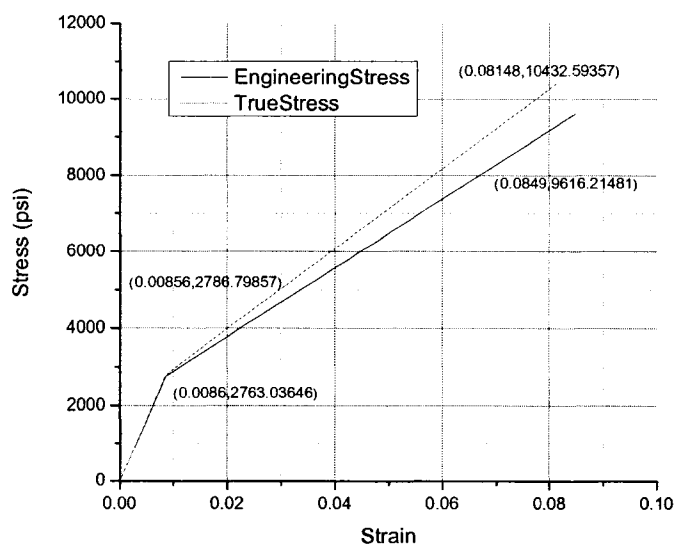


Figure 4.4. True and engineering bilinear model for hoop orientation.

Table 4.2. Material properties for liner.

	Young's Modulus (psi)	Poisson's Ratio	Initial Yield Stress (psi)	Strain Hardening Modulus (psi)	Max. Allowable Effective Plastic Strain
Axial	2.565E5	0.301	3413.85	4.456E4	0.127
Hoop	3.256E5	0.328	2786.8	1.049E5	0.049

The plastic bilinear material model used in the ADINA software assumes the material to be isotropic (i.e., the material properties are the same at all directions). A nonlinear orthotropic plastic material model is also provided in ADINA. But this orthotropic model requires the material parameters in three orthogonal directions. Considering the thickness of the liner, it is hard to get reliable test data for material properties at the direction orthogonal to the liner surface. Thus, a plastic bilinear material model was chosen for the liner material and the material properties at the axial and hoop directions were used to populate this material model. Material properties used as input to the material constitutive model into ADINA are listed in Table 4.3. All parameters for PVC were measured and calculated from Figure 4.5.

Table 4.3. Material properties used for ADINA material models.

	Cast Iron	PVC	Liner
Material Model	Elastic	Plastic	Plastic
	Isotropic	Bilinear	Bilinear
Young's Modulus	14E6Psi	4.85E5Psi	2.565E5Psi
Poisson's Ratio	0.2273	0.42	0.301
Initial Yield Stress	N/A	7760Psi	3413.85Psi
Strain Hardening Modulus	N/A	11840Psi	4.456E4Psi
Max. Allowable Effective Plastic Strain	N/A	0.0478	0.127

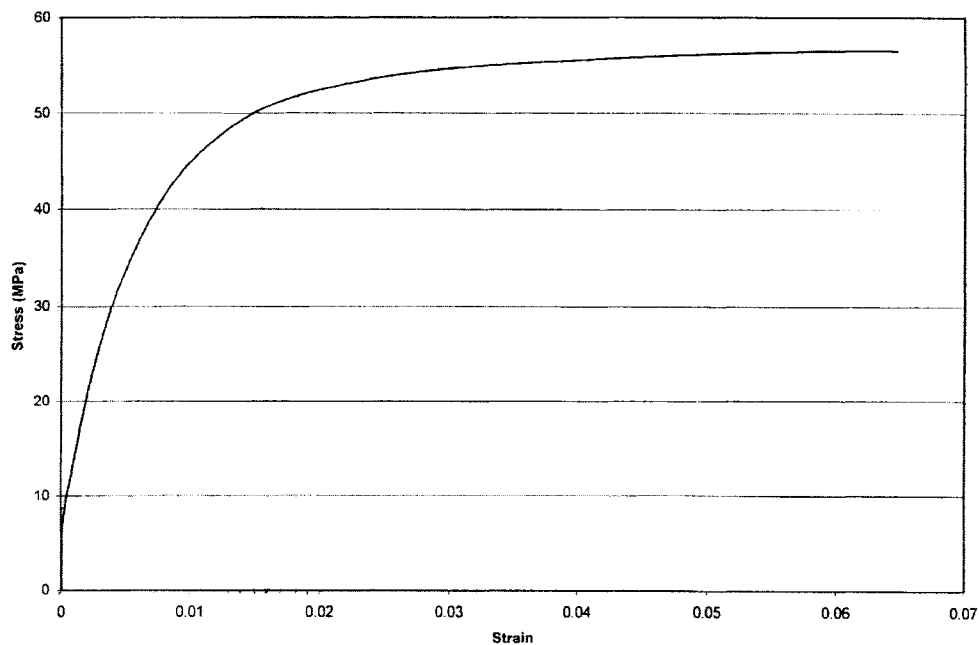


Figure 4.5. Stress-strain curve for class 200 "Blue Brute" PVC pipe.

4.1.3 Element Selection

As discussed in Chapter Two, a 3-D model is needed to simulate the stress and strain distributions, because a non-linear geometrical and material behavior is expected to take place. From the uni-axial tensile test results, described in Chapter Three, it is clear that the liner exhibits a non-linear behavior in the load/width versus strain curve (Figure 3.6). The maximum strain at failure point is well above 10%, which means that a large strain analysis is required.

The utilization of 3-D solid elements is required due to the bulging shape of the liner in the opening area. A large displacement kinematics formulation was chosen because of the large deformation that takes place as the liner bulges out of the opening in the host pipe. As mentioned earlier, the strain at failure is approximately 16.7%, which also suggests that a large strain kinematics formulation is required.

Displacement-based finite element analysis is a procedure that is widely used in such applications. But for the analysis of nearly incompressible media and the analysis of plates and shells, the pure displacement-based finite element procedure is not sufficiently effective. For incompressible media, mixed interpolation, an approach which can be thought of as a special use of the Hu-Washizu variational principal, is efficient [22]. Thus, a mixed interpolation analysis was used in the analysis reported herein.

4.1.4 Contact Conditions and Boundary Conditions

Contact conditions can be specified in ADINA to model the contact behavior between solid elements (2-D and 3-D solids) and/or structural elements (truss, beam, iso-beam or axisymmetric shell, plate, shell and pipe elements).

Contact surfaces are defined as surfaces that are initially in contact or anticipated to come into contact during the response solution. In this study, contact conditions exist between the surface of the liner and the host pipe. The contact between the liner and the host pipe is assumed to be frictionless ($\mu = 0$). The initial penetrations of the nodes are eliminated in the first loading step. Both end surfaces of host pipe and liner are fixed, which means that all degrees of freedom at those surfaces are limited.

4.1.5 Failure Criteria

Many theories have been proposed to predict failure of materials. Considering the plastic phase presented by the liner in this study, the theory used to predict failure of the liner is based on the accumulated plastic strain. Rupture is assumed to occur when the accumulated plastic strain in the complex stress state reaches the maximum plastic strain in the uni-directional tensile test. When the accumulated plastic strain reaches this value in any integration point of an element, that element is considered 'dead' and is removed from the analysis [4]. The load corresponding to the dead element is distributed to neighboring elements. Failure is assumed to be the pressure corresponding to the last load step that resulted in the convergence of the FE model.

4.2 Parameters Study

The burst pressure of a liner is determined by several factors namely: a) the material properties of the host pipe; b) the shape of the gap in the host pipe; c) the gap size; and d) the liner properties. The ASTM method [1] considers the last two factors, but does not consider the effects of the first two factors. Thus, the effects of the host pipe mechanical properties and the shape of the gap in the host pipe require further examination. Finally, the ASTM model considers only monotonically increasing loading

and neglects the effect of cyclic loading. Thus, a method for computing the equivalent monotonic loads of a given number of cyclic loads is needed.

Finite element methods are widely used in many engineering areas. Finite element analysis removes many simplifications and assumptions used in many analytical analyses, and thus can be used to obtain more precise predictions. The reliability of a finite element analysis has to be considered before conducting any parametric study by comparing its predictions with data obtained from experimental testing and analytical solutions. Finite-element solutions will converge to the exact solution of a perfect analytical model as the element size approaches zero. However, computational time for this case will approach infinity. In practice, a mesh size is selected that provides a compromise between accuracy and computational time. The balance between the solution precision and run time is a function of the capacity of the computing system and model complexity. Considering practical engineering conditions, a 1.5" diameter defect is normally the lowest limit which could begin to compromise the integrity of a re-lined water main (pressure range 60~130psi). Thus, a study was undertaken to determine the appropriate mesh size for a PVC host pipe with a 1.5" diameter circular opening.

Table 4.4 presents the liner burst pressure predicted by the FE model for a mesh size ranging from 0.15" to 0.45". Figures 4.6 and 4.7 reveal that as the mesh size is refined, the predicted burst pressure value declines but the differences between the predicted values also become smaller. Also, for a mesh size of 0.25" or smaller, the predicted burst pressure is nearly constant.

Table 4.4. Liner burst pressure result for 1.5 inch defect with different mesh sizes.

Liner Burst Pressure (psi)	Mesh Size (inch)					
	0.15	0.25	0.3	0.35	0.45	0.5
	750	765	800	840	870	885
Difference (psi)		15	35	40	30	15
Percentage of Difference (%)		2	4.575	5	3.571	1.724

According to the results listed in Table 4.4, the percentage difference drops to 2% when the mesh size goes down to 0.25". Considering that a 1.5" diameter defect is the smallest defect size to be considered, a 0.25" mesh size was chosen as a reasonable mesh size for the analysis.

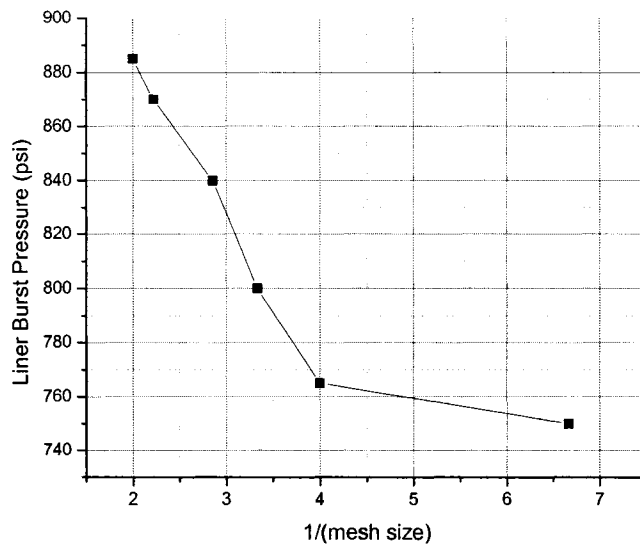


Figure 4.6. Liner burst pressure varies with mesh size.

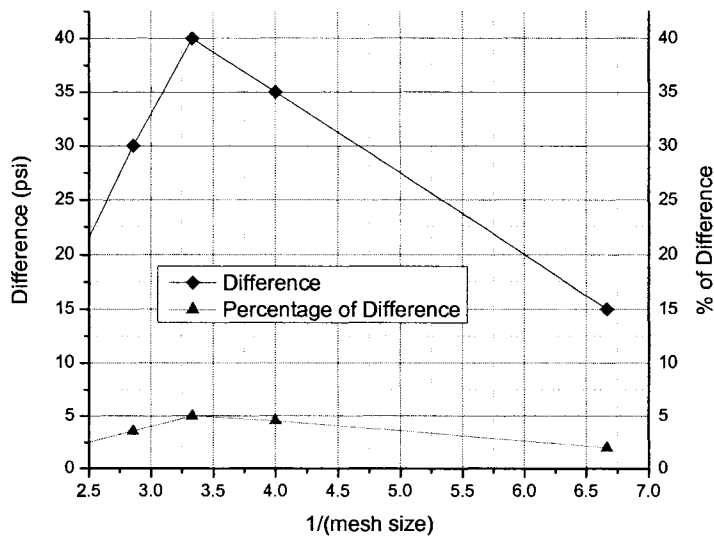


Figure 4.7. Burst pressure difference with mesh size.

Mesh sizes of 0.3" and 0.5" were chosen to compare the burst pressure results for circular defects ranging in diameter from 0.5" to 8" on an 8" internal diameter (9.2" O.D.) PVC host pipe. Table 4.5 and Figure 4.8 present the results for the two mesh sizes.

Table 4.5. Burst pressure results for mesh sizes of 0.3" and 0.5".

Gap diameter	0.5"	1.0"	1.5"	2"	2.5"	3"	4"	5"	6"	7"	8"
0.3Mesh (psi)	1120	950	765	710	685	600	535	400	455	330	300
0.5Mesh (psi)	1220	1060	885	760	680	620	450	420	405	325	385

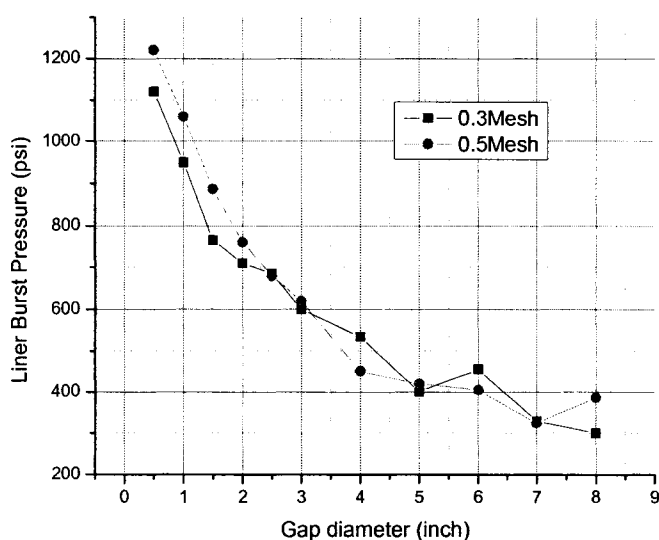


Figure 4.8. Burst pressure results for two mesh sizes.

Table 4.5 and Figure 4.8 display the predicted burst pressure for two mesh sizes, namely 0.3" and 0.5". It can be seen that the predictions made using the two mesh sizes are very close. Considering accuracy and time requirements, the 0.3" mesh was used for defects from 0.5" to 4", while the 0.5" mesh was used for defects from 5" to 8".

4.2.1 Host Pipe Material Properties

Two different materials, cast iron and PVC, were used for the host pipe. Table 4.6 and Figure 4.9 show the burst pressures for two different host pipes with circular defects from 0.5" diameter to 8" diameter. The geometrical parameters for the host pipe and liner are listed in Table 5.1.

From Table 4.6 and Figure 4.9, it can be seen that the predicted liner burst pressures for cast iron and PVC host pipes are quite different when the defect size is relatively small, but the predictions converge as the defect size grows larger.

The host pipe and liner act together to resist the internal pressure, with the host pipe providing confinement to the liner. As the gap size increases, the confinement provided by the host pipe decreases and the internal pressure is resisted mainly by the liner in the gap area. From Table 4.6, Figure 4.9 and Figure 4.10, it can be seen that for a gap size equal to or larger than 4", the internal pressure is mainly supported by the liner and the burst pressure is dominated by the tensile and bending properties of the liner. For a defect size of less than 4", the confinement provided by host pipe contributes to the ability of the liner to resist the internal pressure. This contribution increases significantly as the defect size decreases.

Table 4.6. Burst pressures with circular defects for two host pipes.

Defect Size (inch)	Liner Burst Pressure (psi)		Liner Displacement Magnitude (inch)	
	Cast Iron	PVC	Cast Iron	PVC
0.5	N/A	1120	N/A	0.08015
1	N/A	950	N/A	0.08962
1.5	1470	765	0.1672	0.1319
2	960	710	0.1669	0.2077
2.5	840	685	0.1973	0.2956
3	740	600	0.1324	0.3612
4	425	450	0.1865	0.2455
5	395	420	0.2803	0.3368
6	400	405	0.4043	0.4298
7	365	325	0.4279	0.3620
8	385	385	0.5253	0.5277

N/A: Not Available.

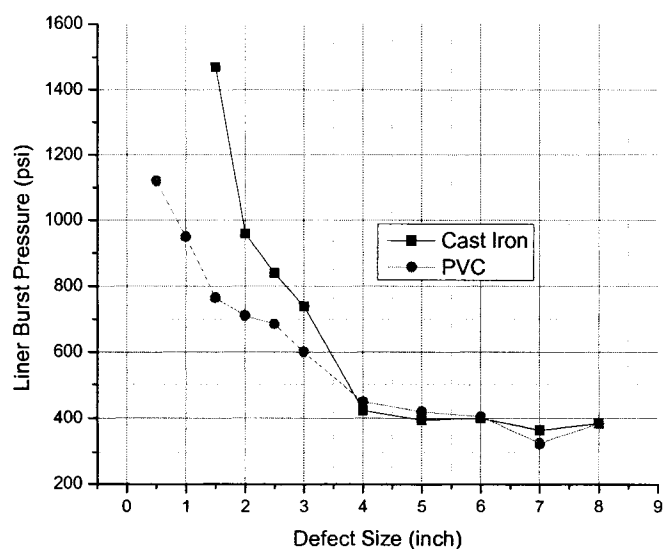


Figure 4.9. Liner burst pressure for cast iron and PVC host pipe with different defect sizes.

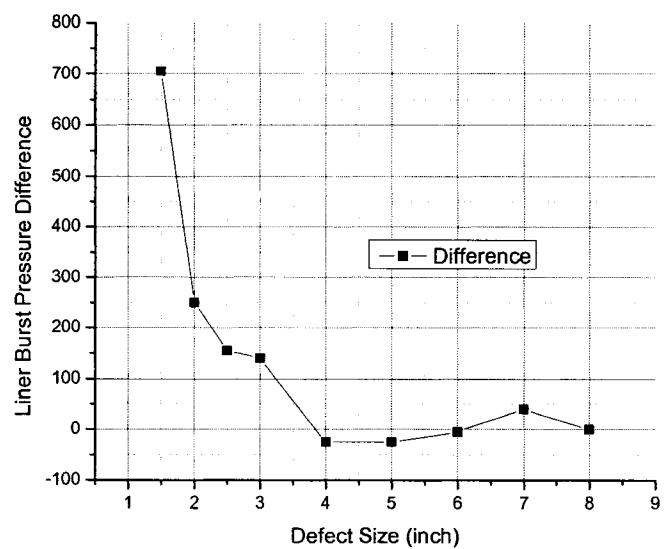


Figure 4.10. Simulated liner burst pressure difference between PVC and cast iron host pipes.

Figures 4.11 and 4.12 display (with same magnification) the deformation of the liner under burst pressure for a 2" circular defect for the cases of cast iron and PVC host pipes, respectively.

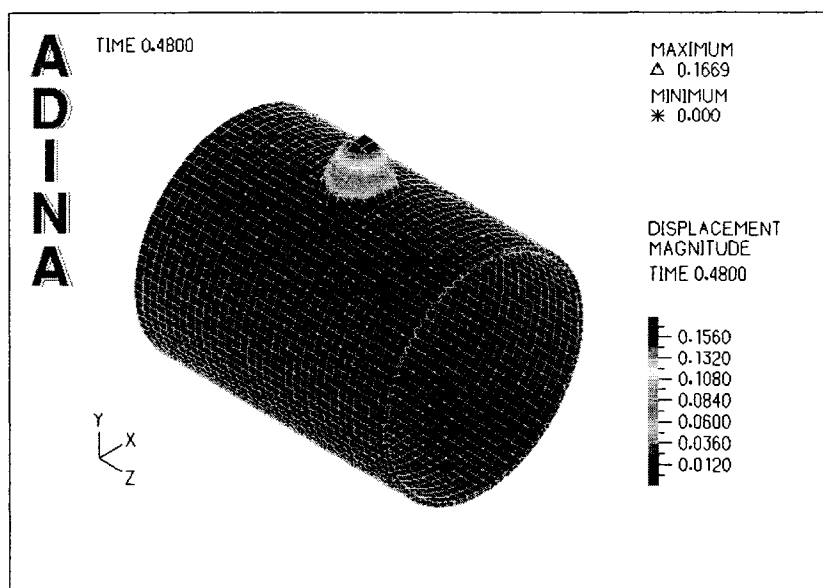


Figure 4.11. Magnified deformation for a 2" diameter defect in a cast iron host pipe.

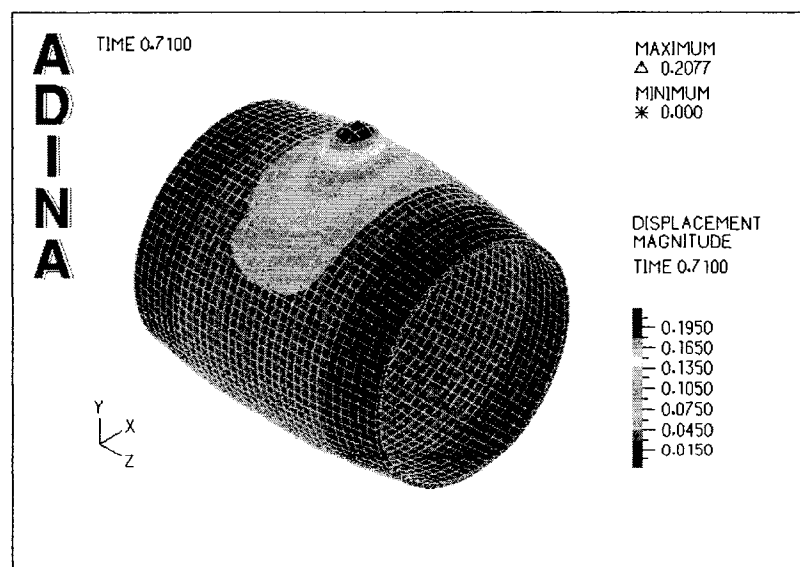


Figure 4.12. Magnified deformation for a 2" diameter defect in a PVC host pipe.

Comparing Figures 4.11 and 4.12, it can be seen that the PVC host pipe itself expands under the internal pressure together with the liner as the pressure increases. A cast iron host pipe, which is a much more rigid material, will not expand with the liner, and will provide significantly stiffer confinement to the liner as the internal pressure increases.

4.2.2 Shape of Gap in Host Pipe

Stress concentration is an important phenomenon in the mechanics of materials. When a stress concentration occurs, the area under consideration experiences higher than average local stresses. The types of discontinuities that cause stress concentrations are: cracks, sharp corners, holes and narrowing of the object. Cracks represent one of the worst types of stress concentration forms. High local stresses can cause the object to fail more easily than its overall size suggests [2]. Design procedures commonly attempt to avoid or reduce stress concentrations. This section focuses on examining the manner in which different defect shapes affect the liner burst pressure and the change in the burst pressure due to stress concentration, defect area and defect orientation.

The burst pressures listed in Table 4.7 show that different defect (gap) shapes with the same cross-sectional area have different burst pressures. With a cross-sectional area of 9 square inches, rectangle and ellipse defect shapes with the long axes in the pipe axial direction have a significantly lower burst pressure than a circular defect. Figures 4.13 and 4.14 show the difference between rectangular defects in two different orientations. When the rectangular defect has its longer dimension in the axial direction, the stress concentration is obvious and the liner burst pressure is significantly less than

that of other geometrical shapes and is also significantly lower than that of same rectangular defect in the hoop orientation.

Table 4.7. Burst pressures with different shape defects for two host pipes.

Defect Shape (inch)	Liner Burst Pressure(psi)	Liner Displacement Magnitude(inch)
Square (3*3)	525	0.3356
Rectangle (1.732*5.196) Axial Direction	395	0.2455
Rectangle (1.732*5.196) Hoop Direction	700	0.3383
Ellipse (2.93;0.977) Axial Direction	400	0.2449
Ellipse (2.93;0.977) Hoop Direction	815	0.4432
Circle (1.693)	760	0.1512

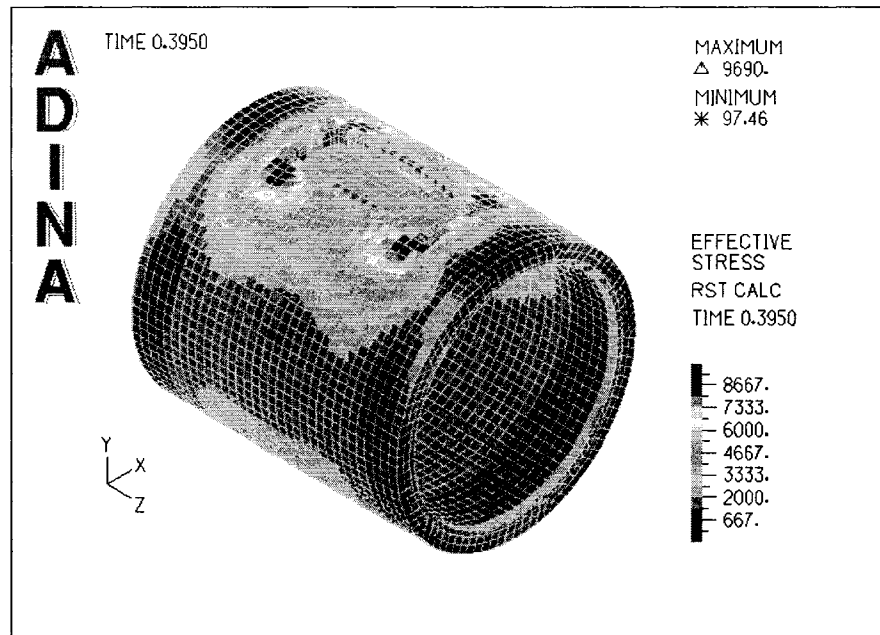


Figure 4.13. Rectangle defect (1.732*5.196) in the axial direction.

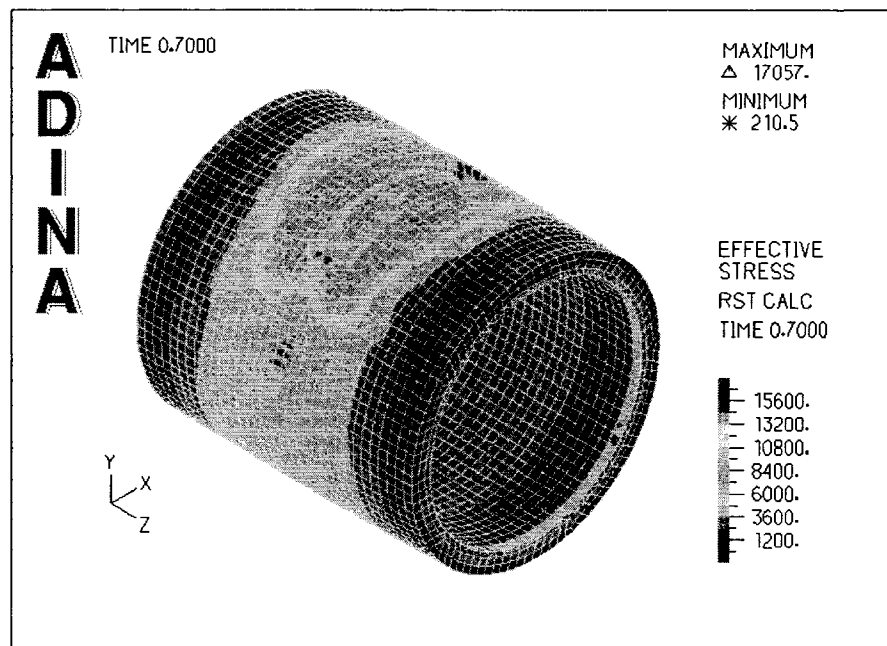


Figure 4.14. Rectangle defect in the hoop direction.

Two simple models can be used to demonstrate this phenomenon. A straight plate under pressure is compared with a curved plate under the same pressure. The displacement at the center point for the straight plate is much larger than that of the curved plate. This means that it is easier for the liner to bulge out of a gap in the axial direction than from a gap in the hoop direction. When the liner bulges out through the gap in the axial direction, it pushes against the corners of the host pipe, causing a stress concentration. For the defect in the hoop direction, the deformation is significantly lower. Thus, the development of stress concentration is delayed and less significantly impacts the liner burst pressure. Figures 4.15 and 4.16 display the deformation for these two simple models.

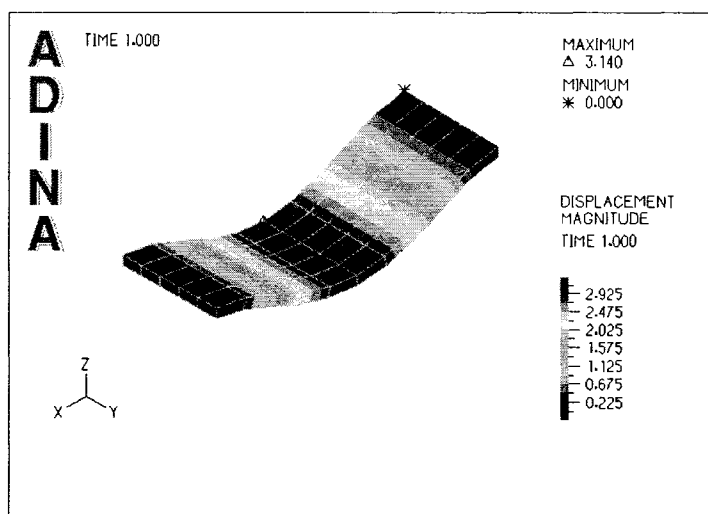


Figure 4.15. Deformation of a straight plate under pressure.

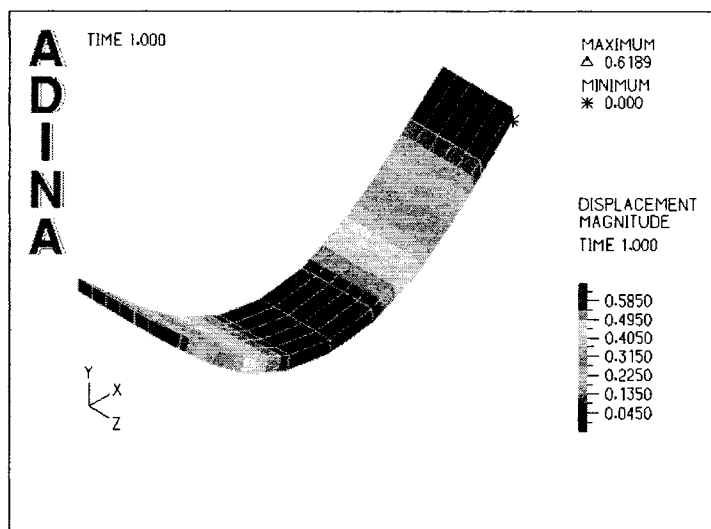


Figure 4.16. Deformation of a curved plate under pressure.

4.3 Results Comparisons between Different Methods

Liner burst pressures for various circular defect sizes and different defect shapes were calculated using the ADINA finite element software. These results are compared with calculations made using ASTM 2207-02, and are summarized in Tables 4.8 and 4.9.

Table 4.8. Burst pressures for circular defects: comparison between finite element analysis and ASTM predictions.

Defect Size (inch)	Liner Burst Pressure (psi)			
	FEA Result		ASTM 2207-02 Result	
	Cast Iron	PVC	Max	Interactive
0.5	N/A	1120	4891	5161
1.0	N/A	950	2445	2581
1.5	1470	765	1630	1720
2	960	710	1223	1290
2.5	840	685	978	1032
3	740	600	815	860
4	425	450	611	645
5	395	420	489	516
6	400	405	407	430
7	365	325	349	368
8	385	385	305	322

Table 4.9. Burst pressures with different defect shapes: Comparison between finite element analysis and ASTM predictions.

Defect Shape	Liner Burst Pressure (psi)		
	FEA Result	ASTM Result	
		Max	Interactive
Square (3*3)	525	815.13	860.215
Rectangle (1.732*5.196) Axial Direction	395	N/A	N/A
Rectangle (1.732*5.196) Hoop Direction	700	N/A	N/A
Ellipse (2.93;0.977) Axial Direction	400	N/A	N/A
Ellipse (2.93;0.977) Hoop Direction	815	N/A	N/A
Circle (1.693)	760	1444	1524

N/A: Not available

The comparison between finite element analysis results and ASTM 2207-02 predicted results are presented in Figure 4.17

. It's clear that the difference increases as the defect size decreases.

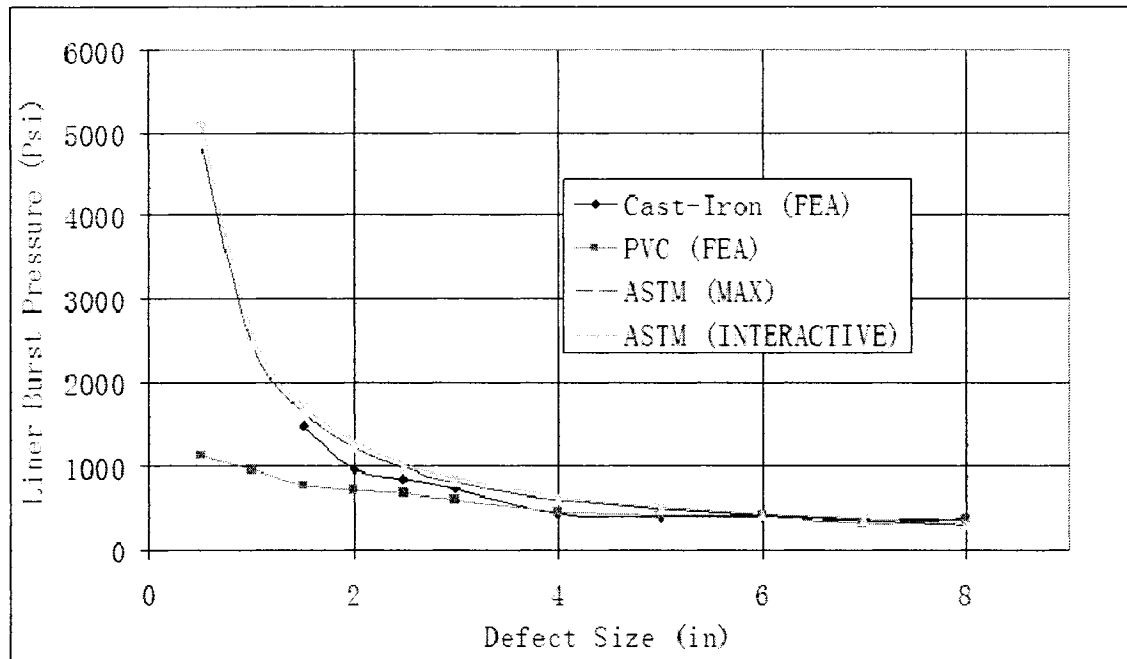


Figure 4.17. FEA results and ASTM 2207-02 predicted values *versus* defect diameter.

To check the failure modes for different defect geometries, it is necessary to check the strain distribution in the liner at the failure point. The strain distribution for the cast-iron host pipe with a 1.5 inch and 6 inch circular defect, a 3×3 inch square defect and a 1.732×5.1963 inch rectangular defect are presented respectively from Figure 4.18 to Figure 4.21.

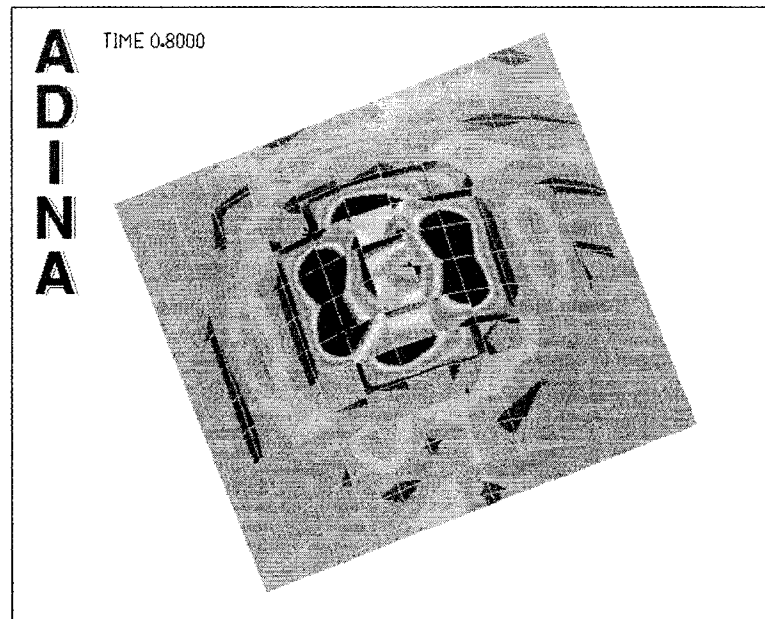


Figure 4.18. Strain distribution for a cast-iron host pipe with a 1.5 inch circular defect.

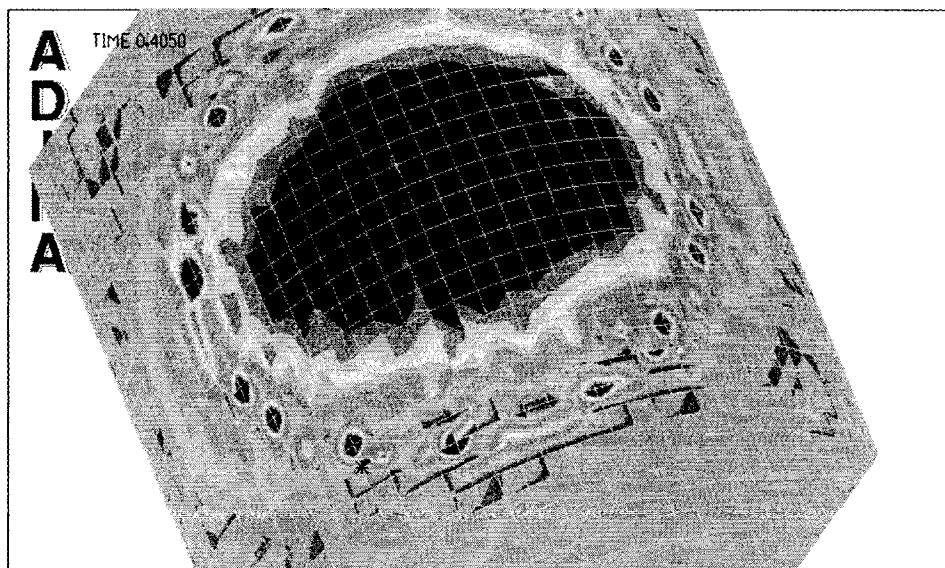


Figure 4.19. Strain distribution for a cast-iron host pipe with a 6 inch circular defect.

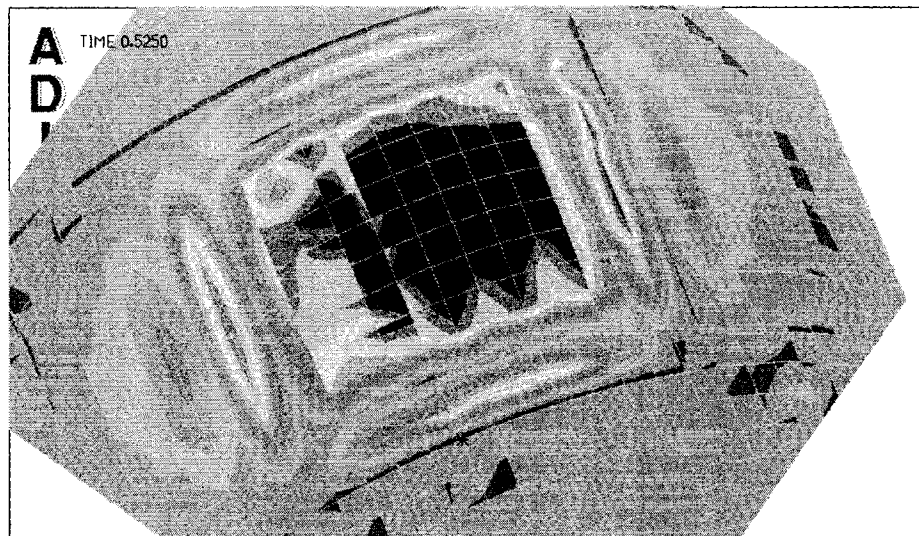


Figure 4.20. Strain distribution for a cast-iron host pipe with a 3×3 inch square defect.

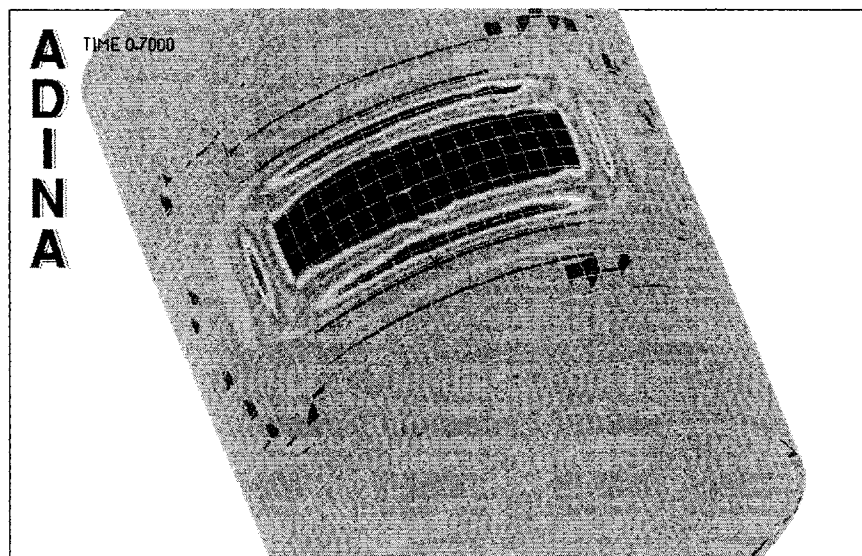


Figure 4.21. Strain distribution for a cast-iron host pipe with a 1.732×5.1963 inch rectangular defect.

From the strain distribution graphs, it's clear that, for circular defects, the failure mode changes from the center of a large area defect to direct (“punching”) shear failure

for a small area defect. Comparing the strain distribution of the different defect geometries, stress concentrations do show on the perimeter of defect. This is in keeping with the experimental observations reported by Hall et al. [2].

4.4 Finite Element Model Verification and Conclusions

For model verification purpose, a cast-iron host pipe with an 8" long and 6" wide ellipse defect was simulated in ADINA to compare with the experimental liner burst pressure result. The simulation result is shown in Figure 4.22.

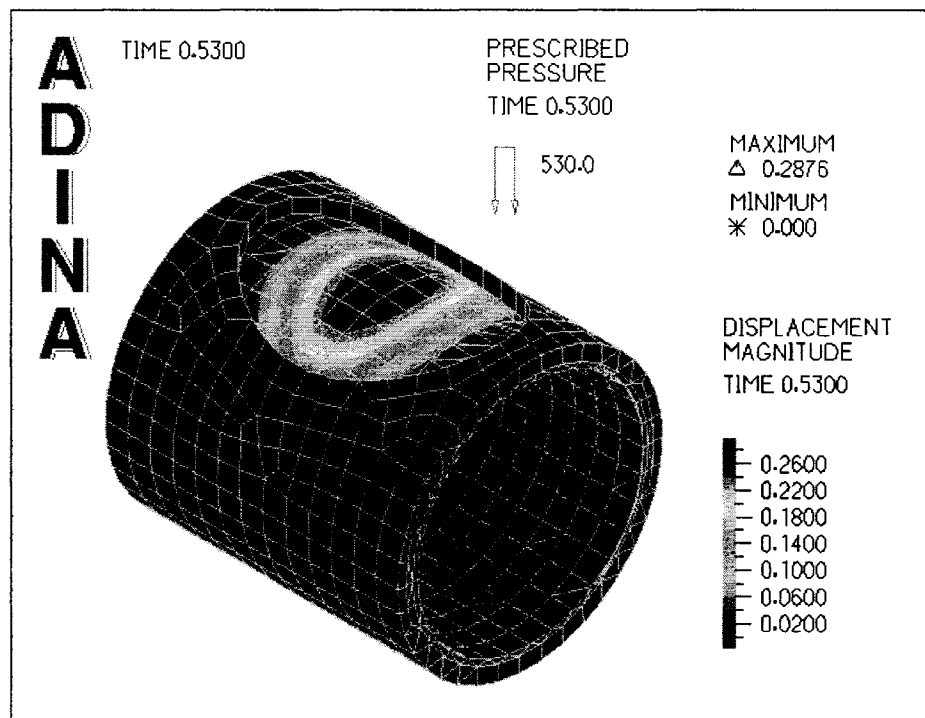


Figure 4.22. Cast-iron host pipe with 8" long and 6" wide defect.

The burst pressure from the finite element analysis is 530 psi and the displacement at the center of the defect is 0.288". The liner burst pressure test results for a cast-iron host pipe with a 6" by 8" defect was reported by Allouche et al (2005) and

Jaganathan et al (2007). The specimen was pressurized in 50 psi increments, with the pressure held at each pressure increment for a minimum of 5 minutes as per the ASTM D3139 leakage test. The test was discontinued at 550 psi due to the difficulties in sealing the bulkheads and the realization that the liner was potentially reaching its ultimate plastic strain and a consequently catastrophic failure. The maximum deformation recorded by the LVDTs at 550 psi was approximately 0.295 inches (7.5 mm). The results from the finite element analysis and the experimental observations are listed in Table 4.10. It can be concluded that the predictions made by the finite element analysis closely correspond to the observed experimental data for the particular experimental test considered.

Table 4.10. Comparison of experimental and simulated burst pressures for a 6 inch x 8 inch elliptical defect.

	Experimental Results	Finite Element Results	Difference
Liner Burst Pressure	550psi	530psi	3.6%
Displacement at Center	0.295inch	0.2876inch	2.5%

CHAPTER FIVE

INFLUENCE OF CREEP EFFECT ON LINER LONG TERM PERFORMANCE

Material deformation is called creep when it occurs as a result of long-term exposure to a steady level of stress that is lower than the yield or ultimate strength of the material. The rate of creep is a function of the material properties, temperature and the magnitude of the externally applied load. Depending on the magnitude of the applied load and its duration, the deformation may become so large that a component can no longer perform its function. Creep does not immediately occur after sudden loading but is the accumulation of plastic strain over a long time period, which could ultimately result in failure of the material under an external load significantly lower than its ultimate short-term capacity. This makes creep deformation a "time-dependent" phenomenon. Creep is usually of concern to engineers when evaluating components that operate under high stresses and/or elevated temperatures over long periods of time.

Under a given level of stress, the strain rate is commonly divided into two regions. The first region, known as primary creep, is characterized by a rapid decline in the strain rate. The strain rate eventually levels off and becomes nearly constant. This is known as secondary, or steady-state, creep. The term "creep strain rate" typically refers to the rate during this secondary stage.

5.1 Creep Experiment

A custom test apparatus, designed and constructed by Hong Lin in 1995 [5], was used for the creep testing. The device is shown in Figure 5.1. The system is able to apply a constant uniform tensile force on the specimen. Both ends of the specimen were clamped in the grips and a weight was applied to the specimen through a lever. The ratio of the cantilever arm to lever arm was 7.0.

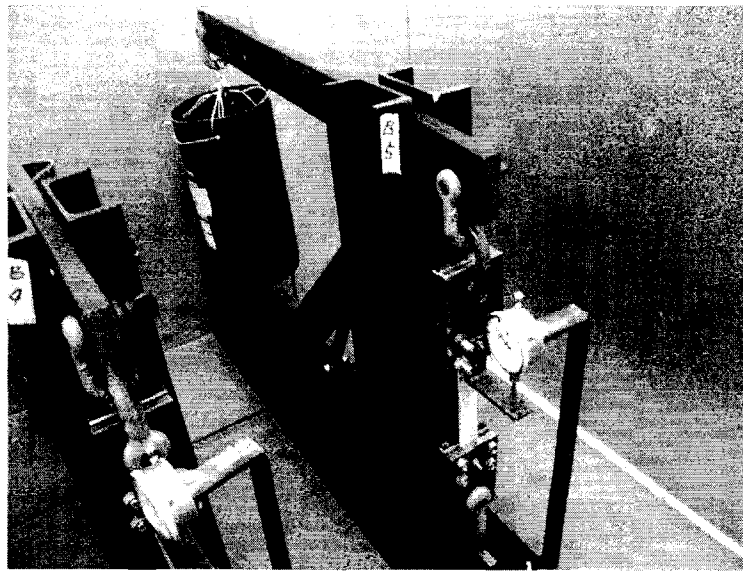


Figure 5.1. Tension loading device.

The test specimens were prepared from “Aqua Pipe®” liner material removed from a 70 year-old 6” diameter cast-iron water main which was relined in 2003 in the City of Hamilton, Ontario, Canada. Following the relining project, several 1.2m long segments of the host pipe were exhumed and delivered to Louisiana Tech University for testing.

The curved liner material was removed from the pipe segment and cut into rectangular shaped specimens for further treatment. The liner material had been cured in

a circular geometry. Thus, to straighten the specimens a small environmental chamber was used to heat the liner sections while pressure was applied simultaneously to “straighten” the specimens. A 48-hour treatment in the heat chamber was applied before commencement of the creep test.

According to ASTM D638-00 and ASTM D2990-95, five stress levels were chosen for the creep test and two specimens were prepared for each level. The dimensions of all specimens are listed in Table 5.1.

Table 5.1. Dimensions of creep test specimens.

	Width	Length	Thickness
A1	0.9718	4.5	0.17336
A2	0.989	4.5	0.17336
A3	N/A	4.5	0.17336
A4	0.9914	4.5	0.17336
A5	0.9922	4.5	0.17336
B1	0.9674	4.5	0.17336
B2	0.9776	4.5	0.17336
B3	0.9742	4.5	0.17336
B4	0.9708	4.5	0.17336
B5	0.9728	4.5	0.17336

Experimental procedures followed ASTM D2290-95. The load was applied rapidly and smoothly to the specimen in 1 to 5 seconds. Deformation measurements were taken in accordance with the following time schedule: 1, 6, 12, 30 minutes; 1, 2, 5, 20 hours; then every 24 hours for 500 hours; every 48 hours from 500 to 1000 hours; every 96 hours from 1000 to 3500 hours and every week from 3500 to 5000 hours.

The applied load and corresponding stress level for each specimen are listed in Table 5.2.

Table 5.2. Applied load and stress level for each specimen.

	Cross Section Area	Applied Load (lbs)	Stress Level (psi)	Percentage of Yield Stress (%)
A1	0.168471	48.1285	285.678	8.368
A2	0.171453	126.8785	740.019	21.677
A3	N/A	201.2535	N/A	N/A
A4	0.171869	270.375	1573.146	46.081
A5	0.172008	350.875	2039.876	59.753
B1	0.167708	48.566	289.587	8.483
B2	0.169477	125.1285	738.321	21.627
B3	0.168887	200.3785	1186.465	34.754
B4	0.168298	262.5	1559.733	45.688
B5	0.168645	342.5625	2031.264	59.501

Test results and strain curves for all specimens are given in Appendix C. Figure 5.2 depicted a typical creep strain vs. time curve (for specimen B5).

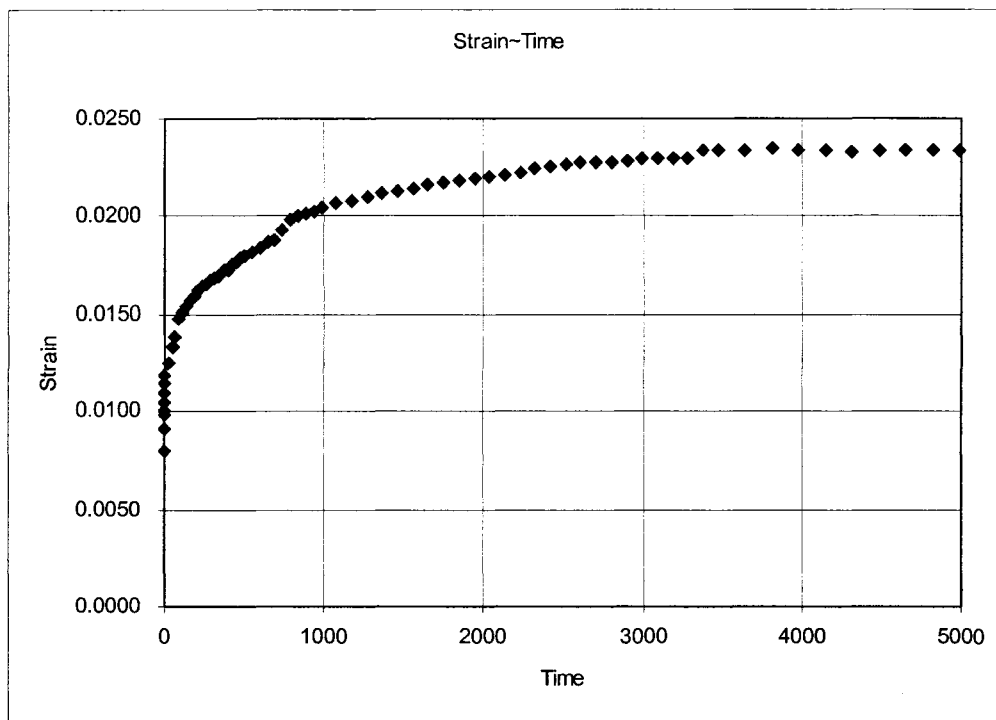


Figure 5.2. Creep strain curve for specimen B5.

5.2 Liner Creep Variation for FE Modeling

5.2.1 Creep Material Models

ADINA's thermo-elasto-plasticity and creep material model is the appropriate material model to be used for the liner in this study. The thermo-elasto-plasticity and creep models include the following features [3]:

- Thermal strains, ${}^t e_{rs}^{TH}$
- Time-independent plastic strains, ${}^t e_{rs}^P$
- Time-dependent creep strains, ${}^t e_{rs}^C$

The constitutive relation used by the model is expressed mathematically as followed:

$${}^t \sigma_{ij} = {}^t C_{ijrs}^E ({}^t e_{rs} - {}^t e_{rs}^P - {}^t e_{rs}^C - {}^t e_{rs}^{TH}) \quad (5.1)$$

Where ${}^t \sigma_{ij}$ is the stress tensor at time t and ${}^t C_{ijrs}^E$ is the elasticity tensor at the temperature corresponding to time t . The tensor ${}^t C_{ijrs}^E$ can be expressed in terms of Young's modulus ${}^t E$ and Poisson's ratio ${}^t \nu$, both of which are temperature dependent.

The thermal strain is calculated from the prescribed nodal point temperature with the coefficient of thermal expansion being temperature dependent. In this research, effect of temperature change was not considered and the creep tests were performed in an environmental chamber under a constant temperature of $70^{\circ} \pm 1$ C.

The plastic strains were calculated using von Mises plasticity model with temperature-dependent material parameters (Young's modulus, strain hardening modulus, Poisson's ratio, yield stress, etc...). Hence, the yield function in isotropic hardening is expressed as:

$${}^t f_y = \frac{1}{2} {}^t s \cdot {}^t s - \frac{1}{3} {}^t \sigma_{yv}^2 \quad (5.2)$$

while in kinematic hardening it is expressed as:

$${}^t f_y = \frac{1}{2} ({}^t s - {}^t \alpha) \cdot ({}^t s - {}^t \alpha) - \frac{1}{3} {}^t \sigma_{yv}^2 \quad (5.3)$$

In ADINA, The effective creep strain is calculated using one of the following Creep Laws:

Power Creep Law (Creep Law 1 [3]):

$${}^t \bar{\epsilon}^C = a_0 {}^t \sigma^{a_1} t^{a_2} \quad (5.4)$$

in which a_0 , a_1 , a_2 are material constants.

Exponential Creep Law (Creep Law 2 [3]):

$${}^t \bar{\epsilon}^C = F(1 - e^{-Rt}) + Gt \quad (5.5)$$

with

$$F = a_0 e^{a_1 {}^t \sigma}; \quad R = a_2 \left(\frac{{}^t \sigma}{a_3} \right)^{a_4}; \quad G = a_5 e^{a_6 {}^t \sigma}$$

in which a_0 to a_6 are material constants; or the eight-parameter Creep Law (Creep Law 3 [3]):

$${}^t \bar{\epsilon}^C = S \cdot T \cdot e^{-H} \quad (5.6)$$

with

$$S = a_0 {}^t \sigma^{a_1}; \quad T = t^{a_2} + a_3 t^{a_4} + a_5 t^{a_6}; \quad H = \frac{a_7}{{}^t \theta + 273.16}$$

in which a_0 to a_7 are material constants.

In the above equations, ${}^t \bar{\epsilon}^C$, ${}^t \sigma$ and ${}^t \theta$ denote the effective creep strain, stress and temperature at time t , respectively.

5.2.2 Data Fitting Methods and Results

For above three creep material models, data fitting and comparison is necessary to find the appropriate material model for the liner material evaluated in this study.

The least squares fitting method based on the Levenberg-Marquardt algorithm (LMA) [23], a commonly used nonlinear least squares fitting algorithm, was used to fit the creep test data and find the material constants for each of the models.

The Levenberg-Marquardt algorithm provides a numerical solution to the mathematical problem of minimizing a sum of squares of several, generally nonlinear, functions that depend on a common set of parameters. The Levenberg-Marquardt algorithm interpolates between the Gauss-Newton algorithm (GNA) [24] and the method of gradient descent. It is a popular curve-fitting algorithm used in many softwares that provide a generic curve-fitting tool. There are three parameters in Creep Law 1 and the fitting results for all specimens are listed in Table 5.3.

Table 5.3. Parameters for Creep Law 1.

Specimens	Parameters		
	a ₁	a ₂	a ₃
A1	0.01146	-0.39556	0.08223
A2	0.01318	-0.34243	0.20113
A3	N/A	N/A	N/A
A4	0.02075	-0.26766	0.17066
A5	0.02519	-0.24124	0.25113
Average	0.017645	-0.31172	0.176288
Standard Deviation	0.006449	0.07043	0.070939
B1	0.0088	-0.42773	0.1495
B2	0.00877	-0.37756	0.25191
B3	0.01341	-0.3186	0.20271
B4	0.02055	-0.26879	0.18479
B5	0.02021	-0.26355	0.21199
Average	0.014348	-0.33125	0.20018
Standard Deviation	0.005822	0.070883	0.037507

The data for specimen A3 is not available because it failed during the loading stage due to the use of an inappropriate loading rate.

There are eight parameters in Creep Law 3 and the fitting results for all specimens are listed in Table 5.4.

Table 5.4. Parameters for Creep Law 3.

Specimen	Parameters							
	A1	a2	a3	a4	a5	a6	a7	a8
A1	0.07369	-0.1421	0.12972	-0.47681	0.13158	-0.47681	0.13158	82.33228
A2	0.07375	-0.13915	0.14592	-0.47177	0.14086	-0.47177	0.14086	89.51646
A3	N/A	N/A	N/A	N/A	N/A	N/A	N/A	N/A
A4	0.09123	-0.10845	0.106	-0.46552	0.09818	-0.46552	0.09818	21.56259
A5	0.06574	-0.14962	0.25117	-0.36072	0.25121	-0.36075	0.25115	130.93894
Average	0.076103	-0.13483	0.158203	-0.44371	0.155458	-0.44371	0.155443	81.08757
Standard Deviation	0.010764	0.018131	0.06411	0.055516	0.066414	0.055501	0.066385	45.09611
B1	0.11355	-0.06705	0.06865	-0.49496	0.06725	-0.49496	0.06725	35.34092
B2	0.09647	-0.09754	0.16245	-0.49252	0.15946	-0.49252	0.15946	94.3049
B3	0.07371	-0.13668	0.18358	-0.46769	0.18207	-0.46769	0.18207	89.86685
B4	0.0808	-0.12456	0.15593	-0.44811	0.1518	-0.44811	0.1518	62.50696
B5	0.07867	-0.1264	0.16461	-0.44779	0.1564	-0.44779	0.1564	69.60297
Average	0.08864	-0.11045	0.147044	-0.47021	0.143396	-0.47021	0.143396	70.32452
Standard Deviation	0.016322	0.028248	0.045015	0.022955	0.044135	0.022955	0.044135	23.67725

In the ADINA software, Creep Law 1 and Creep Law 2 are not available for Thermo-Elastic-Plastic creep materials. Thus, Creep Law 3 was selected for the modeling and the parameters in Table 6.4 were used in the finite element analysis for evaluating the liner's long term performance under constant pressure.

5.3 Finite Element Analysis for Liner Long Term Performance

To check the reliability of the material parameters that were acquired from the data fitting process, a simple model should be analyzed to compare with the experimental results. A liner block (4.5" x 0.98" x 0.173") was modeled in ADINA as shown in Figure 5.3.

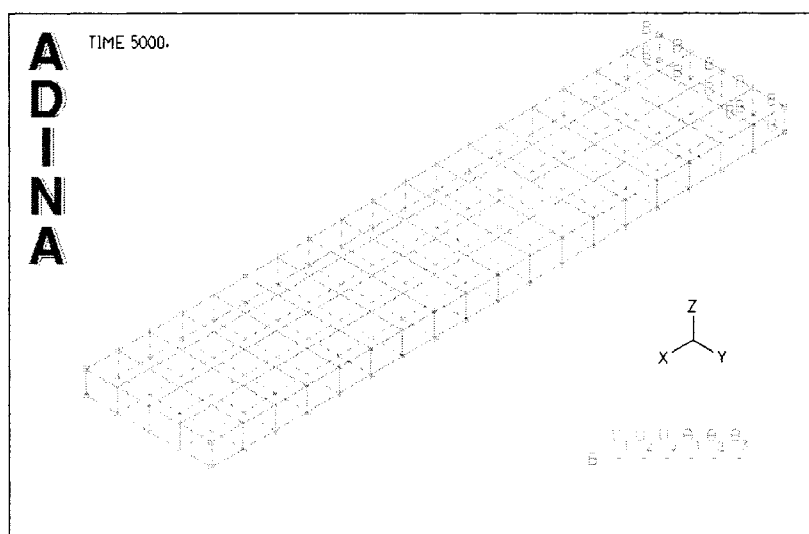


Figure 5.3. Liner block model.

The liner block model was subjected to five different stress levels, identical to those used in the experimental setup, and was analyzed to compute the displacement predicted for a 5,000-hour creep test. A comparison of the predictions given by the finite

element analysis with experimental observations is given in Table 5.5. The response curve for specimen B5 is shown in Figure 5.4.

Table 5.5 Displacement results from finite element analysis and experiments.

	Pressure (psi)	Displacement		Percentage of Difference (%)
		Experiment	FEA	
B1	289.6	0.0168	0.01687	0.416667
B2	738.3	0.0378	0.03783	0.079365
B3	1186.5	0.0538	0.05362	0.334572
B4	1559.7	0.0852	0.08419	1.185446
B5	2031.3	0.1051	0.1039	1.14177

The response curve for specimen B5 is shown in Figure 5.4.

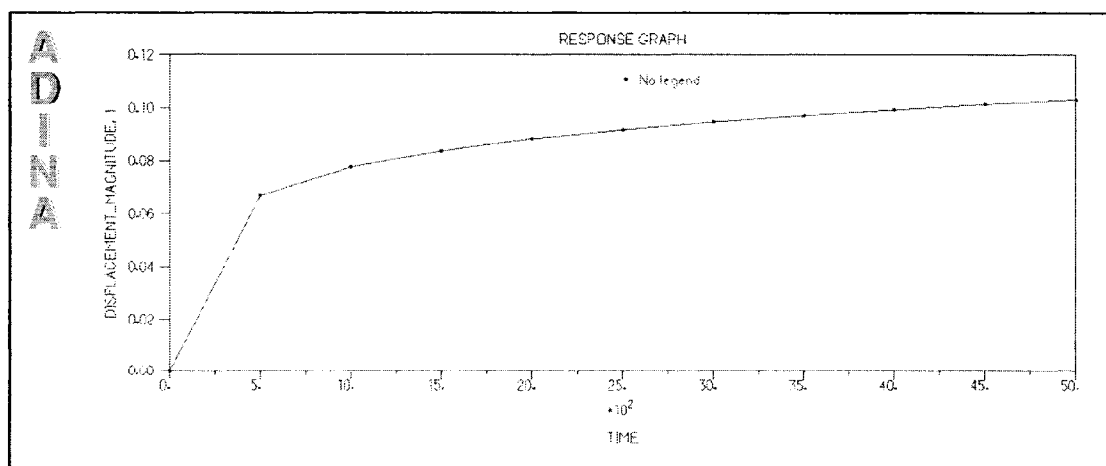


Figure 5.4. Displacement developments for specimen B5 over 5,000 hours.

From Table 5.5 and Figure 5.5, it can be concluded that the ADINA finite element software can accurately predict the liner's long term deformation using the parameters from data fitting along with the eight-parameter creep material model.

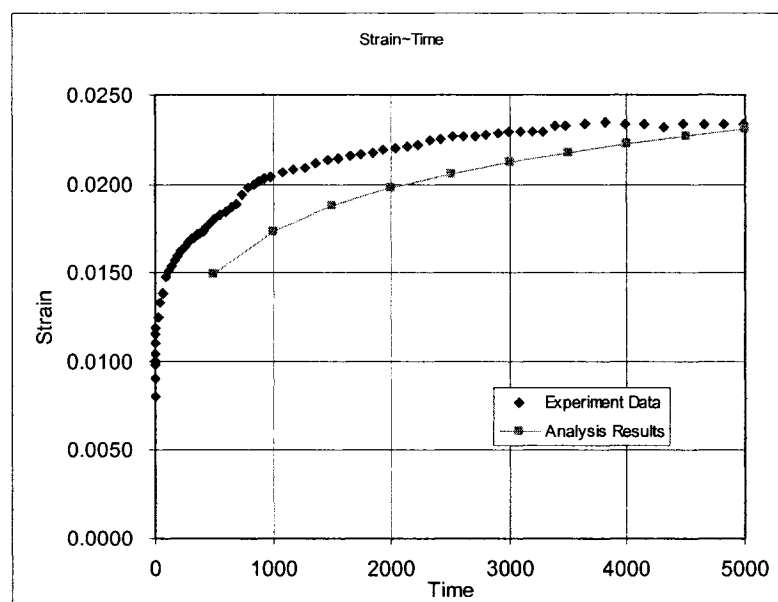


Figure 5.5. Strain comparison between experimental results and analysis results.

An 8" cast-iron host pipe with a 4" diameter circular defect was taken as an example to study the effect of creep on the long term performance of a structural liner in a fully deteriorated pipe. A constant pressure (200 psi) was applied and the analysis was carried out over a 5,000-hour loading period.

Figure 5.6 is the contour plot of the magnitude of the displacement in the liner at 5,000 hours. The displacement scale was enlarged to show the liner deformation. The maximum displacement of the liner is 0.128".

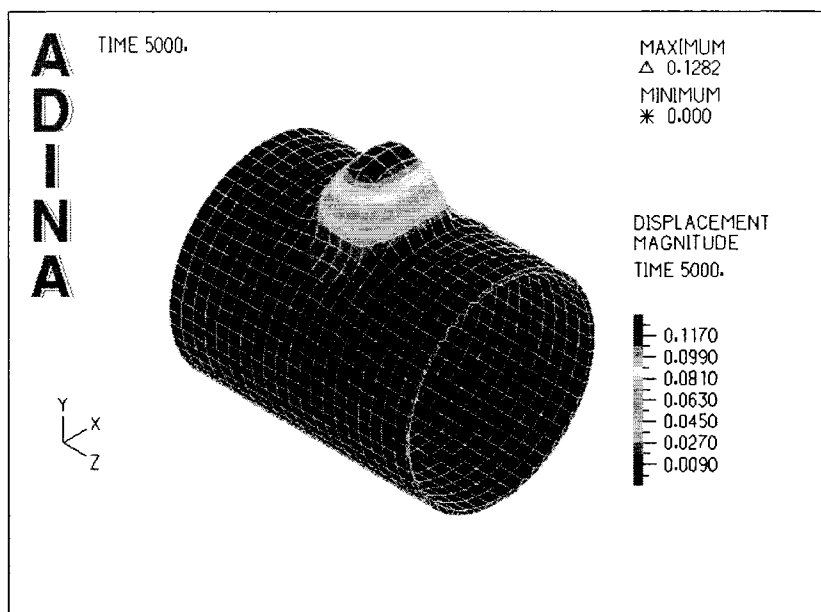


Figure 5.6. Magnified deformation of the liner at 5,000 hours (4" diameter hole in cast-iron pipe).

To compare with the liner response without the creep effect, an 8" diameter cast iron host pipe with a 4" circular defect was analyzed under 200 psi internal pressures. Figure 5.7 shows the displacement magnitude developed under a 200 psi pressure without consideration of the effect of creep. It shows the maximum displacement is 0.06215 inch. Thus, failure to consider creep results in an under-estimate of the liner's maximum deformation by more than 100% for a 4" diameter hole under a pressure of 200 psi for a test period of 5000 hrs.

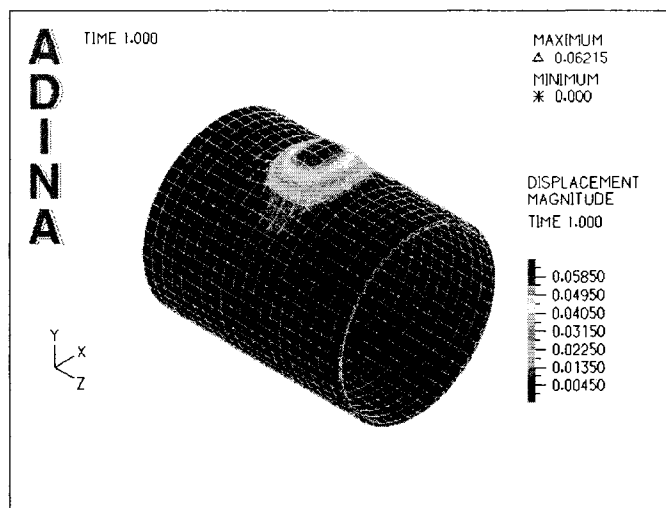


Figure 5.7. Magnified deformation for a 4" diameter defect in a cast iron host pipe (creep is neglected).

Liner creep behavior for a cast iron host pipe with a 4" diameter circular defect was analyzed under a constant pressure of 300 psi.

Figure 5.8 shows the contour plot of the predicted displacement in the liner at 5,000 hours and the picture again is scaled to show the liner deformation more clearly. The maximum displacement of the liner is 0.22 inch.

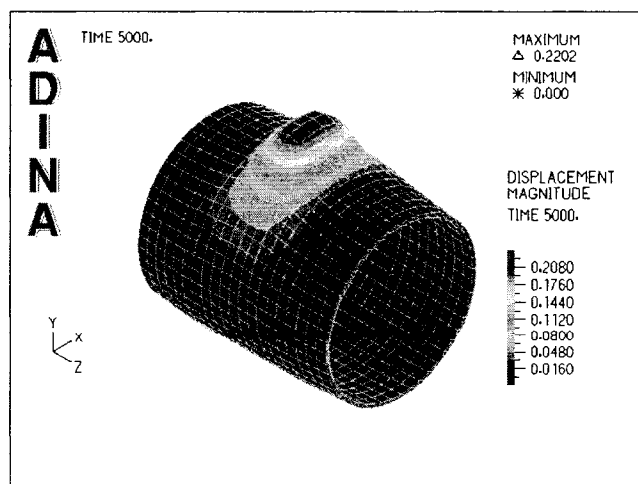


Figure 5.8. Magnified deformation of the liner after 5,000 hours (pressure at 300 psi).

Figure 5.9 displays the element labels in the model. Element number 1951 was chosen as a special model point to track the liner deformation in response to the applied load. Figure 5.10 presents the displacement of the element 1951 over the test duration of 5,000 hours. The displacement increases rapidly at first and the rate becomes slower as time increases. The trend of displacement development shows clearly the creep effect on the liner performance. Figure 5.11 represents the effective creep strain development vs. time for the numerical simulation.

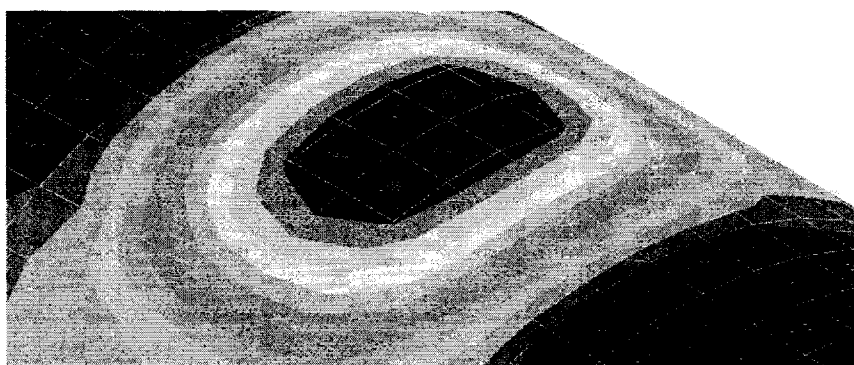


Figure 5.9. Element labels in model.

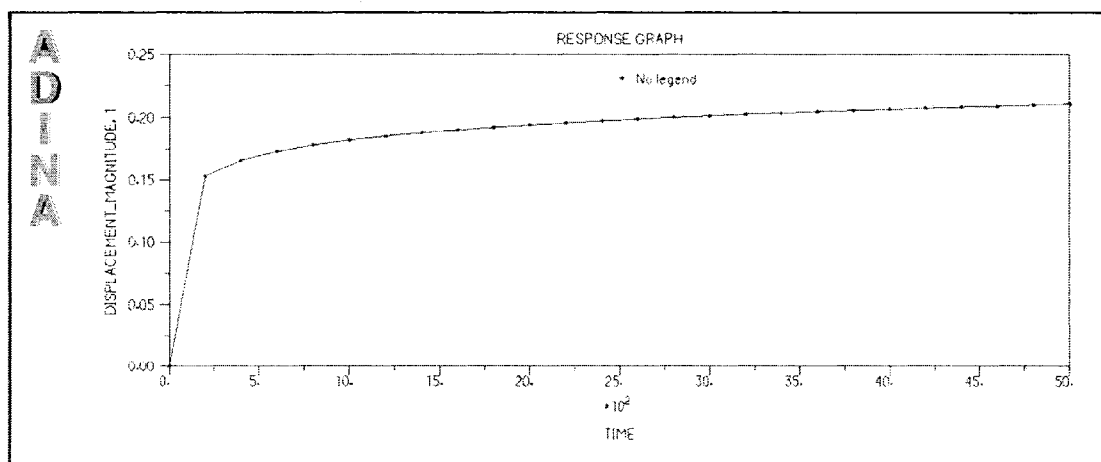


Figure 5.10. Displacement *versus* time (pressure at 300 psi).

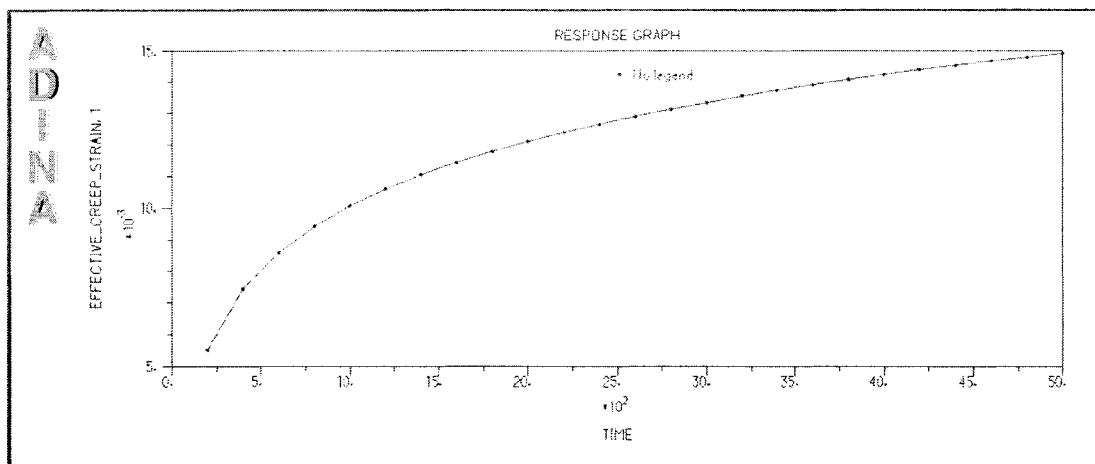


Figure 5.11. Effective creep strain *versus* time (element 1951; pressure at 300 psi).

The results suggest that material creep properties could have a significant effect on the long-term performance of structural liners in a fully deteriorated cast-iron water main. The displacement of the liner with the creep effect considered is much larger than that predicted with the creep effect neglected. Thus, in a fully deteriorated pressure pipe, an operating pressure, that could be considered to be safe under a burst test condition, could result in failure of the liner due to creep strain over a design life of 50 years (438,000 hours). For example, under an operating pressure of 200 psi and based on the creep data collected for the “Aqua Pipe®” liner, failure will occur at about 35 years for a cast-iron host pipe with a 4” circular defect. Another phenomenon that could further accelerate the failure of a liner is cyclic loading due to water hammer effect. This phenomenon is further discussed in Chapter Six.

5.4 Parametric Study

To check the creep effect for different defect sizes, both cast-iron and PVC host pipes were simulated in ADINA with circular defect diameters from 4 inch to 8 inch and

a steady internal pressure of 200 psi. The results are listed in Table 5.6 for cast-iron host pipe and Table 5.7 for PVC host pipe.

Table 5.6. Displacement results with and without creep effect (Cast-iron pipe).

Cast-Iron	Displacement under 200Psi at 5000 Hours	Displacement without creep effect	Difference (%)
4inch	0.1282	0.06215	106.2751
5inch	0.2010	0.1008	99.40476
6inch	0.2463	0.1295	90.19305
7inch	0.2585	0.1460	77.05479
8inch	0.2555	0.1518	68.31357

Table 5.7. Displacement results with and without creep effect for a PVC pipe.

PVC	Displacement under 200Psi at 5000 Hours	Displacement without creep effect	Difference (%)
4inch	0.1538	0.07122	115.9506
5inch	0.2034	0.1008	101.7857
6inch	0.2354	0.1199	96.33028
7inch	0.2449	0.1355	80.73801
8inch	0.2450	0.1426	71.80926

Figure 5.12 shows the displacement of the liner in a cast-iron host pipe at 5,000 hours with and without creep effect. Figure 5.13 shows the percentage difference between these two cases. The percentage difference ranges from about 70% to 105%. The trend of the curve shows that the relative significance of the creep effect increases as the defect

size decreases. It is also obvious that the liner creep effect should not be ignored during liner design.

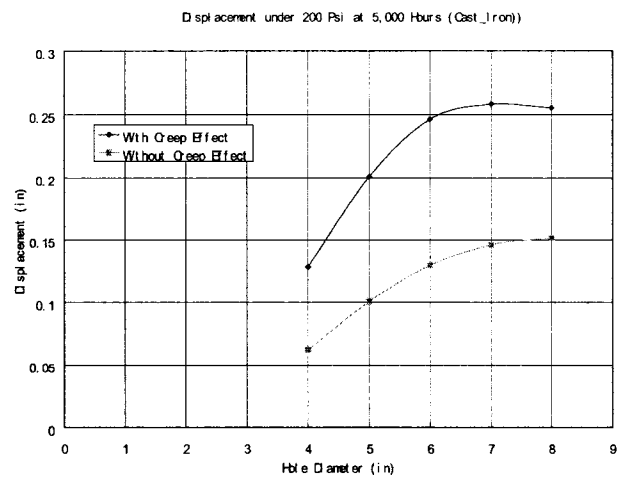


Figure 5.12. Displacement with and without creep effect for cast iron pipe.

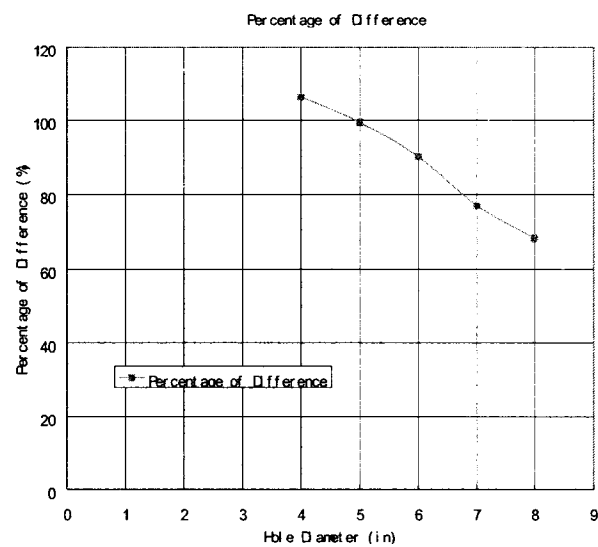


Figure 5.13. Percentage difference with and without creep effect.

Figures 5.14 and 5.15 show the results for a PVC host pipe. The trend shown for the PVC host pipe is similar to that reported above for the cast-iron pipe, with the effect of creep accounting for a 72% to 116% increase in the predicted displacement.

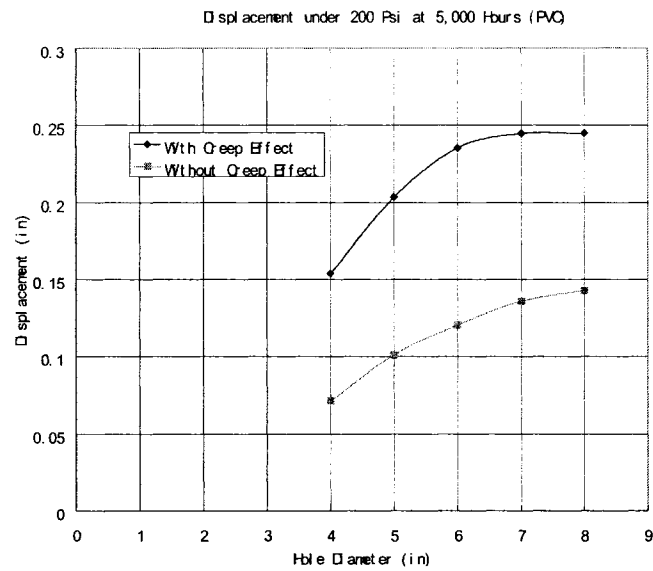


Figure 5.14. Displacement comparison with and without creep effect (PVC pipe).

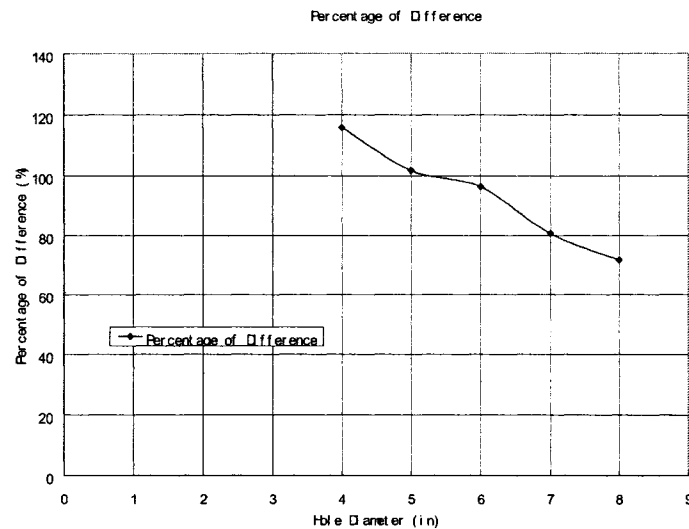


Figure 5.15. Percentage difference with and without creep effect (PVC).

From a design perspective, plastic strain accumulation is more critical for the case of intermediate stress levels (120-200 psi) than for the case of a high stress level (300 psi); also, the creep is more critical in the case of mid-size gaps compared with very large gaps in the host pipe (when the confinement effect of the host pipe is negligible).

From Figure 5.12 to Figure 5.15, it is clear that the significance of creep decreases as the diameter of the defect increases, demonstrating that creep is a significant factor for applications where gaps are in the order of 0.5"-3" in diameter, a gap range that could be expected to develop over the liner's design life of 50 years when lining a fully deteriorated water main.

5.5 Conclusions

From the study in Chapter Five, it is clear that liner creep properties have a significant effect on a liner's long term performance. To achieve a conservative liner system design, a careful consideration of creep effects is needed.

CHAPTER SIX

CYCLIC LOADING EXPERIMENTS

As mentioned in Chapter Two, surge pressure is a major concern in the design of water distribution systems. The cyclic loading experiment described in this chapter is designed to evaluate the effect of cyclic loading conditions on the long term performance of a reinforced liner in a partially deteriorated cast-iron pipe.

6.1 Cyclic Loading Experiment Setup

The equipment used in the cyclic loading experiment represents an enhancement of the custom-made pressure testing system used for the liner burst pressure experiment [18]. The pressure was provided by an air compressor running at 150 psi to 170 psi. Several release valves were used in this system to provide protection for the system and keep the water pressure in the pipeline within the desired range. This device is shown in Figure 6.1 and Figure 6.2. The pressure range utilized in the experiments was 60 psi to 120 psi . This pressure range is the one recorded in the City of Hamilton, Ontario, Canada, and could be considered representative of municipal water distribution systems (normal operating pressure 40-60 psi; surge pressures up to 120 psi). The water hammer frequency was determined to be 3 times per day and could reach a pressure value as high as 120 psi for short time periods (10-20 seconds). The experiment was designed to duplicate these values with the target of 50,000 cycles (equivalent of a 50-year design life)



Figure 6.1. Customer-made pressure testing system.

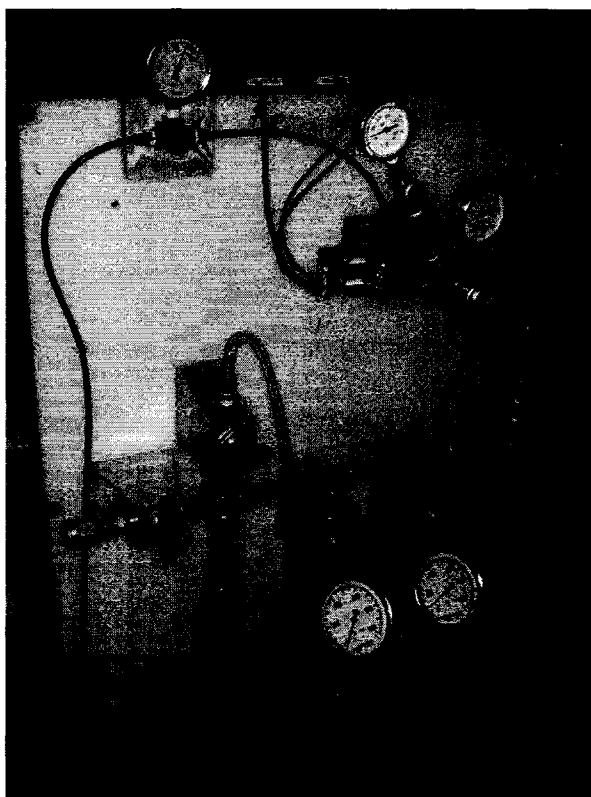


Figure 6.2. Control unit of customer-made pressure testing system.

Four 6" internal diameter PVC pipe specimens were machined and shipped to the City of Hamilton, Canada. They were lined with an "Aqua-Pipe®" Liner (manufactured by Sanexen Environmental Services Inc., Quebec, Canada) by Fer Pal LLC, one of Sanexen's certified installation contractors. The openings machined for the four specimens are shown in Figure 6.3. To simulate the stiffness of a cast-iron host pipe, several steel rings were machined to a diameter somewhat greater than the PVC pipe's spigot outer diameter. A circular opening in the steel ring was machined to expose the opening in the host pipe.



Figure 6.3. Machined PVC host pipe and steel ring.

As shown in Figure 6.4, LVDTs and strain gauges were set up at each hole to record the displacement and corresponding strain at each loading level.

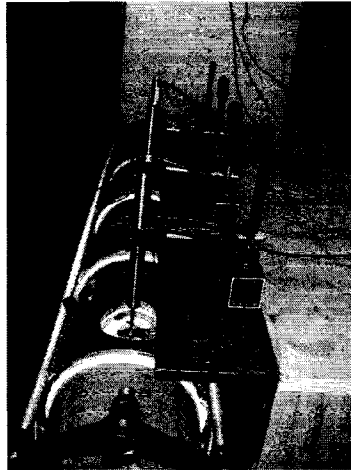


Figure 6.4. LVDTs and strain gauges.

The unit shown in Figure 6.5 is an electro-pneumatic regulator T3111 from Marsh Bellofram. The regulator utilizes a pair of quick-firing solenoid valves and an onboard pressure sensor to precisely control downstream pressure and at the same time achieve accuracy and stability. The supply solenoid valve feeds supply pressure to the downstream application while the exhaust solenoid valve bleeds off any overpressure. By monitoring the onboard pressure sensor (or the user-supplied remote sensor on two-loop units), the electronics rapidly fire one solenoid or the other to maintain the desired set point. The maximum output pressure is 150 psi.

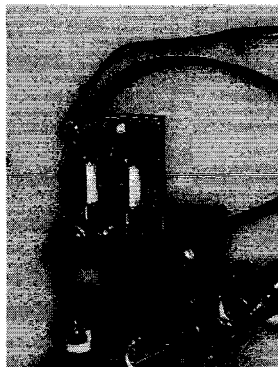


Figure 6.5. Electro-pneumatic regulator T3111.

Several power supplies, presented in Figure 6.6, were used to supply the voltage needed by the regulator, LVDTs, and pressure transducer. A wave generator was used to generate a rectangular command signal wave with high level at 8 V and low level at 4 V. The output pressure corresponding to this rectangular command signal wave was 120 psi at high value and 60 psi at low value.

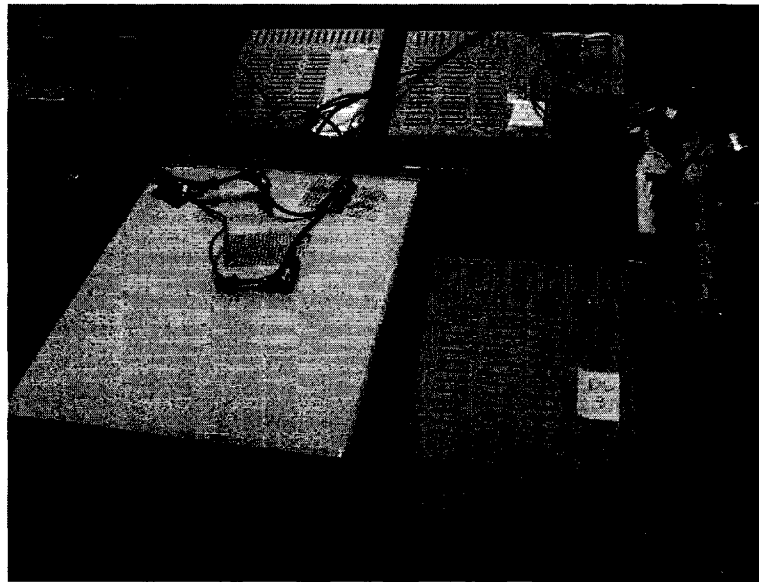


Figure 6.6. Adjustable power supplies and signal monitor.

A rectangular wave of internal pressure is illustrated in Figure 6.7. High level is at 120 psi and the low level is at 60 psi. The duration for each cycle is 40 seconds. The internal water pressure in the pipeline is maintained at 120 psi for 20 seconds and at 60 psi for the next 20 seconds during each loading cycle.

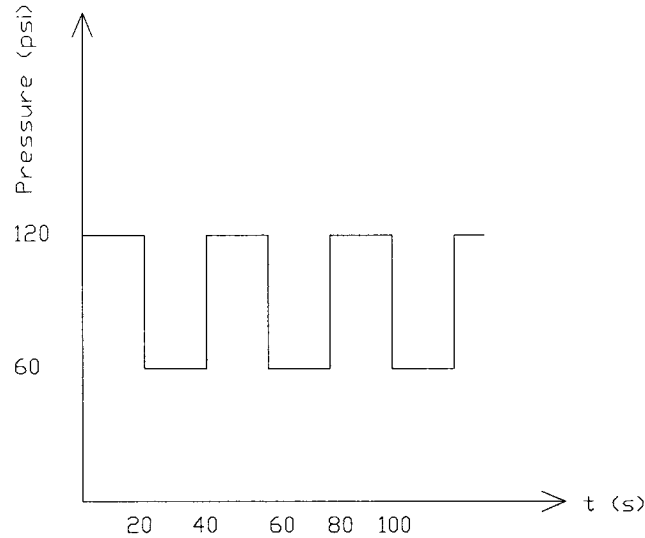


Figure 6.7. Loading cycle illustrations.

In this experiment, 50,000 cycles were performed, a value approximating 50 years of service life. The internal water pressure in the pipe, displacement and strain of the liner were be measured and recorded throughout the experiment.

6.2 Cyclic Loading Experimental Results

Four LVDTs were used to measure the liner displacements at four circular defects with diameter ranging from 2 inch to 4 inch. Strain gauges were also set up at each circular defect as shown at Figure 6.3.

Prior to the commencement of the cyclic loading test, 15 hours of data were collected to establish a baseline for the LVDT and strain gauge recorded values, and determine the level of noise from the instrumentation. Figures 6.8 and 6.9 present samples of the baseline data. The reading drift of LVDT 2 (3 inch defect) is 0.002370 inch (Figure 6.8), while the reading drift of one leg in the strain gauge rosette number 1

(4 inch defect) is 0.000089. The effect of measurement drift is discussed later in this chapter.

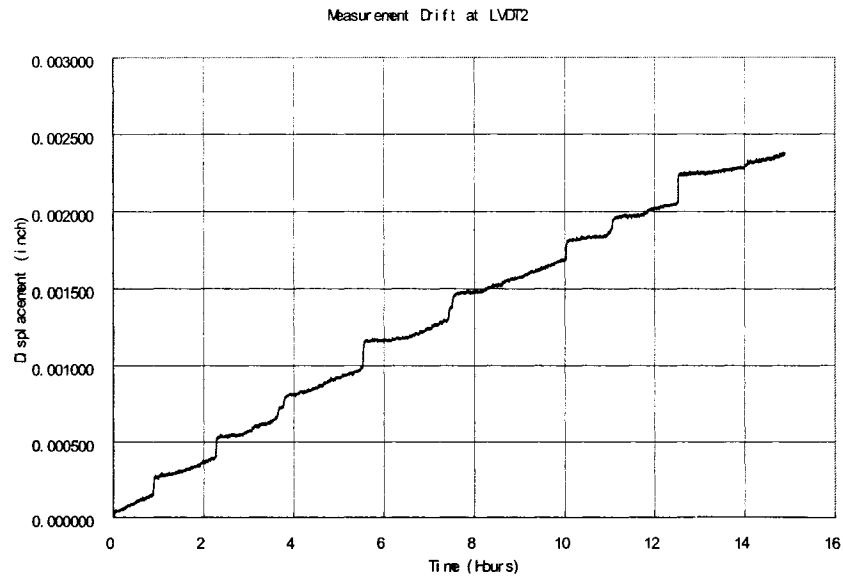


Figure 6.8. Measurement drift at LVDT2 without load.

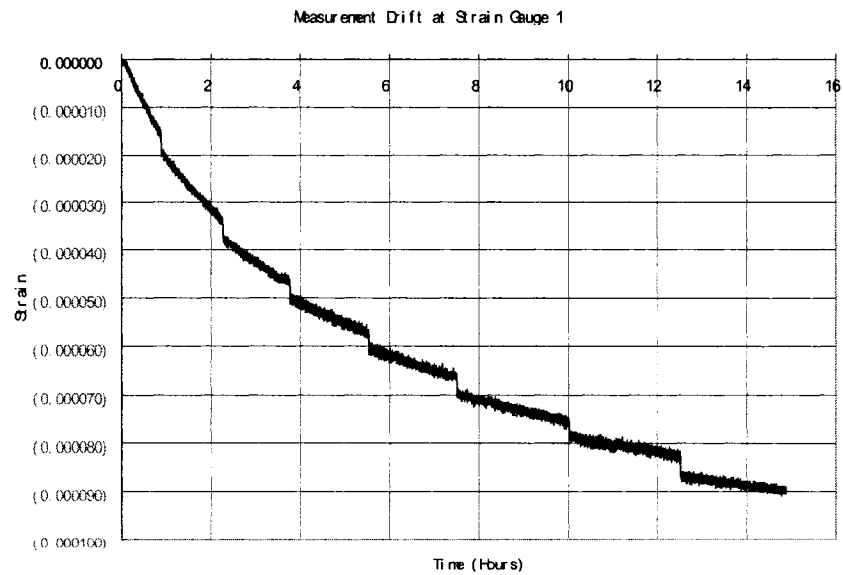


Figure 6.9. Measurement drift at strain gauge 1 without load.

The baselines, listed in Table 6.1, were used as the starting point for calculating the displacements and strains. The strain gauge rosette for the 2 inch circular defect was damaged during the installation, and strain data for this defect size is back calculated based on assumptions of isotropic behavior. Strain curve and strain increase for 2 inch circular defect are presented in Appendix D.

Table 6.1. Baselines for LVDTs and stain gauges.

	LVDT1	LVDT2	LVDT3	LVDT4
Voltage(VDC)	4.324167	8.682206	7.883915	0.011081
Base Reading (inch)	0.870054	1.753981	1.59014	0.607789
	SG1	SG2	SG3	SG4
L (OHM)	349.883434	350.100471	350.360613	350.236554
M (OHM)	349.032326	350.123180	350.047974	N/A
R (OHM)	349.640033	350.352306	350.487587	350.131496

Selected data points chosen from the recorded LVDT data are presented in Appendix D. Displacement values for the 4 inch circular defect are illustrated in Figure 6.10. The increase in liner outward displacement, calculated as percentage, is presented in Figure 6.11.

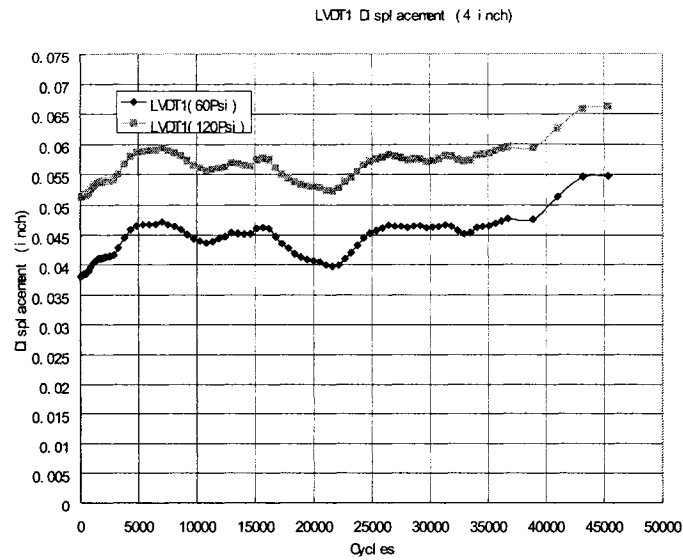


Figure 6.10. LVDT1 displacement developments.

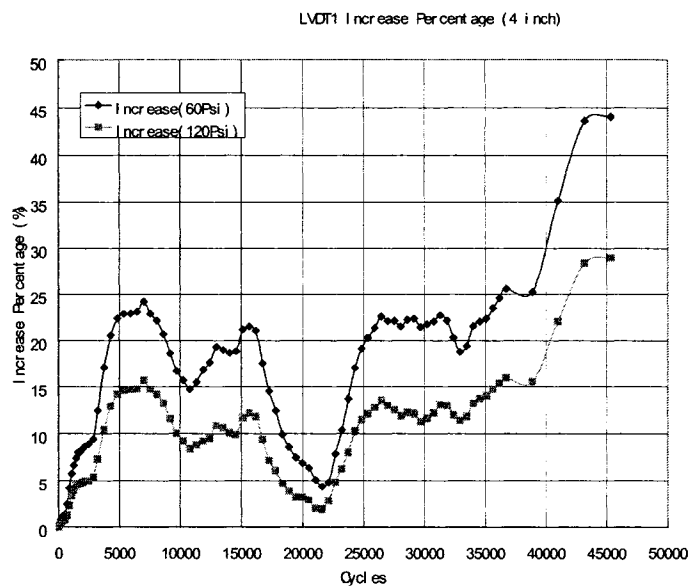


Figure 6.11. LVDT1 displacement increase percentages.

Selected data points for LVDTs 2 through 4 are presented in Appendix D. The strain developments for the 4 inch circular defect are illustrated in Figure 6.12 and the strain increase, expressed in percentage, is presented in Figure 6.13.

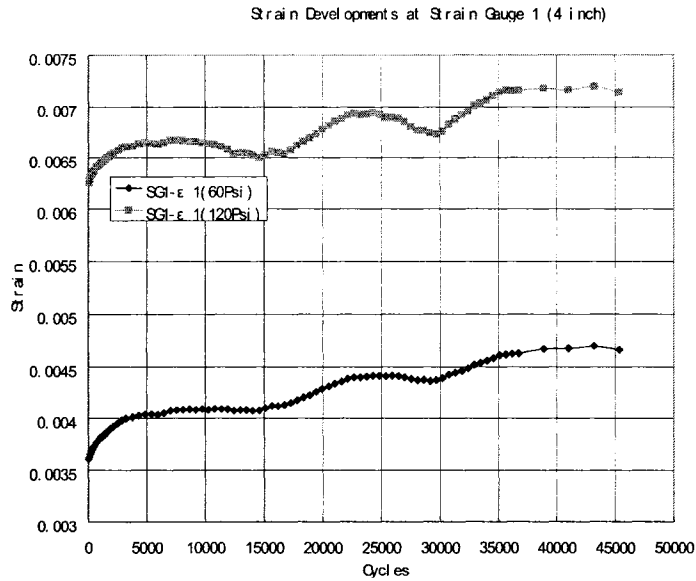


Figure 6.12. Strain developments at 4 inch circular defect.

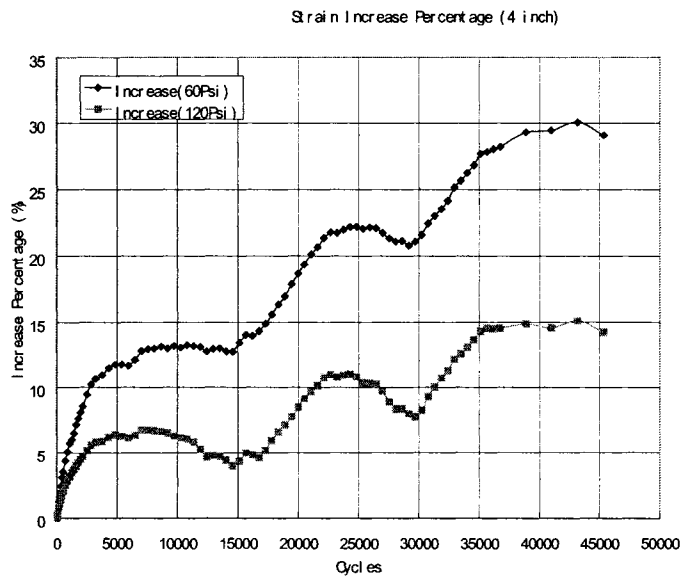


Figure 6.13. Strain increase percentages.

From Figures 6.10 and 6.11 it can be seen that after 45,000 loading cycles the displacement recorded by LVDT1 increases by 29% with respect to the baseline established under a constant pressure of 120 psi, and by 44% with respect to the base line

established at a constant pressure of 60 psi. Due to localized flexure failure of the resin under the repeated loads after about 7000 loading cycles, irregular displacement readings were observed for a period of time, before the trend stabilized again.

From Figures 6.12 and 6.13 it can be seen that after 45,000 loading cycles the strain increase was 15% with respect to the baseline established under a steady pressure of 120 psi and 29% with respect to that established under a steady pressure of 60 psi. While the strain gain rate fluctuates during the test, a clear upward linear trend can be noted from the data. This strain gain under cyclic loading is a clear indication that the stiffness of the liner (i.e., its Young's Modulus) is decreasing gradually under the action of the repeated loading.

The figures in Appendix D for defect 2 through 4 show the same overall trends for displacement and strain gain as those noted for defect 1 (4" hole). As the defect size decreases, the increase in strain gain and displacement over the baseline values also decreases. Thus, it can be stated that the effect of cyclic loading increases as the defect size increase.

Figure 6.14 to Figure 6.17 present the net gain and increase percentage on both strain gauges and LVDTs after about 56,000 loading cycles.

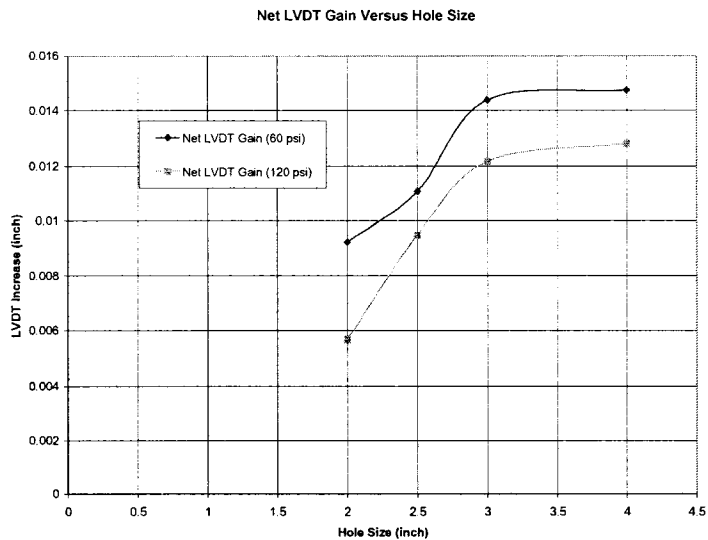


Figure 6.14. Displacement net gain *versus* hole size.

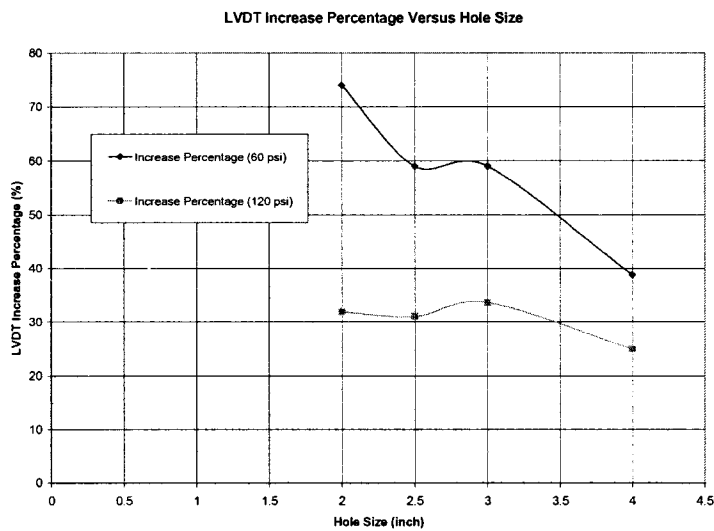


Figure 6.15. Displacement increase percentage *versus* hole size.

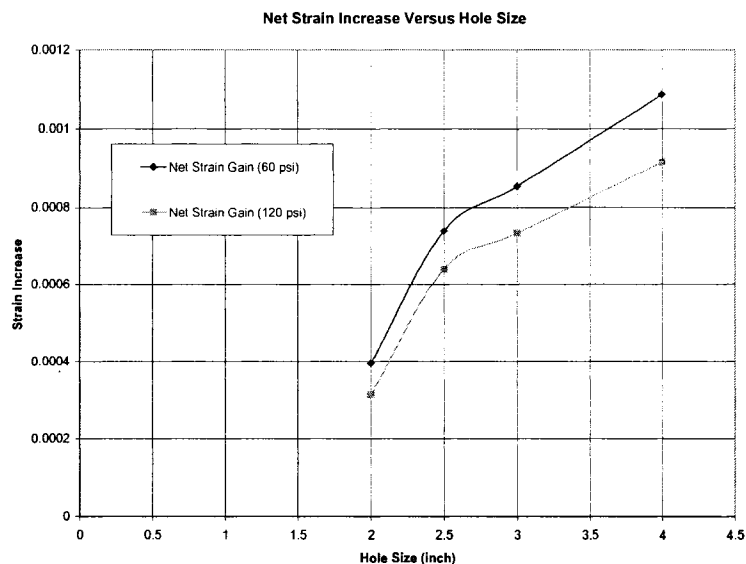


Figure 6.16. Strain net gain *versus* hole size.

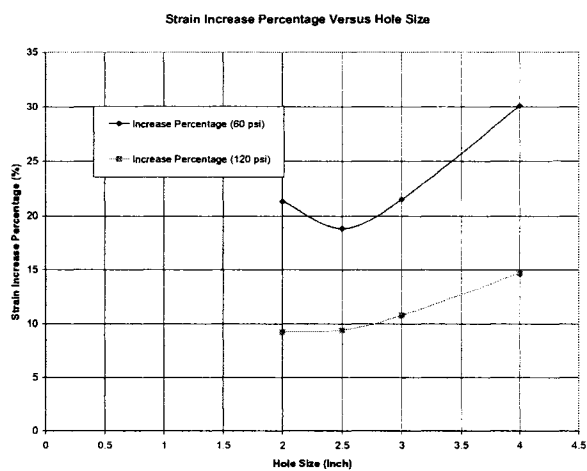


Figure 6.17. Strain increase percentage *versus* hole size .

It is necessary to compare the data under cyclic loading and the data measurement drift recorded during the baseline test. After 45,000 loading cycles the displacement at LVDT 2 has increased by 0.014381". The drift value for LVDT 2 represents approximately 16% of the displacement increase due to the cyclic loading. The drift value in the strain measurements in the left leg of strain rosette 1 was 0.000595. The drift

accounts for 15% of the net strain gain over the test period. As the test progresses, these measurement drifts are expected to play a lesser role, and are unlikely to affect the conclusions from the testing.

One reason for the measurement drift in the instrumentation includes a change in the temperature. The baseline test was started at about 5PM and ended at about 8AM in the morning. The room temperature decreased during the test period. The liner contracted due to temperature drop and change in the moisture content caused a strain decrease. The LVDTs are fastened to steel bracket, and thus readings from the LVDTs could be sensitive to temperature change.

To be able to isolate the net effect of the cyclic loading mechanism from creep on the decline of stiffness value of the cured liner, it is necessary to compare the recorded data under cyclic loading condition with results from the finite element model simulating the response of the liner under the same pressure range with and without creep effect.

A finite element model for a cast iron host pipe with 4" diameter circular defect was analyzed. Figure 6.18 and Figure 6.19 present displacement developments of a cast iron host pipe with 4 inch circular defect subject to uniform internal pressure 120 psi for 552 hours.

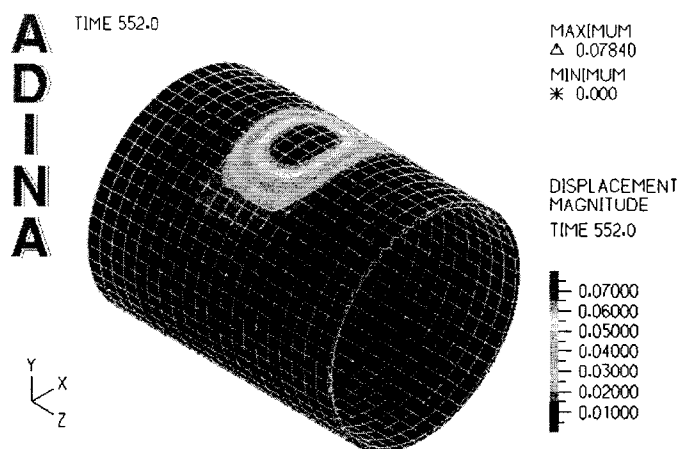


Figure 6.18. Displacement development for 4 inch circular defect for 552 hours.

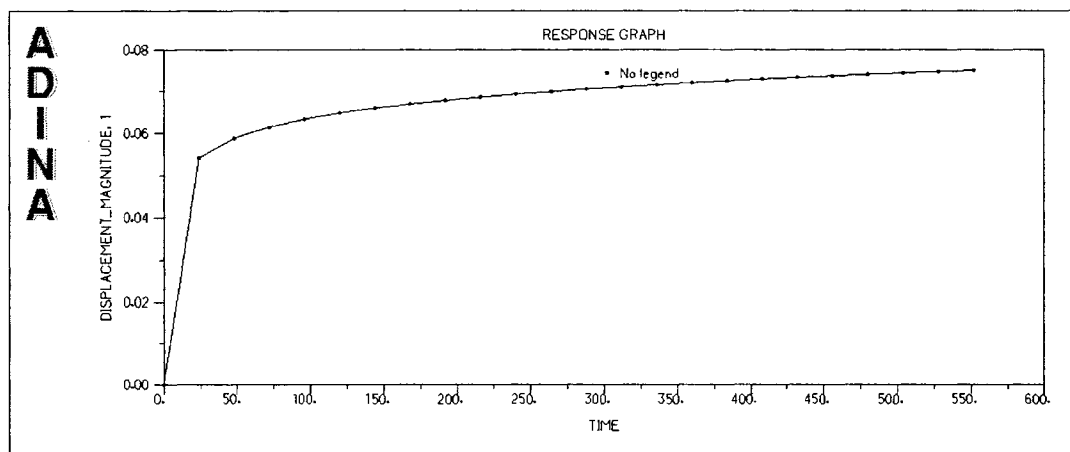


Figure 6.19. Displacement development *versus* time (effect of creep considered; notice primary and secondary creep mechanisms).

Figure 6.20 displays a comparison between the experimental test data and the finite element analysis predictions. The experimental data agrees very well with the numerical data for the primary creep range. A reasonable agreement also exists between the predicted and observed deflections during the secondary creep period, with the overall trends being in close agreement.

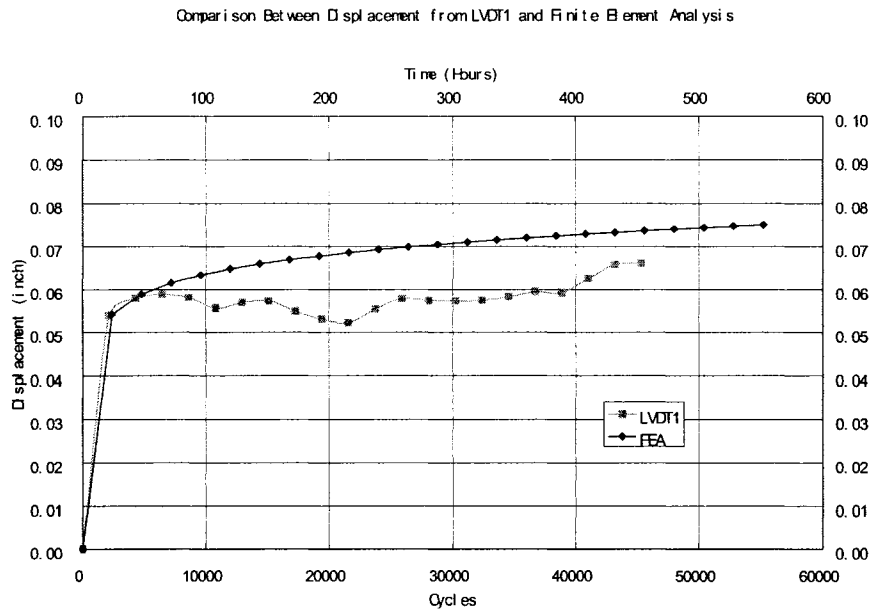


Figure 6.20. Comparison between displacement from LVDT1 and finite element analysis.

Figure 6.21 shows the comparison of the experimental strain data from strain gauge 1 (4 inch circular defect) and the strain predictions from the finite element analysis with consideration of the creep effect. The strain from the cyclic experimental data (60-120 psi) is lower overall than that predicted by the FEA model for creep under a constant pressure of 120 psi for the same time period. An inspection of Figure 6.21 reveals that the difference is attributed mainly to a lower primary creep strain. The secondary creep strain gain under a constant pressure of 120 psi is similar to that observed for a base pressure of 60 psi with cyclic loading up to 120 psi. Thus, it can be concluded that the effect of cyclic loading can be accounted for by calculating the secondary creep gain for peak pressure value (also known as the maximum operating pressure, or MOP) over the design period. The net effect of the cyclic loading can be

roughly approximated by integrating the pressure as a function of time and comparing the areas under the curves, which is about 30% of creep at a level of 120 psi.

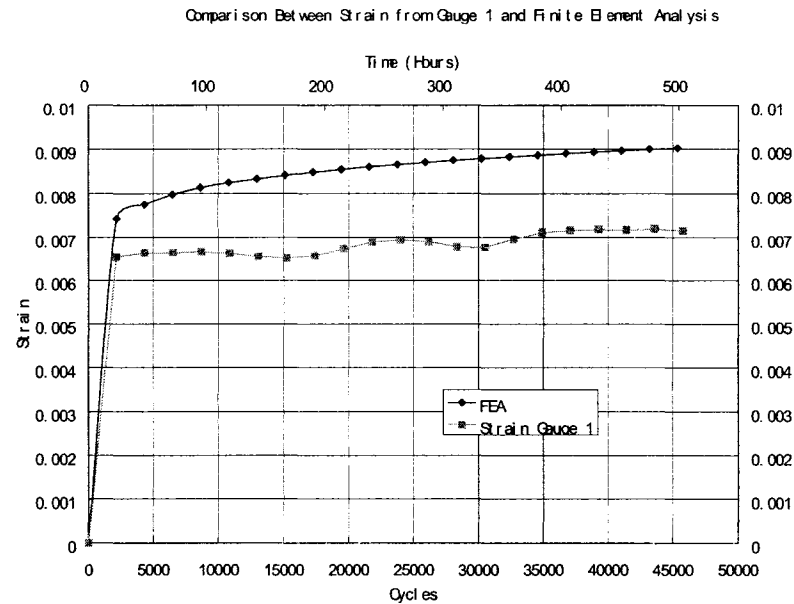


Figure 6.21. Comparison between strain from strain gauge 1 and finite element analysis.

6.3 Conclusions

The results reported in this chapter demonstrate that a cyclic loading mechanism contribute to the progressive failure of a GFR CIPP liner installed in a partially deteriorated cast-iron pipe at operating levels significantly lower than the ultimate burst pressure capacity of the liner. The effect of cyclic loading at a normal operating pressure range of a typical municipal system (60-120 psi) enhances displacement and creep strain gain by as much as 30% over the design life of the liner of approximately 50 years.

From strain data shown in Appendix 'D', a "step" like behavior was observed. From 0-4500 cycles, the creep strain increases due to microscopic cracks in resin under the repeated flexure loading. From 4500-15750 cycles, a steady period is shown. From

15750-22500 cycles, another deterioration mechanism in the composite material (possible partial failure at the fiber-matrix interface) took place, leading to further degradation in the stiffness of the composite's stiffness. From 22500-29250 cycles, a new steady level took place. From 29250-36720 cycles, the impact of yet another deterioration mechanism was observed. This behavioral pattern is typical for a progressive failure of a composite material subjected to fatigue load.

Based on the results reported in this chapter, it can be stated that a design that accounts for the effect of creep at a monotonic pressure level equal to that of the expected water hammer effect (i.e., maximum operating pressure) also accounts for the effect of cyclic loading on a typical liner over the design life of 50 years (assuming 3 water hammer events per day).

CHAPTER SEVEN

POSSIBLE MODIFICATIONS ON THE DESIGN OF PIPELINE REHABILITATION LINERS

Based on the research results reported in Chapters Three through Six, it can be concluded that a liner's long term pressure resistance performance is overestimated by the ASTM 2207-02 design methodology. It is recommended to apply safety factors to the predictions of ASTM F2207-02 to ensure the conservative nature of its predictions.

7.1 Factor for Host Pipe and Defect Variation

Based on the results reported in Chapter Four, the failure mode of a GFR CIPP liner, under static loading, changes from flexure-tensile failure in the case of a large defect in the host pipe (4" or larger) to a direct shear failure ("punch" shear) for smaller defects. Thus different safety factors are recommended based on defect size.

From Table 4.8, it can be seen that the ASTM F2207-02 design methodology can be used safely to predict the bursting pressure for circular defect sizes ranging from 6 inch to 8 inch in diameter. For defect sizes ranging from 1.5 inch to 5 inch, a safety factor from 1.1 to 1.4 should be applied to the ASTM F2207-02, resulting in a reduction in the predicted liner burst pressure. For a flexible pipe (i.e., PVC) the needed safety factors are higher than for the case of a rigid pipe (cast-iron pipe). For a circular defect size less than 1 inch in diameter, the liner burst pressure is controlled by the stress concentration

around the defect edge and failure is governed by a “punch” shear failure mode. It is recommended that the burst pressure rating calculated using ASTM 2207-02 should be reduced by a factor of 3.0 or 4.0 for defects less than 1 inch in diameter.

Based on the results reported in Chapter Four, the design methodology included in ASTM F2207-02 is not capable of calculating the liner burst pressure for the case where the length of the defect is not equal to its width. To estimate the liner burst pressure using the ASTM method for defect shapes other than a square or a circle, it is recommended to use different safety factors based the defect’s longest dimension. It is suggested that an equivalent area method should be used, where the area of the defect is computed and converted to a square shape with an equivalent area. Based on the dimensions of the equivalent square, the ASTM method can then be used to calculate liner burst pressure. When the defect is significantly longer in the axial direction, a safety factor of 2.0 should be applied to the calculated liner burst pressure. When the defect is significantly longer in the hoop direction, a safety factor of 1.2 should be used.

7.2 Factor for Creep Effect and Cyclic Loading Condition

From Chapter Five, it can be concluded that creep strain has a significant effect on the long term performance of a GFR liner installed in a partially deteriorated pressure pipe. Based on the research included in Chapter Five, a safety factor of 1.5 is recommended to be applied to the predicted liner burst pressure.

From the research results reported in Chapter Six, it can be concluded that cyclic loading could make a noticeable contribution to the displacement and plastic strain gain in a liner subjected to stress levels well below the short term burst pressure of the liner and within the normal operation range of a municipal water distribution system. Cyclic

loading amplified the effect of creep strain by approximately 30% beyond that anticipated from creep alone.

The data also indicates that accounting for the creep induced plastic strain assuming a monotonic pressure equal to the maximum operating pressure (MOP) due to expected water hammer effect, is adequate for accounting for the effect of cyclic loading (i.e., for a normal operating pressure of 60 psi and peak pressure of 120 psi, the liner burst pressure would need to be calculated assuming a constant operating pressure equal to 120 psi).

7.3 Conclusions and Recommendations

From the research on CIPP liner design conducted for this thesis, it is suggested that a liner's performance is overestimated by the ASTM F2207-02 methods and could result in structure failure before it reaches its design life at relatively high operating pressures (~300 psi).

When using the methodology proposed in ASTM F2207-02 for calculating the liner burst pressure, host pipe material, defect size and defect shape should all be taken into consideration. To account for these, an additional safety factor ranging from 1.1 to 1.4 for defect sizes larger than 1 inch, and a safety factor of 3 to 4 for defect sizes less than 1 inch should be applied.

Based on the defect orientation for non-circular defects, a safety factor of up to 2.0 should be applied to the calculated liner burst pressure corresponding to the defect's axial or hoop orientation. Also, a safety factor of 2.0 should be applied to account for the creep strain and cyclic loading over the liner's design life.

CHAPTER EIGHT

FURTHER INVESTIGATION OF LINER DESIGN

In this research relating to liner design, the ASTM2207-02 design method has been examined and the influence of the liner material properties, host pipe material properties, defect size and shape, liner creep properties and cyclic loading condition has been analyzed using numerical and experimental methods. Comparing the results between the existing ASTM2207-02 analytical method, finite element analysis and experimental testing, several safety factors are proposed to be applied to the burst pressure predictions made using the methodology given in ASTM2207-02 when predicting the liner's burst pressure.

To gain a better understanding of liner long term performance and provide a reliable but not overly conservative design methodology, the following additional research work is recommended.

1. Liner burst pressure tests for different defect sizes and shapes should be performed to provide experimental data for validating the numerical results reported in this work.
2. 5,000-hour liner creep pressure tests should be performed on lined pipe for different defect sizes at a range of stress levels to validate the numerical results for long-term secondary creep.

3. The cyclic loading test should be repeated for different stress levels and cyclic loading frequencies.
4. Different liner materials should be studied, enabling the development of more general conclusions and recommendations.
5. Stress concentrations due to the presence of point loads (from the bedding material) on the liner outer surface and crack propagation phenomenon should be studied to estimate the effect on liner long term performance.

APPENDIX A

LINER TENSILE EXPERIMENTAL DATA

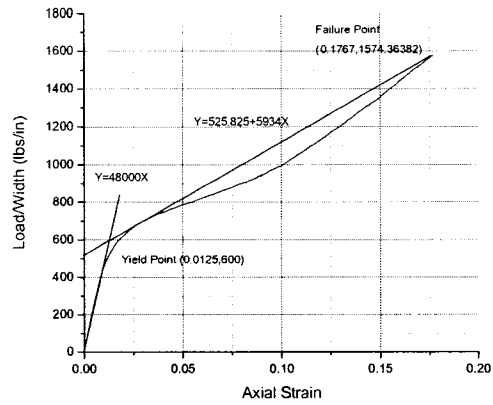


Figure A.1. Load/width *versus* axial strain of axial specimen 1.

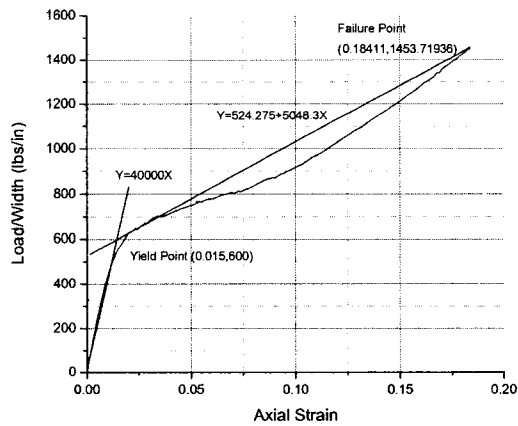


Figure A.2. Load/width *versus* axial strain of axial specimen 2.

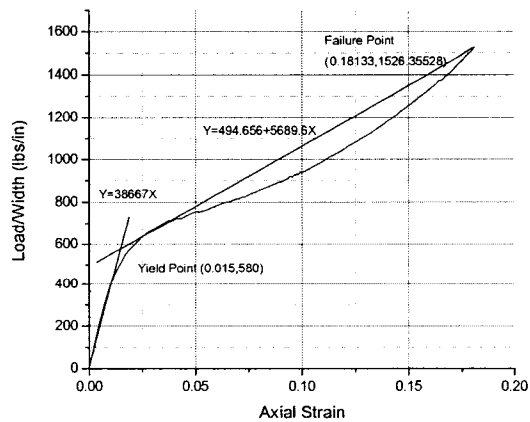


Figure A.3. Load/width *versus* axial strain of axial specimen 3.

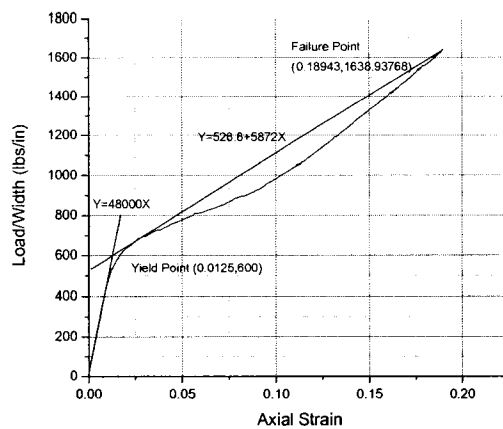


Figure A.4. Load/width *versus* axial strain of axial specimen 4.

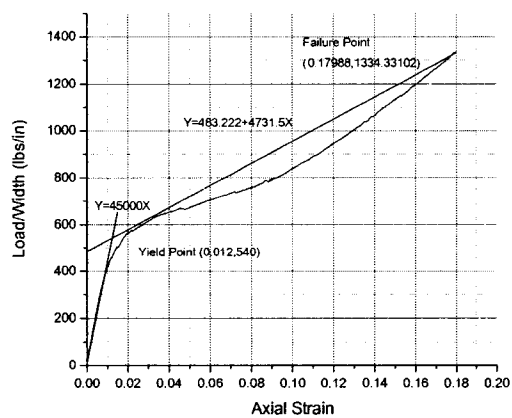


Figure A.5. Load/width *versus* axial strain of axial specimen 5.

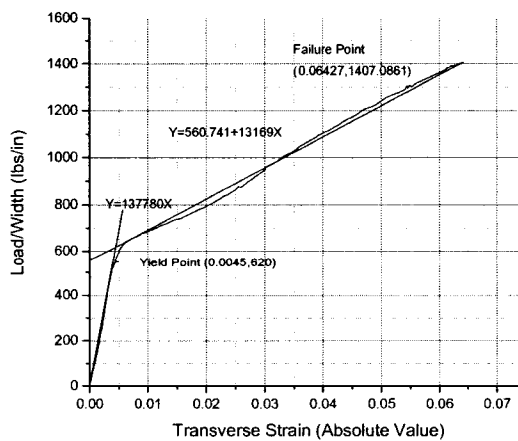


Figure A.6. Load/width *versus* transverse strain of axial specimen 6.

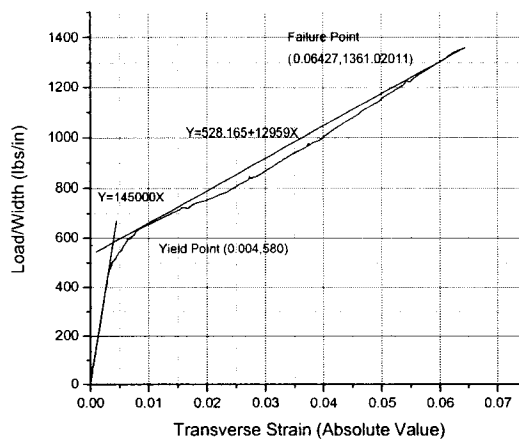


Figure A.7. Load/width *versus* transverse strain of axial specimen 7.

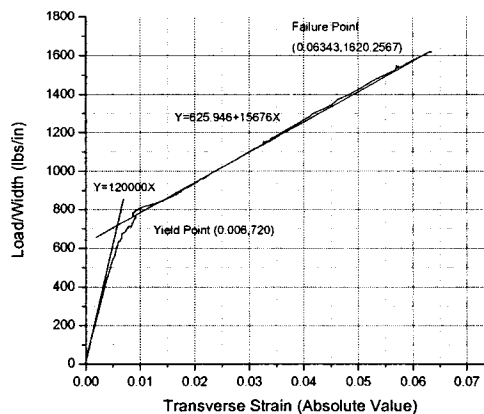


Figure A.8. Load/width *versus* transverse strain of axial specimen 8.

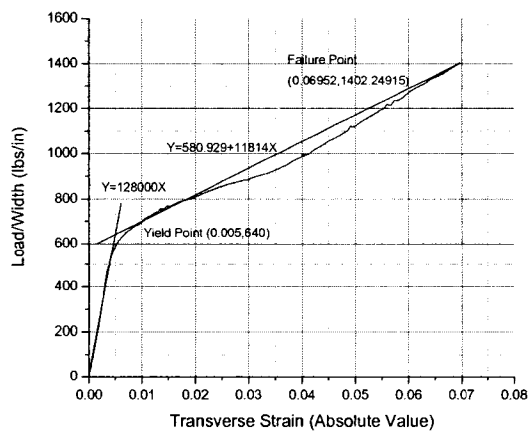


Figure A.9. Load/width *versus* transverse strain of axial specimen 9.

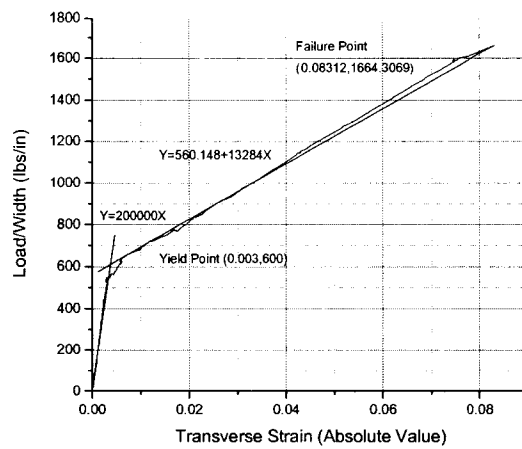


Figure A.10. Load/width *versus* transverse strain of axial specimen 10.

APPENDIX B

MATHCAD® SPREADSHEETS FOR

BURST PRESSURE

B.1 Calculations of Burst Pressure Using Maximum
Stress Criteria

Input data:

E_a is the axial stiffness of the liner

E_h is the axial stiffness of the liner

P is the pressure in the liner

L is the length of the hole

w is the width of the hole

D is the diameter of the host pipe

N_a is the axial load per unit width in the liner

N_h is the hoop load per unit width in the liner

r_a is the axial radius of curvature in the doomed liner

r_h is the hoop radius of curvature in the doomed liner

s_{ah} is the the compliance due to Poisson's effect

ϵ_a is the axial strain in the liner

ϵ_h is the hoop strain in the liner

ϵ_y is the yield strain in the liner

$L := 1$

$w := 1$

$D := 7$

$N_{af} := 1505.54143$

$N_{hf} := 1667.067$

$s_y := 0.011$

$$E_{s1} := 43933.4$$

$$E_{s2} := 5473.44$$

$$E_{h1} := 45619.6$$

$$E_{h2} := 15571.8$$

$$s_{12,1} := 7.02058 \cdot 10^{-6}$$

$$s_{12,2} := 7.47245 \cdot 10^{-5}$$

$$s_{21,2} := 2.576 \cdot 10^{-5}$$

Step 1 : Determining the parameters till the yielding

Guess Values:

$$P_y := 10$$

$$h := 0.06$$

Given:

$$P_y = \frac{1}{\left(\frac{1}{E_{s1} E_{h1}} - s_{12,1}^2\right) \left(\frac{w^2}{8h} + \frac{h}{2}\right)} \left[\frac{1}{E_{s1}} \left[\frac{\left(\frac{w^2}{4h} - h\right) \operatorname{asin}\left(\frac{w}{\frac{w^2}{4h} + h}\right)}{w} - 1 \right] - s_{12,1} \left[\frac{\left(\frac{L^2}{4h} - h\right) \operatorname{asin}\left(\frac{L}{\frac{L^2}{4h} - h}\right)}{L} - 1 \right] \right] \dots$$

$$- \frac{1}{\left(\frac{1}{E_{s1} E_{h1}} - s_{12,1}^2\right) \left(\frac{L^2}{8h} + \frac{h}{2}\right)} \left[-s_{12,1} \left[\frac{\left(\frac{w^2}{4h} - h\right) \operatorname{asin}\left(\frac{w}{\frac{w^2}{4h} + h}\right)}{w} - 1 \right] - \frac{1}{E_{h1}} \left[\frac{\left(\frac{L^2}{4h} - h\right) \operatorname{asin}\left(\frac{L}{\frac{L^2}{4h} - h}\right)}{L} - 1 \right] \right]$$

$$\left[100 \left[\frac{\left(\frac{w^2}{4h} - h\right) \operatorname{asin}\left(\frac{w}{\frac{w^2}{4h} + h}\right)}{w} - 1 \right] \right]^2 + \left[100 \left[\frac{\left(\frac{L^2}{4h} - h\right) \operatorname{asin}\left(\frac{L}{\frac{L^2}{4h} - h}\right)}{L} - 1 \right] \right]^2 = (100 s_y)^2$$

$$\begin{pmatrix} P_y \\ h_y \end{pmatrix} := \operatorname{Find}(P_y, h)$$

$$\begin{pmatrix} F_y \\ h_y \end{pmatrix} = \begin{pmatrix} 226.62 \\ 0.05 \end{pmatrix}$$

$$N_{xy} := \frac{1}{\frac{1}{E_{a1} E_{h1}} - S_{12_1}^2} \left[-S_{12_1} \left[\frac{\left[\left(\frac{w^2}{4 h_y} + h_y \right) \operatorname{asin} \left(\frac{w}{\frac{w^2}{4 h_y} + h_y} \right) \right]}{w} - 1 \right] + \frac{1}{E_{h1}} \left[\frac{\left[\left(\frac{L^2}{4 h_y} + h_y \right) \operatorname{asin} \left(\frac{L}{\frac{L^2}{4 h_y} + h_y} \right) \right]}{L} - 1 \right] \right]$$

$$N_{xy} = 257.737$$

$$N_{hy} := \frac{1}{\frac{1}{E_{a1} E_{h1}} - (S_{12_1})^2} \left[\frac{1}{E_{a1}} \left[\frac{\left[\left(\frac{w^2}{4 h_y} + h_y \right) \operatorname{asin} \left(\frac{w}{\frac{w^2}{4 h_y} + h_y} \right) \right]}{w} - 1 \right] + -S_{12_1} \left[\frac{\left[\left(\frac{L^2}{4 h_y} + h_y \right) \operatorname{asin} \left(\frac{L}{\frac{L^2}{4 h_y} + h_y} \right) \right]}{L} - 1 \right] \right]$$

$$N_{hy} = 272.29$$

$$s_{xy} := \left[\frac{\left[\left(\frac{L^2}{4 h_y} + h_y \right) \operatorname{asin} \left(\frac{L}{\frac{L^2}{4 h_y} + h_y} \right) \right]}{L} - 1 \right]$$

$$s_{hy} := \frac{\left(\frac{w^2}{4 h_y} + h_y \right) \operatorname{asin} \left(\frac{w}{\frac{w^2}{4 h_y} + h_y} \right)}{L} - 1$$

$$s_{xy} = 7.778 \times 10^{-3}$$

$$s_{hy} = 7.778 \times 10^{-3}$$

Step 2 : Determining the parameters from the yielding portion till the failure

$$F_f := 100$$

$$h := 0.06$$

$$s_a := 0.005$$

$$s_f := .005$$

Given

$$s_a = \frac{\left(\frac{L^2}{4h} + h \right) \arcsin \left(\frac{L}{\frac{L^2}{4h} - h} \right)}{L} - 1$$

$$s_h = \frac{\left(\frac{w^2}{4h} + h \right) \arcsin \left(\frac{w}{\frac{w^2}{4h} - h} \right)}{w} - 1$$

$$P_f = \frac{\frac{1}{\left(\frac{1}{E_{a2} E_{t2}} - s_{12_2} s_{21_2} \right)} \left[\frac{1}{E_{a2}} (s_h - s_{hy}) - s_{21_2} (s_a - s_{ay}) \right] + N_{hy}}{\frac{w^2}{8h} - \frac{h}{2}} \cdot \frac{1}{\left(\frac{1}{E_{a2} E_{t2}} - s_{12_2} s_{21_2} \right)} \left[-s_{12_2} (s_h - s_{hy}) - \frac{1}{E_{t2}} (s_a - s_{ay}) \right] + N_{ay}$$

$$N_{hf} = \frac{1}{\left(\frac{1}{E_{a2} E_{t2}} - s_{12_2} s_{21_2} \right)} \left[\left(\frac{1}{E_{a2}} \right) (s_h - s_{hy}) - s_{21_2} (s_a - s_{ay}) \right] + N_{hy}$$

$$\begin{pmatrix} s_h \\ s_a \\ P_f \\ h_f \end{pmatrix} = \text{Find}(s_h, s_a, P_f, h)$$

$$\begin{pmatrix} s_h \\ s_a \\ P_f \\ h_f \end{pmatrix} = \begin{pmatrix} 0.095 \\ 0.095 \\ 2.445 \times 10^3 \\ 0.191 \end{pmatrix}$$

B.2 Calculations of Burst Pressure in ASTM F2207-02 Using Interactive Criteria

$$L := 1$$

$$w := 1$$

$$D := 7$$

$$N_{hf} := 1505.54143$$

$$N_{hf} := 1667.067$$

$$s_y := 0.011$$

$$E_{a1} := 43933.4$$

$$E_{a2} := 5473.44$$

$$E_{h1} := 45619.6$$

$$E_{h2} := 15571.8$$

$$s_{12_1} := 7.02058 \cdot 10^{-6}$$

$$s_{12_2} := 7.47245 \cdot 10^{-5}$$

$$s_{21_2} := 2.576 \cdot 10^{-5}$$

Step 1

Guess values to determine yield pressure

$$P_y := 10$$

$$n := 0.06$$

Given

$$P_y = \frac{1}{\left(\frac{1}{E_{a1} E_{h1}} - s_{12_1}^2 \right) \left(\frac{w^2}{8 h} + \frac{h}{2} \right)} \left[\frac{1}{E_{a1}} \left[\frac{\left[\left(\frac{w^2}{4 h} + h \right) \operatorname{asin} \left(\frac{w}{\frac{w^2}{4 h} + h} \right) \right]}{w} - 1 \right] - s_{12_1} \left[\frac{\left[\left(\frac{L^2}{4 h} + h \right) \operatorname{asin} \left(\frac{L}{\frac{L^2}{4 h} + h} \right) \right]}{L} - 1 \right] \right] \right. \\ \left. - \frac{1}{\left(\frac{1}{E_{a1} E_{h1}} - s_{12_1}^2 \right) \left(\frac{L^2}{8 h} + \frac{h}{2} \right)} \left[-s_{12_1} \left[\frac{\left[\left(\frac{w^2}{4 h} + h \right) \operatorname{asin} \left(\frac{w}{\frac{w^2}{4 h} + h} \right) \right]}{w} - 1 \right] + \frac{1}{E_{h1}} \left[\frac{\left[\left(\frac{L^2}{4 h} + h \right) \operatorname{asin} \left(\frac{L}{\frac{L^2}{4 h} + h} \right) \right]}{L} - 1 \right] \right] \right] \right. \\ \left. \left[100 \left[\frac{\left[\left(\frac{w^2}{4 h} + h \right) \operatorname{asin} \left(\frac{w}{\frac{w^2}{4 h} + h} \right) \right]}{w} - 1 \right] \right]^2 - \left[100 \left[\frac{\left[\left(\frac{L^2}{4 h} + h \right) \operatorname{asin} \left(\frac{L}{\frac{L^2}{4 h} + h} \right) \right]}{L} - 1 \right] \right]^2 \right] = (100 s_y)^2$$

$$\begin{pmatrix} P_y \\ h_y \end{pmatrix} := \text{Find}(P_y, h)$$

$$\begin{pmatrix} P_y \\ h_y \end{pmatrix} = \begin{pmatrix} 226.621 \\ 0.054 \end{pmatrix}$$

$$N_{ay} := \frac{1}{\frac{1}{E_{al} E_{hl}} - S_{12_1}} \left[-S_{12_1} \left[\frac{1}{w} \left[\frac{\left(\frac{w^2}{4 h_y} + h_y \right) \arcsin\left(\frac{w}{\frac{w^2}{4 h_y} + h_y} \right)}{\frac{w^2}{4 h_y} + h_y} \right] - 1 \right] - \frac{1}{E_{hl}} \left[\frac{1}{L} \left[\frac{\left(\frac{L^2}{4 h_y} + h_y \right) \arcsin\left(\frac{L}{\frac{L^2}{4 h_y} + h_y} \right)}{\frac{L^2}{4 h_y} + h_y} \right] - 1 \right] \right]$$

$$N_{ay} = 257.737$$

The axial yield LPW in the liner

$$N_{hy} := \frac{1}{\left(\frac{1}{E_{al} E_{hl}} - S_{12_1} \right)} \left[\frac{1}{E_{al}} \left[\frac{1}{w} \left[\frac{\left(\frac{w^2}{4 h_y} + h_y \right) \arcsin\left(\frac{w}{\frac{w^2}{4 h_y} + h_y} \right)}{\frac{w^2}{4 h_y} + h_y} \right] - 1 \right] - S_{12_1} \left[\frac{1}{L} \left[\frac{\left(\frac{L^2}{4 h_y} + h_y \right) \arcsin\left(\frac{L}{\frac{L^2}{4 h_y} + h_y} \right)}{\frac{L^2}{4 h_y} + h_y} \right] - 1 \right] \right]$$

$$N_{hy} = 272.29$$

The hoop yield LPW in the liner

$$s_{ay} := \frac{\left(\frac{L^2}{4 h_y} + h_y \right) \arcsin\left(\frac{L}{\frac{L^2}{4 h_y} + h_y} \right)}{L} - 1$$

$$s_{hy} := \frac{\left[\frac{\left(\frac{w^2}{4 h_y} + h_y \right) \arcsin\left(\frac{w}{\frac{w^2}{4 h_y} + h_y} \right)}{\frac{w^2}{4 h_y} + h_y} \right]}{w} - 1$$

$$s_{ay} = 7.778 \times 10^{-3}$$

$$s_{hy} = 7.778 \times 10^{-3}$$

Step 2

Guess values

$$E_f := 100$$

$$h := 0.06$$

$$s_a := 0.005$$

$$s_h := 0.005$$

Given

$$s_a = \frac{\left(\frac{L^2}{4 \cdot h} + h\right) \arcsin\left(\frac{L}{\frac{L^2}{4 \cdot h} + h}\right)}{L} - 1$$

$$s_h = \frac{\left(\frac{w^2}{4 \cdot h} + h\right) \arcsin\left(\frac{w}{\frac{w^2}{4 \cdot h} + h}\right)}{w} - 1$$

$$E_f = \frac{\frac{1}{E_{a2}} (s_h - s_{hy}) - S_{21_2} (s_a - s_{ay})}{\left(\frac{1}{E_{a2} E_{h2}} - S_{12_2} S_{21_2}\right)} + N_{hy} \frac{\left[-S_{12_2} (s_h - s_{hy}) + \frac{1}{E_{h2}} (s_a - s_{ay})\right]}{\left(\frac{1}{E_{a2} E_{h2}} - S_{12_2} S_{21_2}\right)} + N_{ay}$$

$$\frac{w^2}{8 \cdot h} + \frac{h}{2} \qquad \frac{L^2}{8 \cdot h} + \frac{h}{2}$$

$$\left[\frac{1}{N_{hy}} \left[\frac{1}{E_{a2}} (s_h - s_{hy}) - S_{21_2} (s_a - s_{ay}) \right]}{\left(\frac{1}{E_{a2} E_{h2}} - S_{12_2} S_{21_2}\right)} + N_{hy} \right]^2 - \frac{1}{N_{hy}} \left[\frac{1}{E_{a2}} (s_h - s_{hy}) - S_{21_2} (s_a - s_{ay}) \right] \frac{1}{N_{hy}} \left[\frac{-S_{12_2} (s_h - s_{hy}) - \frac{1}{E_{h2}} (s_a - s_{ay})}{\left(\frac{1}{E_{a2} E_{h2}} - S_{12_2} S_{21_2}\right)} + N_{ay} \right] = 1$$

$$- \left[\frac{1}{N_{ay}} \left[\frac{-S_{12_2} (s_h - s_{hy}) - \frac{1}{E_{h2}} (s_a - s_{ay})}{\left(\frac{1}{E_{a2} E_{h2}} - S_{12_2} S_{21_2}\right)} + N_{ay} \right] \right]^2$$

$$\begin{pmatrix} s_h \\ s_a \\ E_f \\ h \end{pmatrix} := \text{Find}(s_h, s_a, E_f, h)$$

$$\begin{pmatrix} s_h \\ s_a \\ E_f \\ t_f \end{pmatrix} = \begin{pmatrix} 0.099 \\ 0.099 \\ 2.581 \times 10^3 \\ 0.196 \end{pmatrix}$$

$$N_h := \frac{1}{\left(\frac{1}{E_{a2} E_{h2}} - s_{12_2} s_{21_2} \right)} \left[\frac{1}{E_{a2}} (s_h - s_{hy}) - s_{21_2} (s_a - s_{ay}) \right] - N_{hy}$$

$$N_h = 1.739 \times 10^3$$

$$N_a := \frac{1}{\left(\frac{1}{E_{a2} E_{h2}} - s_{12_2} s_{21_2} \right)} \left[-s_{12_2} (s_h - s_{hy}) + \frac{1}{E_{h2}} (s_a - s_{ay}) \right] - N_{ay}$$

$$N_a = 159.529$$

B.3 Interactive Criteria Conclusion: Liner "Life" and Max Operating Pressure

$$t_f := 50$$

$$T_{emp} := 529.67$$

$$N_{ahbp} := 312.8$$

$$N_{aabp} := 74.7$$

$$N_{maxhoop} := N_{ahbp} \left[0.700 \cdot t_f^{-0.00402} \left[\frac{41.905}{T_{emp}} \left(\frac{1}{T_{emp}} - \frac{1}{529.67} \right) \right] \right]$$

$$N_{maxhoop} = 215.543$$

APPENDIX C

LINER CREEP EXPERIMENTAL DATA

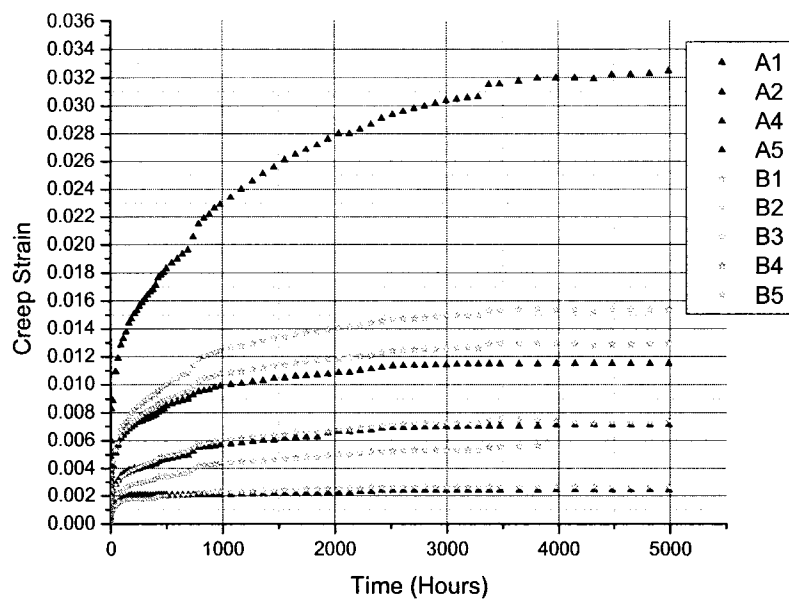
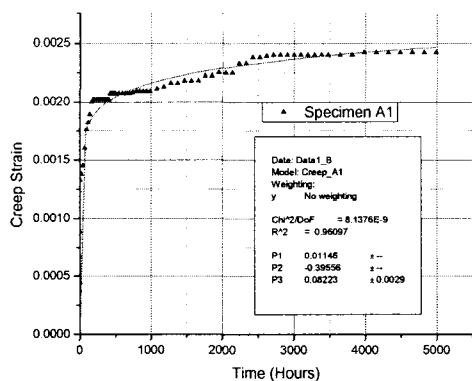
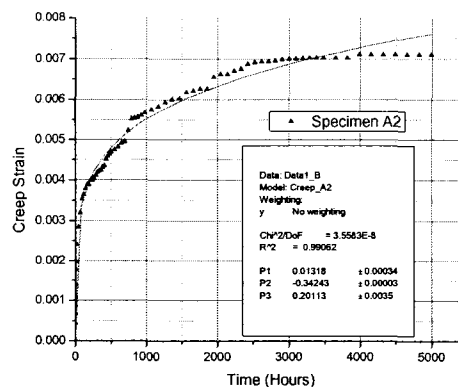


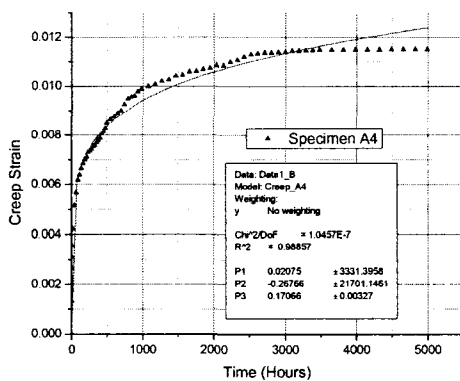
Figure C.1. Liner creep experimental data.



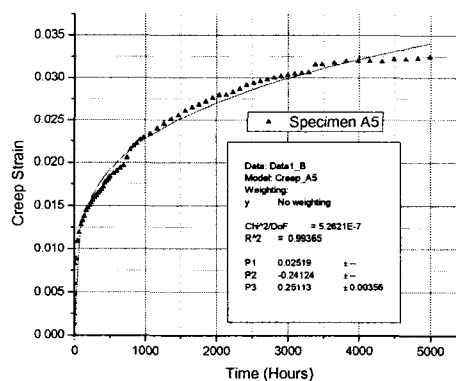
(a)



(b)



(c)



(d)

Figure C.2. Liner creep experimental data and fitting for specimens. (a) A1, (b) A2, (c) A4, and (d) A5.

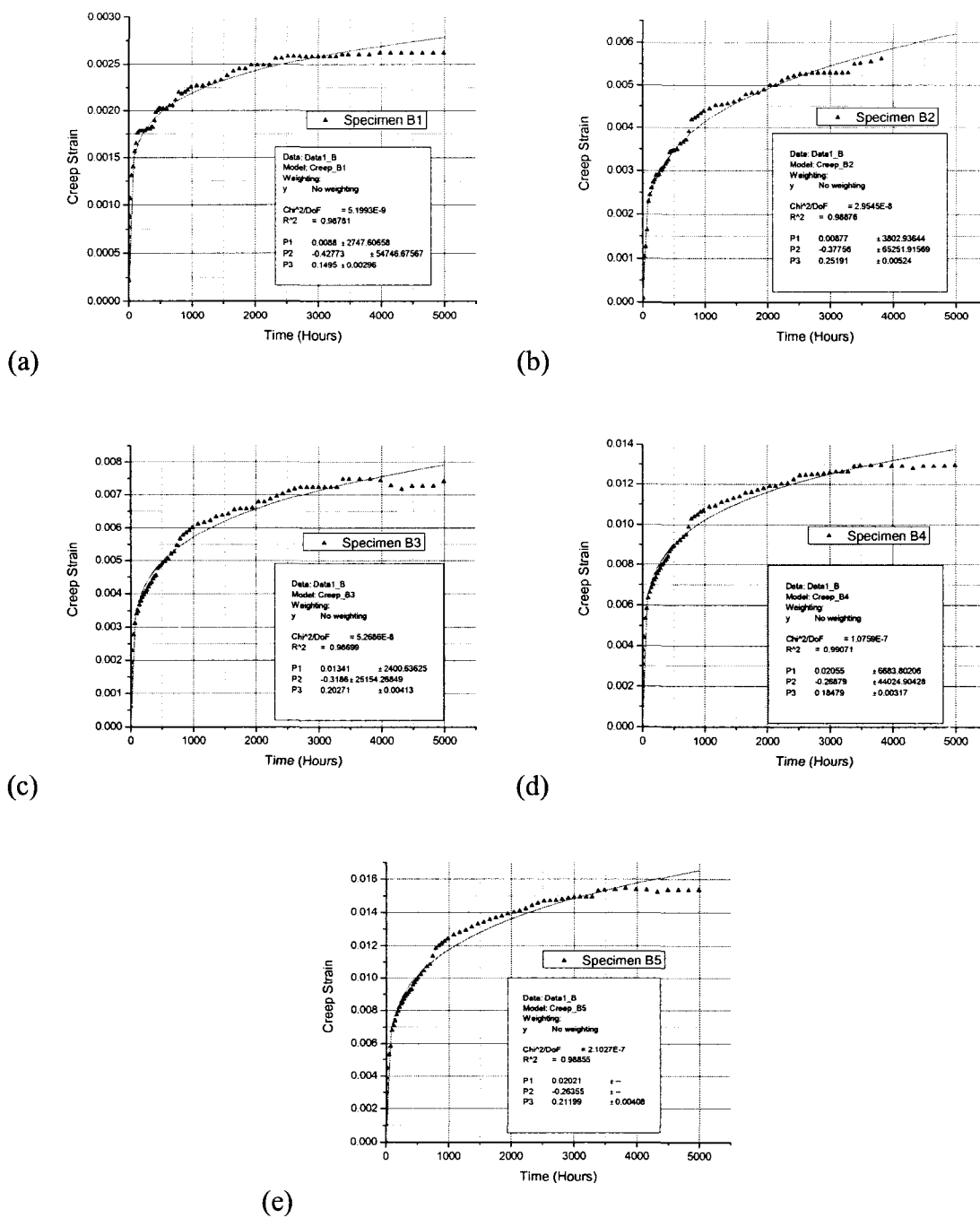


Figure C.3. Liner creep experimental data and fitting for specimens. (a) B1, (b) B2, (c) B3, (d) B4, and (e) B5.

APPENDIX D

CYCLIC LOADING EXPERIMENT DATA

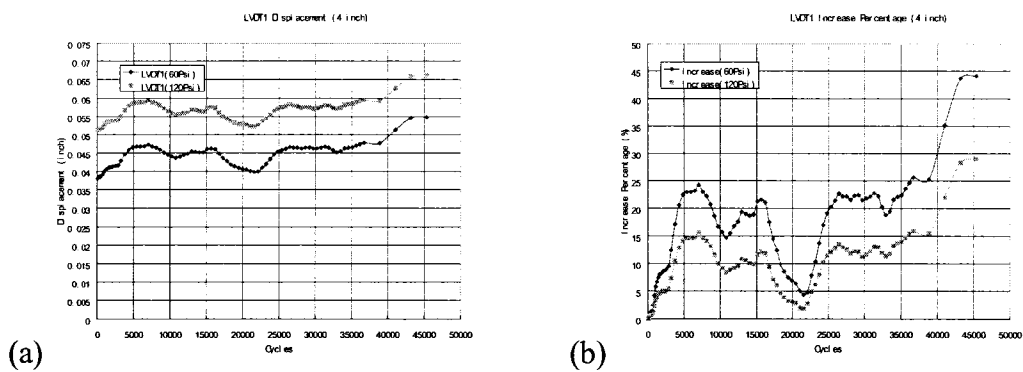


Figure D.1. LVDT1 (a) displacement and (b) increase percentage.

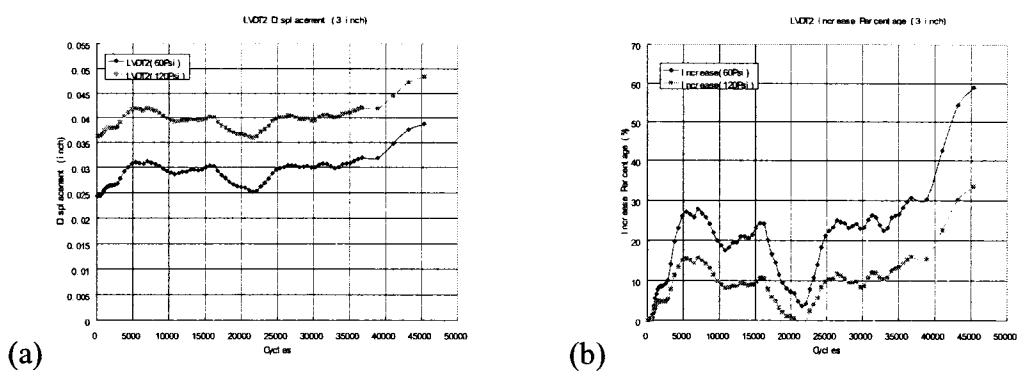


Figure D.2. LVDT2 (a) displacement and (b) increase percentage.

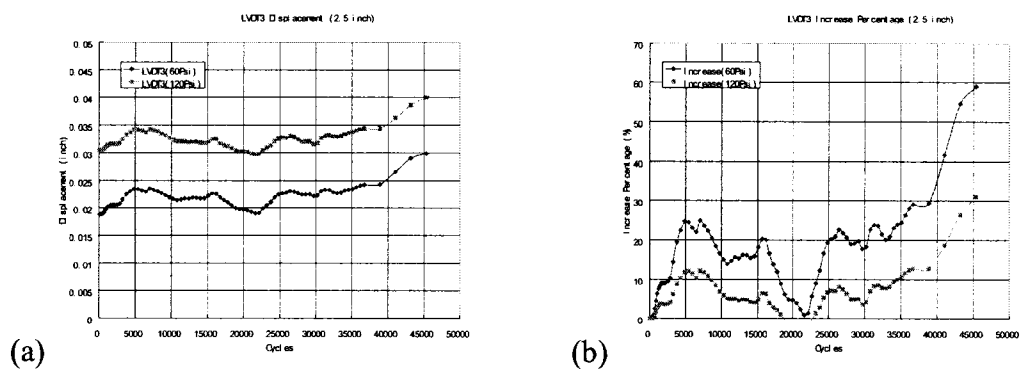


Figure D.3. LVDT3 (a) displacement and (b) increase percentage.

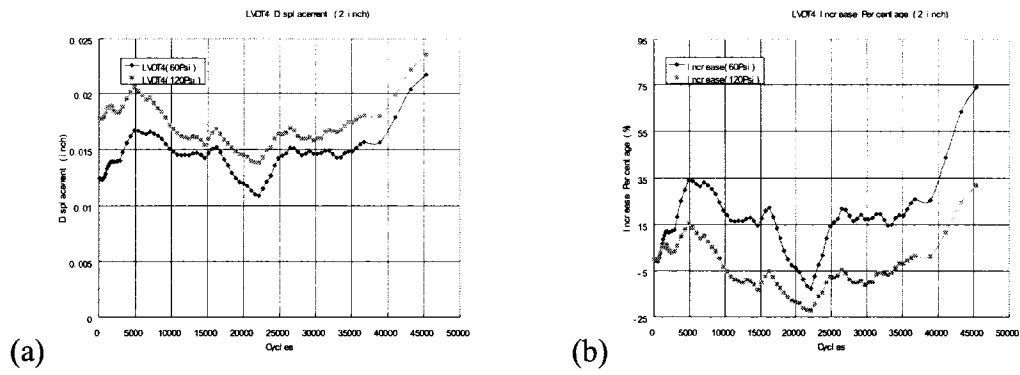


Figure D.4. LVDT4 (a) displacement and (b) increase percentage.

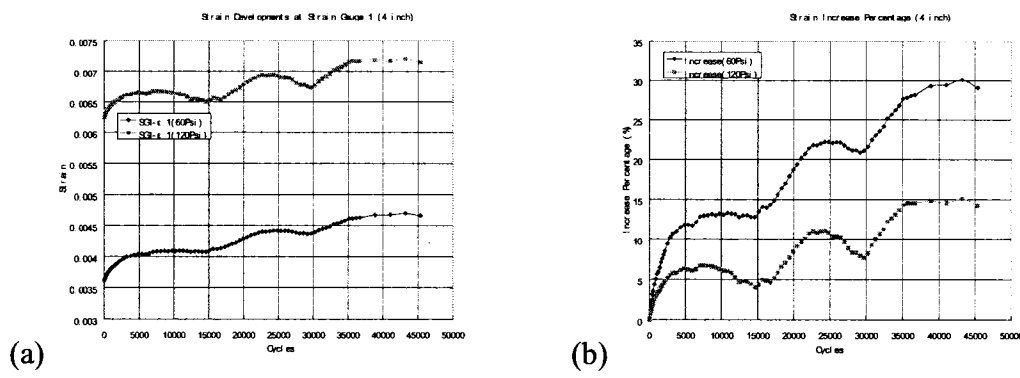


Figure D.5. Strain Gauge 1 (a) strain development and (b) increase percentage.

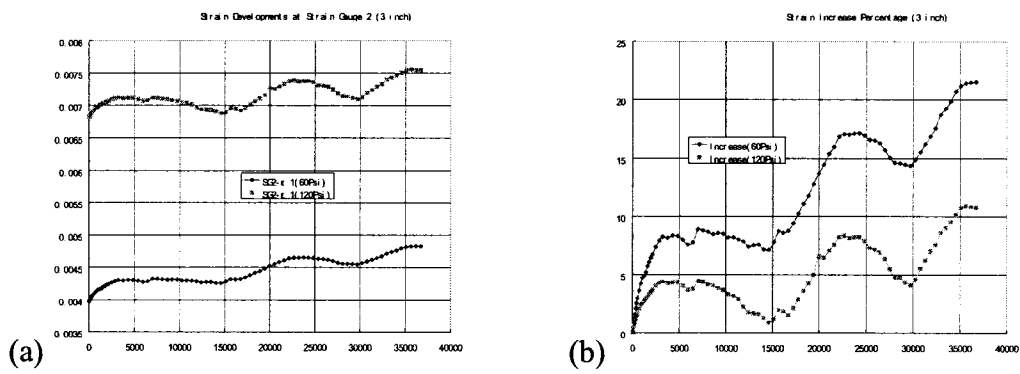


Figure D.6. Strain Gauge 2 (a) strain development and (b) increase percentage.

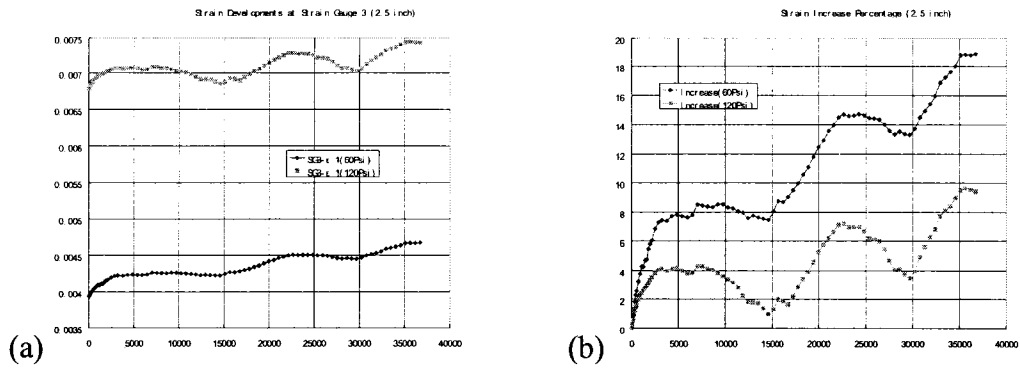


Figure D.7. Strain Gauge 3 (a) strain development and (b) increase percentage.

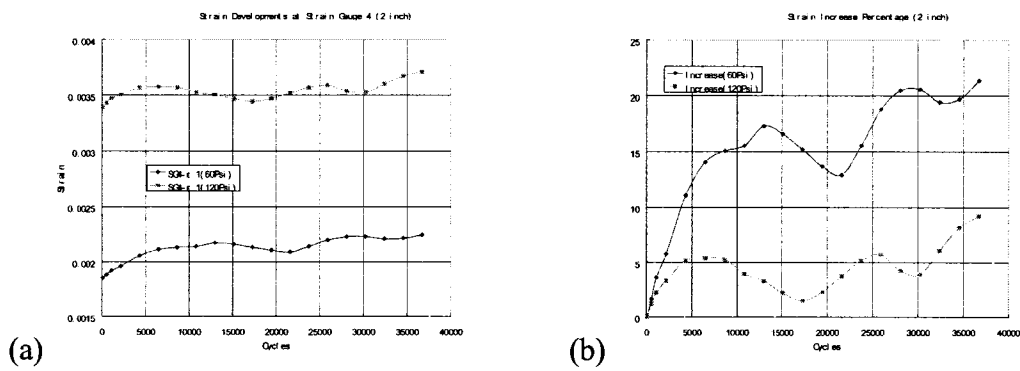


Figure D.8. Strain Gauge 4 (a) strain development and (b) increase percentage.

REFERENCES

- [1] American Society for Testing and Materials F 2207-02, standard.
- [2] Hall, D., et al, "Fabrication and Testing of Pipe Linings for the Gas Industry", final report to GTI (2003).
- [3] Release notes, ADINA System 8.1, 2003.
- [4] Reference manual, ADINA
- [5] Lin, Hung, "Creep Characterization of Cured-in-Place-Pipe Material under Tension, Compression, and Bending," (M.S. thesis, Louisiana Tech University, 1995).
- [6] Findley, W. N. and Gautam Khosla, "An Equation for Tension Creep of Three Unfilled Thermoplastics," *Society of Petroleum Engineers Technical Journal* (December, 1956): 20-25.
- [7] Jaeger, J. C. and Cook, N. C. W., *Fundamental of Rock Mechanics* (New York: John Wiley, 1976), 304-316.
- [8] Findley, W. N., "26-year Creep and Recovery of Poly (Vinyl Chloride) and Polyethylene," *Polymer Engineering and Science* 27 (1987):582-585.
- [9] American Society of Civil Engineers (ASCE), "ASCE Manuals and Reports on Engineering Reports No. 63," *ASCE* (1984): 203-217.
- [10] Findley, W. N., "Creep Characteristics of Plastics," *Symposium on Plastics, American Society for Testing and Materials* (1944):18.
- [11] O'Connor, D. G. and Findley, W. N., "Influence of Normal Stress on Creep in Tension and Compression of Polyethylene and Rigid Polyvinyl Chloride Copolymer," *Society of Petroleum Engineers Transactions* (October, 1962): 273-284.
- [12] Horsley, R. A., "Thermoplastics-Mechanical Properties and Design," *Mechanical Performance and design of Polymers, Applied Polymer Symposia No. 17*, Delatycki, O. Eds. (New York: Interscience Publishers, Division of John Wiley & Sons, 1971).

- [13] Bergen, R. L., Jr. and Wolstenholme, W. E., "Stress Relaxation and Creep Measurements of Some Thermoplastic Materials," *Society of Petroleum Engineers Technical Journal* (November, 1960): 123-124.
- [14] Zhao, Q., "Finite Element Simulation of Creep Buckling of Cured-in-Place-Pipe Liners under External Pressure," (Ph.D. dissertation, Louisiana Tech University, 1999).
- [15] Lu, X., "Finite Element Analysis for Cured-in-Place-Pipe encased in Oval Host Pipes," (M.S. thesis, Louisiana Tech University, 1999).
- [16] Zhu, M., "Computational Investigation of Stress, Contact Condition, and Buckling of Thin-Walled Pipe Liners," (Ph.D. dissertation, Louisiana Tech University, 2000).
- [17] EL-Sawy, K., and Moore I. D., "Stability of Loosely Fitted Liners used to Rehabilitate Rigid Pipes," *Journal of Structural Engineering* 124, (1998):1350-1357.
- [18] Falter, B., "Structural Design of Linings," *Proceedings of the International Conference on Underground Infrastructure Research* (June, 2001): 49-56.
- [19] Allouche, E., "Examining the effect of internal loads on liner in a partially deteriorated pressure pipe," *Technical report to the City of Hamilton* (2005).
- [20] Jaganathan, Arun Prakash, J., "Determination of the Impact of Longitudinal Folds on the Pressure Rating of Cured-in-Place-Pipe Liners," (M.S. thesis, Louisiana Tech University, 2005).
- [21] Allouche, E., "Experimental and numerical evaluation of impact of folds on the pressure rating of Cured-in-Place-Pipe liners," *22nd International No Dig Conference* (Hamburg, Germany, 2004).
- [22] Klaus-Jürgen Bathe, *Finite Element Procedures* (Prentice Hall, 1996).
- [23] Online: http://en.wikipedia.org/wiki/Levenberg-Marquardt_algorithm, (last accessed: December 28, 2006).
- [24] Online: http://en.wikipedia.org/wiki/Gauss-Newton_algorithm, (last accessed: December 28, 2006).